GRAVITY'S EFFECT ON CENTRIFUGAL PENDULUM VIBRATION ABSORBERS

By

Thomas Michael Theisen

A THESIS

Submitted to
Michigan State University
in partial fulfillment of the requirements
for the degree of

MASTER OF SCIENCE

Mechanical Enginering

2011

ABSTRACT

GRAVITY'S EFFECT ON CENTRIFUGAL PENDULUM VIBRATION ABSORBERS

By

Thomas Michael Theisen

This work describes an analytical investigation of the effects of gravity on the dynamics and performance of centrifugal pendulum vibration absorbers (CPVAs). CPVAs are passive devices, consisting of movable masses suspended on a rotor, which act to reduce torsional vibrations in internal combustion engines and other rotating systems. When the system axis of rotation is not vertical, gravity acts directly on the absorbers, and can affect system behavior at low rotor speeds. The investigation is based on a mathematical model that is studied using perturbation methods and numerical simulations. The effects of gravity are captured by a parameter γ, and are examined for different absorber designs and operating conditions, paying particular attention to cases relevant to internal combustion engines. It is found that the steady state system response can be divided into two cases, depending on the order n of the applied torque that leads to torsional vibrations. In the general case, $n \neq 1, 2$, the absorber response to gravity and the applied torque are essentially uncoupled, and the system response can be systematically explored by the introduction of an equivalent system order tuning parameter. In the special cases, $n = 1, 2$, nonlinear interactions from gravity can alter the order n system response in a nontrivial manner. Specifically, we consider the $n = 2$ case, in which a superharmonic response of the absorbers can occur, and the features of this response depend on the number of absorbers N and other system parameters. These predictive results will be of use in the design of CPVAs for automotive engines currently being developed for low speed idle conditions.

To my family current and future.

ACKNOWLEDGMENTS

I would like to take this opportunity to thank all those who have helped me along my journey. This achievement would not have been possible without the support and encouragement of friends, family and coworkers. I would like to thank Dr. Brian Feeny and Dr. Steven Shaw. Dr. Feeny, without your knowledge of perturbation techniques I would not have been able to learn and grasp the skills needed to complete this thesis. Dr. Shaw, it was your constant encouragement and ability to look at problems from a different perspective that carried me through difficulties. I'd also like to thank Alan Haddow, it is because of him that I initially became involved and interested in CPVA's. Thank you to Bruce Geist of Chrysler, your insight on the application of CPVA was instrumental in the development of this thesis. I am thankful to have worked with Ryan Monroe and Brendan Vidmar, without their expertise and experience I would have been lost. Thanks to all the others who have been involve in my research in too many ways to list, Venkat Ramakrishnan, Scott Strachan, Rickey Caldwell, Nick Miller, Michael Farmer, Brian Rockwell and Jelena Paripovic. A special thanks to Carl Coppola, without his help I may have never made it through Dr. Feeny's nonlinear vibration class. Thank you to the National Science Foundation and Chrysler Group LLC for their support of this research. Lastly I'd like to thank my family, without their support and guidance this would never have been achieved.

TABLE OF CONTENTS

LIST OF TABLES

LIST OF FIGURES

Chapter 1

Introduction

Centrifugal pendulum vibration absorbers (CPVAs) are passive devices used to reduce engine order torsional vibrations, that is, twisting vibrations at frequencies proportional to the mean engine speed, in rotating systems. In these systems the constant of proportionality is referred to as the engine order. A CPVA is essentially a mass that moves along a path relative to the rotor, driven by centrifugal effects and the rotor torsional vibrations. The key feature of CPVAs is that their natural frequency is also proportional to the mean rotor speed, and the constant of proportionality for the absorber is referred to as the absorber order. When the absorber is designed with its order close to the engine order, it will react in a manner that counteracts the applied torque, thereby smoothing vibrations. The aim of this work is to gain an understanding of the effects of gravity on centrifugal pendulum vibration absorbers (CPVAs) and their effectiveness in reducing torsional vibrations in systems in which the axis of rotation is horizontal. This problem is motivated by the proposed use of CPVAs in automotive engines, for which gravitational effects become comparable with centrifugal effects at and near engine idle speeds.

Automotive fuel economy standards in the United States continue to increase. One of the ways that progress can be made towards reaching these goals is by lowering engine idle speeds. The lower the engine idle speed, the less fuel it will consume during idling, thus resulting in improvement of the vehicle's fuel economy. However, as in most cases, this fuel savings does not come for free. Lower idle speeds amplify engine torsional vibrations that arise from the cylinder firing pulses. These torsional vibrations are undesirable from a consumer stand point, and can even cause failure if severe enough. It has long been known that CPVAs can reduce torsional vibrations using less inertia than flywheels. In all previous studies of CPVAs gravity has been considered to be small relative to centrifugal effects, and has thus been ignored. This thesis will consider the effects of gravity on the dynamic response of CPVAs, showing that it can have a substantial impact when engine speeds are low.

It is shown that it is important to include these gravitational effects when the parameter $\gamma = g/(R_0\Omega^2)$, which is the ratio of gravitational to centripital acceleration, is 0.02 or greater for $n = 1.5$, and 0.015 or greater for $n = 2$, with reasonable inertia ratios in the range 5%-20%. The corresponding range of engine speeds depends, of course, on the distance from rotor center to absorber center of mass, R_0. For typical automotive engines, R_0 is in the range of 0.05-0.1 meters, which implies that one should consider gravitational effects for rotor speeds below about 70-99 radians/second, that is, about 660-950 rpm for $n = 1.5$ and below about 80-115 radians/second, that is, about 775-1100 rpm for $n = 2$. These are precisely in the range of engine idle speeds. In this work it is shown that gravity, which provides order one excitation directly to the absorbers, can be considered separately from the order n oscillating torque acting on the rotor except when $n = 1, 2$. The $n = 2$ case is considered

in detail, since it has practical application to four cylinder engines, and it is shown that the response depends on the number of absorbers employed. In many cases the response of individual absorbers can have different amplitudes, even though they are subjected to the same loading conditions from gravity and the rotor dynamics. The $n = 1$ case is left for future study.

1.1 History and Background

The history and background of CPVAs, also sometime referred to as Adaptive Tuned Vibration Absorbers (ATVA), can be found in detail in the literature, for example, the works of Alsuwaiyan [1], Schmitz [16], Nester [13], Vidmar [18], Wedin [19], Ker Wilson [22] and Monroe [11]. For the purpose of this thesis, only selected parts of this background are described.

CPVAs were first conceived in the early 1900's. During WWII advancements in the power to weight ratio of piston aircraft engines led to increased torsional vibrations, which were severe enough to lead to failures in the engine unless addressed in some manner [22]. The application of CPVAs as a way of reducing these torsional vibration is discussed by Den Hartog [7], Ker Wilson [22] and Newland [15]. A key feature of CPVAs is that they are tuned to a given engine order, as opposed to given frequency, and thus they remained tuned at all engine speeds. Two of the main features discussed in the early development of CPVAs were the means of suspending the absorbers, and methods of achieving the desired tuning. The bifilar (two point) suspension design, as shown in Figure 1.1, allows the absorber to take the place of existing engine counterweights, and achieve higher tuning orders in a compact

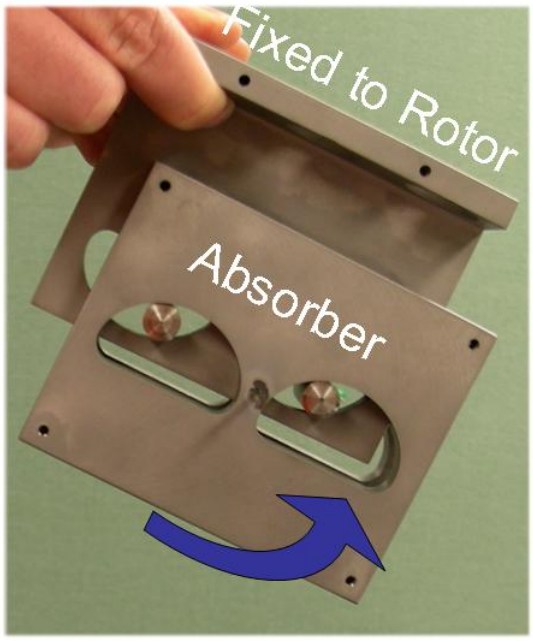

Figure 1.1: Picture of bifilar type absorber. For interpretation of the references to color in this and all other figures, the reader is referred to the electronic version of this thesis.

package, as desired in piston engines.

Early absorber designs were based on a circular path for the absorber center of mass (COM). The nonlinear effects of the circular path were first explored in a paper by Den Hartog [8], who noted that the effective absorber tuning decreases as the absorber amplitude increases, an effect known as nonlinear softening. Newland [15] examined these effects in detail, focusing on the performance of CPVAs, and showed that a jump instability, and associated hysteresis in the response, can occur at moderate absorber amplitudes. Newland suggested that slightly overtuning circular path absorbers is beneficial to their performance, a practice still in use for circular path absorbers. Madden patented a bifilar absorber design for application on helicopter rotors, using a new concept for the path of the absorber COM, specifically, a cycloidal path. The cycloidal path absorber allows the pendulum's tuning to stay closer to a constant, compared to that of circular path, when the absorber amplitude

increases. When a cycloidal path absorber is experiencing high amplitudes of vibration, it's tuning does not decrease like that of a circular path absorber, it actually slightly hardens, which avoids the nonlinear jump [10]. Denman expanded on these ideas for nonlinear absorber tuning by introducing the tautochronic epicycloidal path [5]. This is the path that leads to constant order at all amplitudes, a result which was known to Huygens, and applied to absorbers by Denman. These path issues were further explored in the works of Shaw and co-workers, including Lee and Shaw [9], Alsuwaiyan [1], Chao and Shaw [3] and Geist [6], in which a general class of paths that includes circles, epicycloids, and cycloids, were explored. The general path formulation allows for the systematic study of a variety of paths with both linear and nonlinear tuning.

The stability of the synchronous response of systems of multiple identical absorbers was examined first by Lee, Chao, and Shaw [4], then Alsuwaiyan [1] and then Shaw and Geist [17]. These works focus on characterizing two distinct kinds of stabilities of a synchronous motion: those that correspond to the dangerous nonlinear jump that can occur (described above), and those that break the symmetry of the synchronous response. It is found that a nearly cycloidal path absorber with a slight linear over tuning provides the best results with regards to stability [1, 17]. Additionally it was found that the epicycloidal and cycloid path absorbers do not undergo nonlinear jump behaviors, as do circular path absorbers. These analytical predictions have been verified by simulation and experimental studies [1, 17, 13, 16]. The effects of small imperfections, that is, small differences in tuning and damping, between absorbers was also considered by Alsuwaiyan and Shaw [2], and it was found that this can lead to localized responses in which subsets of absorbers are essentially inactive, leading to a number of undesirable effects. A solution to avoid these problems is proposed by increasing

the linear detuning, such that it is large compared to the imperfections that may exist.

Nester provides the most systematic experimental study of circular absorber systems [13, 14]. The overall system response was compared against analytical predictions and simulations. The instability that corresponds to the dangerous nonlinear jump was explored experimentally with a single absorber system. It was found that this instability occurs and must be avoided, since the absorber becomes a vibration amplifier in this mode. A common discrepancy that appeared between the analytical model, the numerical results, and the experimental results is that this jump occurred at a lower torque level than predicted. Systems with four circular path absorber were also tested experimentally and non-unison responses were observed. However, at low torque levels the non-unison behavior still exists, which does not align with the analytical predictions, and is still not completely understood. In terms of practical engine applications, tests were done with 7.5% overtuned (order 2.15) circular path absorbers in an eight cylinder engine that was run in four cylinder mode, corresponding to cylinder deactivation [13]. Accelerometer data was collected from the vehicle and showed a significant decrease in vibration levels when the absorbers were employed.

Epicycloidal path absorbers were examined experimentally, and compared against analytical predictions, by Schmitz [16]. The effect of linear detuning was examined in detail for these absorbers. Non-unison responses of a two absorber system were also seen during experiments, even at low levels of forcing when the absorbers were tuned close to the excitation order. This is consistent with analytical predictions.

In a recent MS thesis, Wedin [19] examined a different arrangement for absorbers. In this work, CPVAs were coupled with a dual mass flywheel, a system developed by LuK Group and successfully marketed to Mercedes-Benz and BMW. Wedin's thesis reviews many types

of absorbers, including the simple pendulum type, the bifilar type, and the roller type, and epicycloid paths are also considered. Wedin's work focuses on modeling and simulations in an attempt to consider vibrations of additional downstream powertrain components, and their effects on absorber performance.

Bifilar absorbers use rollers as part of their design. Denman developed a model that considers the effects of roller inertia on the equations of motion (EOM), and how this can be accounted for in linear absorber tuning [5]. These results were extended by Monroe, who solved the nonlinear tuning problem for a bifilar absorber with rollers, and derived a tautochronic absorber path that accounts for roller inertia [11].

The transient behavior of absorbers was recently examined by Monroe [11], who developed a method for predicting the overshoot for absorbers that respond when the rotor is suddenly subjected to an applied oscillating torque. This is highly relevant to engines that employ cylinder deactivation, where absorber overshoot must be taken into account in designs, so that the absorbers do not exceed their rattle space limits. It was found that overshoot can be characterized by two parameters: a damping parameter and a system parameter that combines the excitation amplitude, the order detuning, and the system nonlinearity. Experiments were run to mimic cylinder deactivation in order to examine transient responses and compare the analytical model and experiment; this was done using circular path absorbers (the same as those used by Nester) . The results demonstrate the utility of the simple analytical results in predicting the transient overshoot [11].

1.2 Thesis Outline

The remainder of this thesis is organized as follows: In Chapter 2 the mathematical model for a rotor/absorber system is developed, the EOM motion are derived using a Lagrangian approach, and the EOM are non-dimensionalized. This extends previous work by the inclusion of gravity, using an appropriate term in the potential energy. As part of the discussion, the formulation of the absorber path is discussed and the EOM are derived for a general path. However, for purposes of this research, only circular paths will be considered, since they are sufficient to demonstrate the dynamical features of interest. In this Chapter it is also shown that under certain symmetry-related conditions, the effects of gravity cancel out, a result that is useful throughout the entire thesis. Once the EOM are obtained in the desired form, they are scaled so that they can be analyzed using the Method of Multiple Scales.

In Chapter 3, the Method of Multiple Scales is described and applied to the scaled EOM. It is shown that, in contrast to previous work on absorbers, there are special cases that lead to resonant interactions between the applied torque, the gravity, and the absorbers. These cases, which depend on the tuning order and the number of absorbers, are identified and the system steady-state response for the most interesting and relevant cases are analyzed in detail. It is shown that the analytical predictions coincide well with numerical simulations of the full EOM. The results are then analyzed to determine their potential implications for system response, and to identify the conditions under which they are relevant in automotive applications. Chapter 4 provides a discussion of the results and a description of some outstanding related problems.

Chapter 2

The Equations of Motion

In this chapter the equations of motion (EOM) for CPVAs will be derived and scaled in a manner convenient for perturbation analysis. The equations of motion will include the effects due to gravity, which is relevant in systems for which the axis of rotation is not perfectly vertical. Previous works, specifically, those of Alusuwain [1] and Schmitz [16], outline the process that is followed to derive the EOM for absorbers that utilize a general path. The general path equations are made specific for a circular path, thus allowing for comparisons with the results of Nester [13] and Vidmar [18].

The first step is to develop the kinetic and potential energies for the system, from which the EOM can be derived using Lagrange's equations. Once the EOM have been found they are non-dimensionalized to identify important non-dimensional parameters, and to prepare the EOM for perturbation analysis. Specifically, the equations are scaled to identify small effects, so that they can be evaluated through the method of multiple scales (MMS). The MMS provides equations that approximate the slowly varying (relative to the excitation) dynamics of the amplitudes and phases of the CPVAs. These equations are analyzed for

steady-state responses that account for gravity. A stability analysis of these equations is left for future work.

2.1 Model Development

The EOM for CPVAs are derived using Lagrange's equations,

$$\frac{\partial}{\partial t}\left(\frac{\partial L}{\partial \dot{q_k}}\right) - \frac{\partial L}{\partial q_k} = Q_k \tag{2.1}$$

where q_k are the generalized coordinates, Q_k are the generalized forces, and L is the Lagrangian, which is equal to the kinetic energy minus the potential energy:

$$L = T - V. \tag{2.2}$$

Figure 2.1 shows a diagram of the model that is used to develop the EOM, and Table 2.1 provides a description of symbols used in the diagram. The model shows only one absorber, but is easily generalized to account for N absorbers. In practical applications two or more absorbers are desired for balancing and packaging. It is assumed that if more than one absorber is being used, they are equally spaced around the rotor; this allows for some beneficial simplifications in the EOM. The generalized coordinates can be seen to be θ for the rotor angle and S_j for the absorbers. It is assumed that all absorbers are of bifilar construction for this analysis, so that the absorbers do not rotate relative to the rotor. This allows the absorber to be modeled by a point mass located at the absorber's center of mass (COM), and the absorber moment of inertia about its COM is simply included with that of the rotor. Pendulum absorbers with single point suspensions rotate relative to the rotor,

and this changes the analysis [13]. However, a comparison can be made between these two types of models, as described in Appendix 4.2.

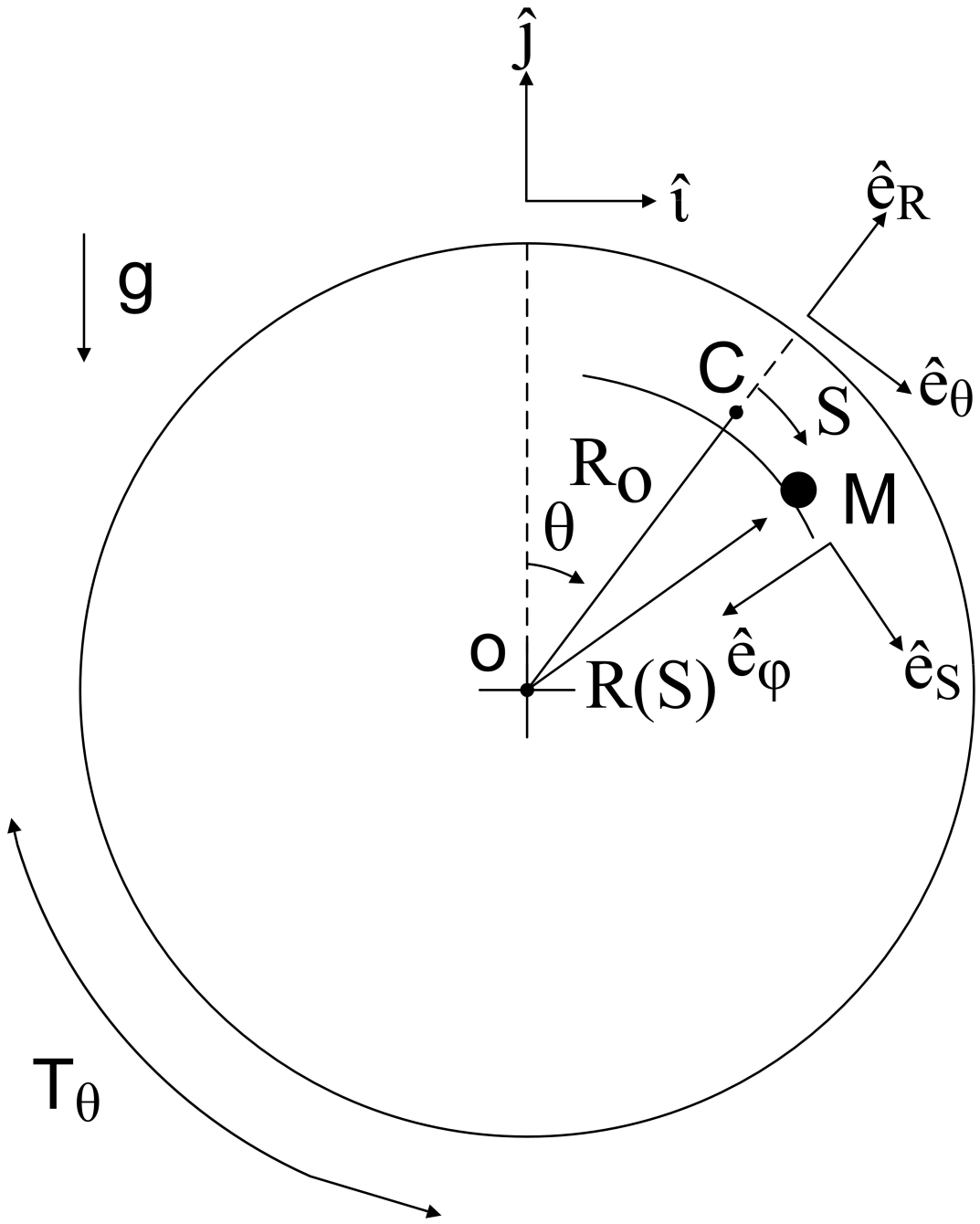

Figure 2.1: Diagram of absorber model.

Table 2.1: Description of symbols used in Figure 2.1.

Symbol	**Description**
O	Center of rotor
C	Position of point mass when the path length is zero
M	Instantaneous position of point mass
R_o	Distance from point O to point C
$R(S)$	Instantaneous distance from point O to point mass
S	Path length
θ	Rotor angle
T_θ	Torque on rotor
g	Gravity
$\hat{\imath}$	Unit vector that is fixed in space and perpendicular to $\hat{\jmath}$
$\hat{\jmath}$	Unit vector that is fixed in space and perpendicular to $\hat{\imath}$
$\hat{e}_R$	Unit vector that is attached to the rotor and perpendicular to $\hat{e}_\theta$
$\hat{e}_\theta$	Unit vector that is attached to the rotor and perpendicular to $\hat{e}_R$
$\hat{e}_S$	Unit vector that is attached to the point mass and perpendicular to $\hat{e}_\phi$
$\hat{e}_\phi$	Unit vector that is attached to the point mass and perpendicular to $\hat{e}_S$

2.1.1 Kinetic Energy

The kinetic energy of the system can be separated into two parts, the kinetic energy of the rotor and the kinetic energy of the absorbers,

$$T = T_{\text{rot}} + \sum_{j=1}^{N} T_j \tag{2.3}$$

where T_j is used to identify the kinetic energy for the j^{th} absorber. The kinetic energy of the rotor is simple and given by,

$$T_{\text{rot}} = \frac{1}{2} J_{\text{rot}} \dot{\theta}^2 \tag{2.4}$$

where J_{rot} is the inertia of the rotor plus that of the absorbers about their respective COM, and $\dot{\theta}$ is the rate of rotor angular rotation. Each pendulum has a kinetic energy of,

$$T_j = \frac{1}{2} m_{p_j} \vec{v}_j \cdot \vec{v}_j \tag{2.5}$$

where m_j is the mass of the j^{th} absorber and $\vec{v}_j$ is the velocity of the absorber. Referring to Figure 2.1, the absorber velocity can be decomposed into two parts: the velocity of point C relative to the origin O plus the velocity of the COM relative to point C.

$$\begin{aligned} \vec{v}_{j(M/C)} &= \dot{S}_j \hat{e}_S \\ \vec{v}_{j(C/O)} &= R(S_j)\dot{\theta}\hat{e}_\theta \end{aligned} \tag{2.6}$$

This leads to the velocity of the j^{th} absorber being given by,

$$\vec{v}_j = \vec{v}_{j(M/C)} + \vec{v}_{j(C/O)} = R(S_j)\dot{\theta}\hat{e}_\theta + \dot{S}_j \hat{e}_S. \tag{2.7}$$

In order to formulate the kinetic energy of the absorbers in terms of the state variables, some relationships for unit vectors and the path function $R(S_j)$ are needed. First, for the unit vectors note that,

$$\begin{aligned} \hat{e}_\theta \cdot \hat{e}_\theta &= 1, \\ \hat{e}_S \cdot \hat{e}_S &= 1, \\ \hat{e}_\theta \cdot \hat{e}_S &= \cos\phi. \end{aligned} \tag{2.8}$$

From Figure 2.2 it can be seen that,

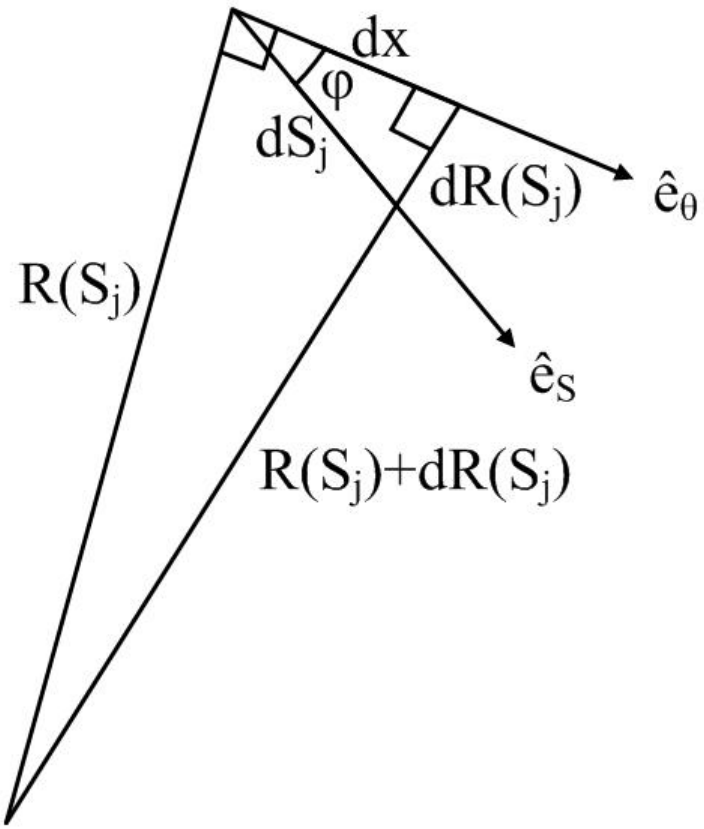

Figure 2.2: Diagram of path consideration.

$$\cos(\phi) = \frac{dx}{dS}. \tag{2.9}$$

Using the Pythagorean theorem it is seen that,

$$dS_j^2 = dx^2 + dR^2, \tag{2.10}$$

which leads to,

$$\frac{dx}{dS_j} = \sqrt{1 - \left(\frac{dR(S_j)}{dS_j}\right)^2}. \tag{2.11}$$

Now $R(S_j)\dot{\theta}\hat{e}_\theta$ can be restated in terms of $R(S_j)$ and its derivatives, as follows,

$$R(S_j)\hat{e}_\theta \cdot \hat{e}_S = \sqrt{R^2(S_j) - R^2(S_j)\left(\frac{dR(S_j)}{dS_j}\right)^2}. \tag{2.12}$$

Note that in some previous formulations the following relationship is used,

$$R^2(S_j)\left(\frac{dR(S_j)}{dS_j}\right)^2 = \frac{1}{4}\left(\frac{dR^2(S_j)}{dS_j}\right)^2. \tag{2.13}$$

The term in equation (2.12) is conveniently expressed by the following path function, $\tilde{G}(S_j)$, is convenient for the EOM, defined using equations (2.12), and (2.13), and given by,

$$\tilde{G}(S_j) = \sqrt{R^2(S_j) - \frac{1}{4}\left(\frac{dR^2(S_j)}{dS_j}\right)^2}. \tag{2.14}$$

In terms of the expressions given above, the system's kinetic energy is given by,

$$T = \frac{1}{2}J_{\text{rot}}\dot{\theta}^2 + \frac{1}{2}m_{p_j}[R^2(S_j)\dot{\theta}^2 + \dot{S_j}^2 + 2\dot{\theta}\dot{S_j}\tilde{G}(S_j)]. \tag{2.15}$$

2.1.2 Potential Energy

When gravity can be ignored, for example, for rotors running at high speeds ($\Omega >> \sqrt{g/R}$), or for rotors with a vertical axis of rotation, the absorber system can be accurately modeled without a potential energy component. When gravity must be accounted for, for example, in systems with a horizontal axis of rotation running at low speeds, the model must include a gravitational potential energy. The rotor speeds over which gravity can be ignored, as well as those for which gravity must be included, are characterized in detail subsequently. For this work it is assumed that the rotor spins about a fixed, perfectly horizontal axis, which implies that the gravitational potential energy comes solely from the vertical position of the absorbers, and is given by,

$$V = \sum_{j=0}^{N} V_{p_j} \tag{2.16}$$

where

$$V_{p_j} = m_{p_j} g h_j \tag{2.17}$$

where g is gravity and h_j is the vertical distance from the fixed rotor center O to the COM. For this purpose, it is convenient to express the distance $R(S_j)$ in terms of an x component $X_{p_j}(S_j)$ and a y component $Y_{p_j}(S_j)$, such that the absorber position vector can be expressed as (see Figure 2.1),

$$-R(S_j)\hat{e}_\phi = Y_{p_j}(S_j)\hat{e}_R + X_{p_j}(S_j)\hat{e}_\theta. \tag{2.18}$$

These components are described in more detail subsequently for different paths. In order to find h_j, one must project $R(S_j)$ onto the fixed reference frame ($\hat{\imath}$ and $\hat{\jmath}$), as shown in Figure

2.1. The required relationships between the rotating vectors ($\hat{e}_R$, $\hat{e}_\theta$) and ($\hat{\imath}$, $\hat{\jmath}$) are given by,

$$\hat{e}_R = \sin(\theta_j)\hat{\imath} + \cos(\theta_j)\hat{\jmath}, \tag{2.19}$$

$$\hat{e}_\theta = \cos(\theta_j)\hat{\imath} - \sin(\theta_j)\hat{\jmath}. \tag{2.20}$$

where

$$\theta_j = \theta + \psi_j \quad \text{where} \quad \psi_j = (j-1)\frac{2\pi}{N}, \tag{2.21}$$

is the rotor angle, θ_j, for absorber j is defined in terms of the segmental angle ψ_j, to give the angular position of the j^{th} absorber relative to $\theta = 0$. Using these in equation (2.18) gives,

$$\begin{aligned} -R(S_j)\hat{e}_\phi = &[Y_{p_j}(S_j)\sin(\theta_j) + X_{p_j}(S_j)\cos(\theta_j)]\hat{\imath} \\ &+ [Y_{p_j}(S_j)\cos(\theta_j) - X_{p_j}(S_j)\sin(\theta_j)]\hat{\jmath}. \end{aligned} \tag{2.22}$$

The potential energy for the j^{th} absorber is thus given by,

$$V_{p_j} = m_{p_j} g[Y_{p_j}(S_j)\cos(\theta_j) - X_{p_j}(S_j)\sin(\theta_j)]. \tag{2.23}$$

2.1.3 Lagrange's Equations

Now that the kinetic and potential energies have been determined, Lagrange's method can be used to find the EOM. Note that dissipation and applied torques will subsequently be included by generalized forces. The Lagrangian is given by,

$$L = \frac{1}{2}J_{\text{rot}}\dot{\theta}^2 + \sum_{j=1}^{N}[\frac{1}{2}m_{p_j}[R^2(S_j)\dot{\theta}^2 + \dot{S_j}^2 + 2\dot{\theta}\dot{S_j}\tilde{G}(S_j)]] - \sum_{j=1}^{N}[mg[Y_{p_j}\cos(\theta_j) - X_{p_j}\sin(\theta_j)]], \tag{2.24}$$

where the generalized coordinates are θ and S_j. The generalized forces Q_k are, for the rotor,

$$Q_\theta = -c_o\dot{\theta} + T_0 + T_\theta \sin(n\theta + \tau), \tag{2.25}$$

which includes rotor viscous resistance and applied torques, and for the j^{th} absorber damping is accounted for using a viscous model,

$$Q_{S_j} = -c_{a_j}\dot{S}_j. \tag{2.26}$$

In these generalized forces, n is the engine order, c_o is the rotor resistance coefficient, T_0 is the mean torque, T_θ is the amplitude of the alternating torque at order n with a phase of τ (allowing this torque to be phased relative to gravity), and c_{a_j} is the absorber damping coefficient. The engine order is based on the number of cylinders in an engine, for example, for a four stroke engines with N_C cylinders, the engine order is half of the number of cylinders, $n = \frac{N_C}{2}$.

Using Lagrange's method the rotor EOM is found to be,

$$\begin{aligned} J_{\text{rot}}\ddot{\theta} + \sum_{i=1}^{N} m_{p_j}[R^2(S_j)\ddot{\theta} + \frac{dR^2(S_j)}{dS}\dot{S}_j\dot{\theta} + \tilde{G}(S_j)\ddot{S}_j + \frac{d\tilde{G}(S_j)}{dS}\dot{S}_j{}^2 \\ - g(X_p(S_j)\cos(\theta_j) + Y_p(S_j)\sin(\theta_j)] = -c_o\dot{\theta} + T_0 + T_\theta \sin(n\theta + \tau), \end{aligned} \tag{2.27}$$

and the absorber EOM are given by,

$$m_{p_j}[\ddot{S}_j + \tilde{G}(S_j)\ddot{\theta} - \frac{1}{2}\frac{dR^2(S_j)}{dS}\dot{\theta}^2 + g(-\frac{dX_p(S_j)}{dS}\sin(\theta_j) + \frac{dY_p(S_j)}{dS}\cos(\theta_j))] = -c_{a_j}\dot{S}_j. \tag{2.28}$$

These form the basis of the analysis that follows.

2.1.4 General Path Absorbers

A quite general formulation is used to describe the path for the absorber COM, as described in detail by Denman [5] and used in subsequent studies [17, 1, 16, 11, 19]. The general path contains a two parameter family of epicycloids that range from circles to cycloids, both of which are special cases of epicycloids. It is beneficial to describe these paths by the local radius of curvature at every point on its path,

$$\rho_j^2 = \rho_{o_j}^2 - \lambda_j^2 S_j^2, \tag{2.29}$$

where ρ_j is the instantaneous radius of curvature, ρ_{o_j} is the radius of curvature of the path at the vertex, and $\lambda_j \in [0, 1]$ describes the amplitude dependent characteristics of the path. When $\lambda_j = 0$, the path is a circle, and when $\lambda_j = 1$ the path is a cycloid. Another case of importance is the tautochronic path, described below, for which,

$$\lambda_{j_t} = \sqrt{\frac{\tilde{n}_j}{(\tilde{n}_j^2 + 1)}}, \tag{2.30}$$

where n_j is the tuning order of the absorber.

Nonlinearities of this system manifest themselves in two different ways: nonlinear coupling through the rotor and a nonlinear restoring force acting on the absorbers. Circular paths provide a softening type of nonlinear restoring force, while cycloids are hardening. The tautochronic path is of importance because it results in a purely linear restoring force acting on the absorber. The detailed expressions for the (x, y) components for these paths

are given in Tables 2.2, 2.3, and 2.4. In terms of these two path parameters the linear tuning order is found from small amplitude vibration analysis, and is given by,

$$\tilde{n}_j = \sqrt{\frac{(R_{o_j} - \rho_{o_j})}{\rho_{o_j}}}, \tag{2.31}$$

as described in [5, 1].

Table 2.2: Description of circular path.

Circular Path	
λ_j	0
S_j	$\rho_{o_j}\phi_j$
$X_p(S_j)$	$\frac{\rho_{o_j}}{1-\lambda_j^2}(\sin(\phi_j)\cos(\lambda_j\phi_j) - \frac{\lambda_j^2 S_j}{\rho_{o_j}}\cos(\phi_j))$
$Y_p(S_j)$	$R_{o_j} + \frac{\rho_{o_j}}{1-\lambda_j^2}(\cos(\phi_j)\cos(\lambda_j\phi_j) + \frac{\lambda_j^2 S_j}{\rho_{o_j}}\sin(\phi_j) - 1)$

Table 2.3: Description of epicycloid path.

Epicycloid Path	
λ_j	$0 < \lambda_j < 1$
S_j	$\frac{\rho_{o_j}}{\lambda_j}\sin(\lambda_j\phi_j)$
$X_p(S_j)$	$\frac{\rho_{o_j}}{1-\lambda_j^2}(\sin(\phi_j)\cos(\lambda_j\phi_j) - \frac{\lambda_j^2 S_j}{\rho_{o_j}}\cos(\phi_j))$
$Y_p(S_j)$	$R_{o_j} + \frac{\rho_{o_j}}{1-\lambda_j^2}(\cos(\phi_j)\cos(\lambda_j\phi_j) + \frac{\lambda_j^2 S_j}{\rho_{o_j}}\sin(\phi_j) - 1)$

Table 2.4: Description of cycloid path.

Cycloid Path	
λ_j	1
S_j	$\rho_{o_j} \sin(\phi_j)$
$X_p(S_j)$	$\frac{1}{2}\rho_{o_j}(\phi_j + \frac{1}{2}\sin(2\phi_j))$
$Y_p(S_j)$	$R_{o_j} - \frac{1}{4}\rho_{o_j}(1 - \cos(2\phi_j))$

In Tables 2.2, 2.3, and 2.4 the angle ϕ is used to describe the effective angle of rotation of the absorber as measured from the radial line passing through the rotor center and the absorber vertex [5]. In each case, ϕ can be determined as a function of S_j, and then $X_p(S_j)$ and $Y_p(S_j)$ can be expressed as functions of S_j. Once $X_p(S_j)$ and $Y_p(S_j)$ have been defined, it can be verified that

$$R^2(S_j) = X_p(S_j)^2 + Y_p(S_j)^2. \tag{2.32}$$

2.1.5 Transformation of Independent Variable

The EOM have, as usual, time as the independent variable. However, due to the applied torque dependence on the rotor angle θ, it is convenient to use θ as the independent variable. This requires a change of coordinates, as described in detail, for example, in [1]. For the rotor speed we define a non-dimensional variable ν as,

$$\nu = \frac{\dot{\theta}}{\Omega}, \tag{2.33}$$

where Ω is the the mean speed of the rotor. Thus, fluctuations in rotor speed about its mean are described by deviations in ν from unity. The chain rule is used to find the relationships

between derivatives with respect to time and derivatives with respect to θ, which are given by,

$$\ddot{\theta} = \frac{d^2\theta}{dt^2} = \frac{d}{dt}(\frac{d\theta}{dt}) = \frac{d}{dt}(\Omega\nu) = \Omega\frac{d}{dt}(\nu) = \Omega\frac{d\nu}{d\theta}\frac{d\theta}{dt} = \Omega^2\nu\nu', \tag{2.34}$$

for the rotor angular acceleration, and generally by,

$$\dot{\star} = \frac{d\star}{dt} = \frac{d\star}{d\theta}\frac{d\theta}{dt} = \frac{d\star}{d\theta}\nu\Omega = \nu\Omega(\star)', \tag{2.35}$$

$$\ddot{\star} = \frac{d^2\star}{dt^2} = \frac{d^2\star}{d\theta^2}(\frac{d\theta}{dt})^2 + \frac{d\star}{d\theta}(\frac{d^2\theta}{dt^2}) = \nu^2\Omega^2(\star)'' + \Omega^2\nu\nu'(\star)'. \tag{2.36}$$

Equations (2.27) and (2.28) can now be transformed to θ dependent variable form, and are given by,

$$\begin{aligned} J_{\text{rot}}\Omega^2\nu\nu' + \sum_{j=1}^{N} m_{p_j}[R^2(S_j)\Omega^2\nu\nu' + \frac{dR^2(S_j)}{dS}\nu^2\Omega^2 S_j' + \tilde{G}(S_j)[\nu^2\Omega^2 S_j'' + \Omega^2\nu\nu' S_j'] \\ + \frac{d\tilde{G}(S_j)}{dS}\nu^2\Omega^2 S_j'^2 - g(X_p(S_j)\cos(\theta_j) + Y_p(S_j)\sin(\theta_j)] \\ = -c_o\nu\Omega + T_0 + T_\theta\sin(n\theta + \tau), \end{aligned} \tag{2.37}$$

$$\begin{aligned} m_{p_j}[\nu^2\Omega^2 S_j'' + \Omega^2\nu\nu' S_j' + \tilde{G}(S_j)\Omega^2\nu\nu' - \frac{1}{2}\frac{dR^2(S_j)}{dS}\Omega^2\nu + \\ g(-\frac{dX_p(S_j)}{dS}\sin(\theta_j) + \frac{dY_p(S_j)}{dS}\cos(\theta_j))] = -c_{a_j}\nu\Omega S_j'. \end{aligned} \tag{2.38}$$

2.1.6 Nondimensionalization

The next step is to non-dimensionalize these equations to reduce the number of parameters. We begin with the dynamic states of the system, and then turn to parameters. The rotor speed has been nondimensionalized by the introduction of ν, and the nondimensional absorber displacement is defined by $s_j = S_j/R_{o_j}$. Then, dividing equation (2.37) by $J_{\text{rot}}\Omega^2$

and equation (2.38) by $m_{p_j}\Omega^2 R_{o_j}$ yields the following non-dimensional EOM,

$$\begin{aligned}\nu\nu' + \frac{b_o}{N}\sum_{j=1}^{N}[x(s_j)\nu\nu' + \frac{dx(s_j)}{ds}\nu^2 s_j' + \tilde{g}(s_j)[\nu^2 s_j'' + \nu\nu' s_j'] + \frac{d\tilde{g}(s_j)}{ds}\nu^2 s_j'^2 \\ - \gamma(x_p(s_j)\cos(\theta_j) + y_p(s_j)\sin(\theta_j))] = -\mu_o\nu + \Gamma_0 + \Gamma_\theta \sin(n\theta + \tau),\end{aligned} \tag{2.39}$$

$$\begin{aligned}\nu^2 s_j'' + \nu\nu' s_j' + \tilde{g}(s_j)\nu\nu' - \frac{1}{2}\frac{dx(s_j)}{ds}\nu \\ + \gamma(-\frac{dx_p(s_j)}{ds}\sin(\theta_j) + \frac{dy_p(s_j)}{ds}\cos(\theta_j)) = -\mu_{a_j}\nu s_j',\end{aligned} \tag{2.40}$$

in which several nondimensional parameters and functions have been introduced, as follows:

$$\begin{gathered}b_o = \frac{I_o}{J_{\text{rot}}}, \quad I_o = m_o R_{o_j}^2, \quad m_o = \sum_{j=1}^{N} m_{p_j}, \quad \frac{S_j}{R_{o_j}} = s_j, \quad \frac{\tilde{G}(S_j)}{R_{o_j}} = \tilde{g}(s_j), \quad \frac{c_a}{m_{p_j}\Omega} = \mu_a, \\ \frac{c_o}{J_{\text{rot}}\Omega} = \mu_o, \quad \frac{T_0}{J_{\text{rot}}\Omega^2} = \Gamma_0, \quad \frac{T_\theta}{J_{\text{rot}}\Omega^2} = \Gamma_\theta, \quad \frac{R^2(S_j)}{R_{o_j}^2} = x(s_j), \quad \frac{X_p(S_j)}{R_{o_j}^2} = x_p(s_j), \\ \frac{Y_p(S_j)}{R_{o_j}^2} = y_p(s_j), \quad \frac{g}{R_{o_j}\Omega^2} = \gamma_j.\end{gathered} \tag{2.41}$$

The functions $x_p(s_j)$ and $y_p(s_j)$ are specified by the selection of the path. Using the fact that $S_j = s_j R_{o_j}$, as well as the relation $\frac{R_{o_j}}{\rho_{o_j}} = 1 + \tilde{n}_j^2$ from equation (2.31), it can be found that for epicycloidal paths,

$$\begin{aligned}x_p(s_j) = &\frac{1}{(1-\lambda_j^2)}[\sin(\frac{\arcsin(s_j\lambda_j(1+\tilde{n_j}^2))}{\lambda_j})\sqrt{\frac{1}{(1+\tilde{n_j}^2)^2} - (s_j^2\lambda_j)^2} \\ &- \lambda_j^2 s_j \cos(\frac{\arcsin(s_j\lambda_j(1+\tilde{n_j}^2))}{\lambda_j})],\end{aligned} \tag{2.42}$$

and

$$y_p(s_j) = -1 - \frac{1}{(1-\lambda_j^2)}[\cos(\frac{\arcsin(s_j\lambda_j(1+\tilde{n_j}^2))}{\lambda_j})\sqrt{\frac{1}{(1+\tilde{n_j}^2)^2} - (s_j^2\lambda_j)^2} - \lambda_j^2 s_j \sin(\frac{\arcsin(s_j\lambda_j(1+\tilde{n_j}^2))}{\lambda_j}) - 1]. \tag{2.43}$$

Taking the derivatives of equations (2.42) and (2.43) we obtain, after simplifications,

$$x_p'(s_j) = \cos\left[\frac{\arcsin(\lambda_j(1+\tilde{n_j}^2)s_j)}{\lambda_j}\right] \tag{2.44}$$

and

$$y_p'(s_j) = \sin\left[\frac{\arcsin(\lambda_j(1+\tilde{n}_j^2)s_j)}{\lambda_j}\right]. \tag{2.45}$$

Additionally, a Taylor Series expansions of $x_p(s_j)^2 + y_p(s_j)^2 = r^2(s_j)$ in s_j is useful for some calculations, and is given by,

$$x(s_j) = 1 - \tilde{n}^2 s_j^2 + \kappa_{1_j} s_j^4 + \ldots, \tag{2.46}$$

where

$$\kappa_{1_j} = \frac{1}{12}(\tilde{n}_j^2 + 1)^2(\tilde{n}_j^2 - \lambda_j^2(1+\tilde{n}_j^2)). \tag{2.47}$$

It is noted that there are special forms of the path functions for circular and cycloidal paths, as mentioned above. However, the general epicycloid expresssions with $\lambda = .01$ and $\lambda = .99$ model the circular and cycloidal paths, respectively, quite accurately, and are used here.

This completes the formulation of the terms needed for the EOM. Next, the EOM are scaled to identify small parameters, so that perturbation analysis can be performed.

2.1.7 Scaling

In order to proceed with perturbation analysis, the EOM (2.39) and (2.40) need to be scaled using a small bookkeeping parameter ϵ that reflects the relatively small effects of forcing, damping, gravity, and nonlinearity, when compared to centrifugal and inertial effects. The scalings of these small parameters and variables by ϵ are chosen so that these effects are captured by a relatively simple perturbation analysis. Several terms in equations (2.39) and (2.40) need to be scaled by ϵ in order for the desired overall scaling to be achieved. Specifically,

$$b_O = \epsilon^B \ , \ \nu = 1 + \epsilon^W w \ , \ \nu' = \epsilon^W w' \ , \ s_j = \epsilon^P p_j \ , \ s_j' = \epsilon^P p_j' \ , \ s_j'' = \epsilon^P p_j'', \ \kappa_1 = \kappa_0 \epsilon^{-B}$$
$$\Gamma_\theta = \epsilon^F \tilde{\Gamma_\theta} \ , \ \gamma_j = \epsilon^G \tilde{\gamma}_j \ , \ \mu a_j = \epsilon^L \tilde{\mu} a_j \ , \ \tilde{n}_j = n(1 + \epsilon^Q \sigma_j) \ , \ \Gamma_0 - \mu_O \nu = \mathcal{O}(\epsilon^D), \tag{2.48}$$

which are described here. The inertia ratio b_O is small parameter the rotor inertia J is considerably larger than the total absorber inertia I_O. The applied oscillating torque Γ_θ is small since it is scaled by the rotational kinetic energy of the system. Due to this torque, the rotor velocity $\dot{\theta}$ is not a constant but has small variations compared to its mean value, accounted for by $\epsilon^W w$. The absorber oscillation amplitudes s_j are small compared to the radial distance R_{O_j}. The path nonlinearity is scaled so that it will be retained (this scaling is not standard, since the power of ϵ is negative, but provides useful results). The gravity parameter γ is small compared to the centripetal acceleration $R_{O_j}\Omega^2$. The absorber damping parameter μ_a is small, since it is proportional to the damping ratio, and these absorbers are lightly damped. It has been shown in previous work that a small level of detuning between the excitation and absorber orders is beneficial, and this is captured by $\epsilon^Q \sigma$. The detuning will be stated by σ or as a percent detuning, $100 * \frac{\tilde{n}-n}{n}$. For a nearly constant rotor speed

to be maintained, the difference between the mean applied torque Γ_0 and bearing resistance torque $\mu_o \nu$ must be small and, in fact, it is assumed that the scaling exponent D is such that this difference does not appear in the resulting model (this assumption is required for the analysis to carry through, and fortunately, it allows for useful results to be obtained).

These scalings and series expansions are used in the absorber path functions, resulting in the following simplified expressions,

$$\begin{aligned}
x(s_j) &= 1 - n_j^2 \epsilon^{2P} p_j^2 + {\kappa_0}_j \epsilon^{3P} p_j^4 \qquad \frac{dx(s_j)}{ds_j} = -2n_j^2 \epsilon^P p_j + 4{\kappa_0}_j \epsilon^{2P} p_j^3 \\
\tilde{g}(s_j) &= 1 - \frac{(n_j^2 + n_j^4)\epsilon^{2P} p_j^2}{2} \qquad \frac{d\tilde{g}(s_j)}{ds_j} = -(n_j^2 + n_j^4)\epsilon^P p_j \\
x_p(s_j) &= \epsilon^P p_j - \frac{(1+n_j^2)^2 \epsilon^{3P} p_j^3}{6} \qquad \frac{dx_p(s_j)}{ds_j} = 1 - \frac{(1+n_j^2)^2}{2}\epsilon^{2P} p_j^2 \\
y_p(s_j) &= -1 + \frac{(1+n_j^2)}{2}\epsilon^{2P} p_j^2 \qquad \frac{dy_p(s_j)}{ds_j} = (1+n_j^2)\epsilon^P p_j
\end{aligned} \tag{2.49}$$

It is also convenient to assume that each absorber in the system is identical in terms of mass, damping, and path, even though the absorbers may not have identical responses. Under this assumption,

$$R_{o_j} = R_o \quad \rho_{o_j} = \rho_o \quad \lambda_j = \lambda \quad \gamma_j = \gamma \quad \sigma_j = \sigma \quad {\kappa_0}_j = \kappa_0 \quad n_j = n \quad \tilde{\mu}a_j = \tilde{\mu}a. \tag{2.50}$$

Substitution of equations (2.48), (2.49), and (2.50) into equations (2.39) and (2.40), an expanded form for the EOM is obtained, as follows,

$$\begin{aligned}
&n^2 p_j \epsilon^P + p_j'' \epsilon^P + 2n^2 \sigma p_j \epsilon^{P+Q} + \tilde{\mu}a p_j' \epsilon^{L+P} + w' \epsilon^W - \tilde{\gamma} \sin(\theta_j) \epsilon^G - 2\kappa_o p_j^3 \epsilon^{3P} \\
&\qquad + (1+n^2)\tilde{\gamma} p_j \cos(\theta_j) \epsilon^{P+G} + \text{HOT} = 0
\end{aligned} \tag{2.51}$$

and

$$(-\tilde{\Gamma_\theta}\sin(n\theta+\tau))\epsilon^F + (w' + \frac{1}{N}\sum_{j=1}^{N} p_j'' + \frac{1}{N}\sum_{j=1}^{N}\gamma\sin(\theta_j))\epsilon^{2P} + \text{HOT} = 0, \tag{2.52}$$

where HOT refers to terms of higher order in ϵ. It is crucial that the parametric excitation term $(1+n^2)\tilde{\gamma}p_j\cos(\theta)\epsilon^{P+G}$ be retained, since it describes an important effect of gravity on the system. To capture this effect, along with the forcing, damping, detuning, and path nonlinearities, the following values are select for the scaling: $P = \frac{1}{2}$, $G = \frac{1}{2}$, $W = 1$, $Q = \frac{1}{2}$,$L = \frac{1}{2}$, $B = \frac{1}{2}$, $D = \frac{3}{2}$ and $F = 1$.

The final result for the expanded EOM, that retains the important effects, is given by,

$$p_j'' + n^2 p_j - \tilde{\gamma}\sin(\theta_j))\epsilon^{\frac{1}{2}} + (2n^2\sigma p_j + \tilde{\mu}_a p_j' + w' - 2\kappa_o p_j^3 + (1+n^2)\tilde{\gamma}p_j\cos(\theta_j))\epsilon = 0 \tag{2.53}$$

for the absorbers, and

$$(w' - \tilde{\Gamma}_\theta\sin(n\theta+\tau) + \frac{1}{N}\sum_{j=1}^{N} p_j'' + \frac{1}{N}\sum_{j=1}^{N}\gamma\sin(\theta_j))\epsilon = 0, \tag{2.54}$$

for the rotor, where the higher order terms have been dropped.

It is convenient at this point to note that with this scaling one can decouple the rotor EOM from those of the absorbers. This is done by solving for w' in equation (2.54) and substituting the result into equation (2.53). The result is divided by $\epsilon^{\frac{1}{2}}$ and expanded in ϵ,

yielding,

$$
\begin{aligned}
&[p_j'' + n^2 p_j - \tilde{\gamma}\sin(\theta_j)[+\epsilon^{\frac{1}{2}}[2n^2\sigma p_j + \tilde{\mu}_a p_j' - 2\kappa_O p_j^3 \\
&+ (1+n^2)\tilde{\gamma} p_j \cos(\theta_j) + \tilde{\Gamma}_\theta \sin(n\theta+\tau) - \frac{1}{N}\sum_{j=1}^{N} p_j'' + \frac{1}{N}\sum_{j=1}^{N}\gamma\sin(\theta_j) = 0.
\end{aligned}
\tag{2.55}
$$

The leading order terms can be used to solve for p_j'', as

$$
p_j'' = \tilde{\gamma}\sin(\theta_j) - \tilde{n}^2 p_j. \tag{2.56}
$$

This is used to replace p_j'' in the order $\epsilon^{\frac{1}{2}}$ term in equation 2.55, and the result is simplified using the method described in Appendix 4.2, which shows that $\sum_1^N \sin(\theta_j) = 0$. Additionally, it is convenient to define $\epsilon^{\frac{1}{2}} = \hat{\epsilon}$. This results in the final equation that used for the detailed analysis presented in the next chapter,

$$
\begin{aligned}
&(p_j'' + n^2 p_j - \tilde{\gamma}\sin(\theta_j)) + \hat{\epsilon}(2n^2\sigma p_j - 2\kappa_O p_j^3 + (1+n^2)\tilde{\gamma} p_j\cos(\theta_j) \\
&\quad + \frac{1}{N}\sum_{j=1}^{N} n^2 p_j + \tilde{\mu}_a p_j' + \tilde{\Gamma}_\theta \sin(n\theta+\tau)).
\end{aligned}
\tag{2.57}
$$

Note that this equations contains leading order effects of damping, order detuning, as well as a cubic nonlinearity. Additionally, it should be noticed that the equation has small parametric forcing due to gravity, hard (nonresonant) direct forcing due to gravity, and soft forcing due to the (resonant) oscillating torque. In the next chapter we determine approximations for the response of the system using perturbation methods applied to equation (2.57).

Chapter 3

Analysis and Results

In this chapter the method of multiple scales will be used to develop the slow flow equations. For different resonance cases based on the order of forcing. The most interesting case is when the forcing order equals two. In this case it will be shown that the solution to the slow flow equations varies based on the number of absorbers that are being used. It will be shown that from the slow flow equations the absorber amplitude can be solved for as a function of the detuning (σ), damping (μ_a), path nonlinearity (κ_0), gravity (γ), forcing order (n) and absorber spacing (ψ_j). It should be noted that κ_0 is dependent on the type of path defined, which has is defined by λ and the tuning of the absorbers ($\tilde{n}$). Additionally the rotor acceleration can be estimated from the slow flow equations in conjunction with the scaled equations. This allows the effect of gravity on performance to be analyzed easily.

3.1 Method of Multiple Scales

The method of multiple scales is used to determine the slow flow equations. Nayfeh and Mook [12] describe this method in their book in more depth. Only the math for our specific

application will be shown. In the method of multiple scales it is assumed that the response involves different time scales. In this problem the EOM have changed from a time dependence to a rotor angle dependence. This change has no effect on the procedure. The response can be defined by

$$p_j = X_{0_j}(\theta_0, \theta_1, \theta_2, ...) + \epsilon X_{1_j}(\theta_0, \theta_1, \theta_2, ...) + \epsilon^2 X_{2_j}(...) + ... \tag{3.1}$$

which leads to

$$p'_j = D_0 X_{0_j} + \epsilon D_0 X_{1_j} + \epsilon D_1 X_{0_j} + O(\epsilon^2) \tag{3.2}$$

and

$$p'' = D_0^2 X_0 + \epsilon D_0^2 X_1 + 2\epsilon D_0 D_1 X_0 + O(\epsilon^2) \tag{3.3}$$

where j is the absorber index, D_0 is the partial derivative with respect to the rotor angle scale θ_0, and D_1 is the partial derivative with respect to the rotor angle scale θ_1, and so forth for higher-order expansions. Equations (3.1), (3.2), (3.3) and (2.22) can then be plugged into equation (2.57). This will give a rather large equation but only the first two orders of ϵ are considered important for this analysis. Separating coefficients of like powers of ϵ leads to

$$\epsilon^0 : D_0^2 X_{0_j} + n^2 X_{0_j} = \tilde{\gamma} \sin(\theta + \psi_j) \tag{3.4}$$

$$\begin{aligned} \epsilon^1 : D_0^2 X_{1_j} + n^2 X_{1_j} = & -2D_0 D_1 X_{0_j} - 2n^2 \sigma X_{0_j} - \frac{n^2}{N} \sum_{k=1}^{N} X_{0_k} \\ & - (1 + n^2)\tilde{\gamma} \cos(\theta_j) X_{0_j} + 2\kappa_0 X_{0_j}^3 - \tilde{\mu}_a D_0 X_{0_j} - \tilde{\Gamma}_\theta \sin(n\theta + \tau) \end{aligned} \tag{3.5}$$

which are partial differential equations.

The solution for X_{0_j} in equation (3.4) is harmonic and contains both a homogeneous solution as well as a particular solution. For this analysis a cosine will be used for the homogeneous response and will be written in exponential form with amplitude a_j and phase α_j which are functions of θ, as they are constants of integration of a partial differential equation. This leads to the following solution for equation (3.4):

$$X_{i0} = C_j e^{in\theta 0} + \bar{C}_j e^{-in\theta 0} + \Lambda_j e^{i\theta 0} + \bar{\Lambda}_j e^{-i\theta 0} \tag{3.6}$$

where

$$\begin{aligned} C_j = \frac{1}{2} a_j e^{i\alpha_j} \quad \& \quad \bar{C}_j = \frac{1}{2} a_j e^{-i\alpha_j} \\ \Lambda_j = \frac{i\tilde{\gamma}}{2(1-n^2)} e^{i\psi_j} \quad \& \quad \bar{\Lambda}_j = \frac{-i\tilde{\gamma}}{2(1-n^2)} e^{-i\psi_j} \end{aligned} \tag{3.7}$$

and C_j is a function of θ_1. Now the solution found in equation (3.6) can be plugged into equation (3.5) such that

$$\begin{aligned} \epsilon^1 : \; & D_0^2 X_{1_j} + n^2 X_{1_j} = -2C_j' in e^{in\theta 0} - 2n^2\sigma(C_j e^{in\theta 0} + \Lambda_j e^{i\theta 0}) \\ & - \frac{n^2}{N} \sum_{k=1}^{N} (C_k e^{in\theta 0} + \Lambda_k e^{i\theta 0}) - \Delta e^{i\psi_j} (C_j e^{i\theta 0(1+n)} + \bar{C}_j e^{i\theta 0(1-n)} + \Lambda_j e^{i2\theta 0} + \bar{\Lambda}_j) \\ & + 2\kappa_0 (C_j^3 e^{i3n\theta 0} + 3C_j^2 \bar{C}_j e^{in\theta 0} + 6C_j \bar{C}_j \Lambda_j e^{i\theta 0} + 3\bar{C}_j^2 \Lambda_j e^{i\theta 0(1-2n)} \\ & + 3C_j^2 \Lambda_j e^{i\theta 0(1+2n)} + 3\bar{C}_j \Lambda_j^2 e^{i\theta 0(2-n)} + 3C_j \Lambda_j^2 e^{i\theta 0(2+n)} + \Lambda_j^3 e^{i3\theta 0} \\ & + 6C_j \Lambda_j \bar{\Lambda}_j e^{in\theta 0} + 3\Lambda_j^2 \bar{\Lambda}_j e^{i\theta 0}) - \tilde{\mu}_a (C_j in e^{in\theta 0} + \Lambda_j i e^{i\theta 0}) + \frac{i\tilde{\Gamma}\theta}{2} e^{i\tau} e^{in\theta 0} + C.C. \end{aligned} \tag{3.8}$$

where here $(\;)' = \frac{d(\;)}{d\theta}$, and

$$\Delta = \frac{(1+n^2)\tilde{\gamma}}{2} \tag{3.9}$$

3.1.1 Slow Flow Equations

In the method of multiple scales the slow flow equations are determined by eliminating the secular terms in equation (3.8). The order of the absorbers relative to the order of excitation has an impact on what terms will be secular. There are four different cases that can be considered. The special cases are $\tilde{n} = 1$, $\tilde{n} = 2$ and $\tilde{n} = 3$. Other orders of the absorbers fall into the general case. The case when $n = 1$ will not be explored in this work.

3.1.1.1 Case 1 : $n \neq 1,\ 2,\ 3$

This is the general case; it directly applies to engines with $3, 5, 7, 8$ or more cylinders. When all of the secular terms are collected and equated to zero the following is found:

$$(2nC_j'i + 2n^2\sigma C_j + \frac{n^2}{N}\sum_{k=1}^{N} C_k - \kappa_0(6C_j^2\bar{C}_j + 12C_j\Lambda_j\bar{\Lambda}_j) + n\tilde{\mu}_a C_j i - \frac{i\tilde{\Gamma}_\theta}{2}e^{i\tau})e^{in\theta}0 = 0 \tag{3.10}$$

Plugging in C_j, $\bar{C}_j$, Λ_j, $\bar{\Lambda}_j$ and Δ and separating into real and imaginary parts, the slow flow equations are obtain as

$$\begin{aligned}
\textbf{RE}: \quad & -a_j\alpha_j' + na_j\sigma + \frac{n}{2N}\sum_{k=1}^{N}[a_k\cos(\alpha_k - \alpha_j)] - \frac{3}{4n}\kappa_0 a_j^3 \\
& - \frac{3}{2}\frac{\kappa_0 a_j\tilde{\gamma}^2}{n(1-n^2)^2} - \frac{\tilde{\Gamma}_\theta}{2n}\sin(\alpha_j - \tau) = 0 \\
\textbf{IM}: \quad & a_j' + \frac{n}{2N}\sum_{k=1}^{N}[a_k\sin(\alpha_k - \alpha_j)] + \frac{\tilde{\mu}a}{2}a_j - \frac{\tilde{\Gamma}_\theta}{2n}\cos(\alpha_j - \tau) = 0.
\end{aligned} \tag{3.11}$$

When $\gamma = 0$ the slow flow equations give the same results as those found by Alsuwaiyan [1].

3.1.1.2 Case 2 : $n = 2$

This is the case of a four cylinder engine. When all the secular terms are collected and equated to zero the following is found:

$$\begin{aligned}(2nC_j'i + 2n^2\sigma C_j + \frac{n^2}{N}\sum_{k=1}^{N} C_k - \Delta\Lambda_j e^{i\psi_j} - \kappa_0(6C_j^2\bar{C}_j + 12C_j\Lambda_j\bar{\Lambda}_j) \\ + n\tilde{\mu}_a C_j i - \frac{i\tilde{\Gamma}_\theta}{2}e^{i\tau})e^{in\theta}0 = 0\end{aligned} \tag{3.12}$$

Plugging in C_j, $\bar{C}_j$, Λ_j, $\bar{\Lambda}_j$, from equations (3.7) and Δ from equation (3.9) and separating into real and imaginary parts produces the slow flow equations as

$$\begin{aligned}\textbf{RE}: \quad & -a_j\alpha_j' + na_j\sigma + \frac{n}{2N}\sum_{k=1}^{N}[a_k\cos(\alpha_k - \alpha_j)] - \frac{3}{4n}\kappa_0 a_j^3 \\ & - \frac{3}{2}\frac{\kappa_0 a_j\tilde{\gamma}^2}{n(1-n^2)^2} - \frac{\tilde{\Gamma}_\theta}{2n}\sin(\alpha_j - \tau) - \frac{(1+n^2)\tilde{\gamma}^2}{4n(1-n^2)}\sin(2\psi_j - \alpha_j) = 0 \\ \textbf{IM}: \quad & a_j' + \frac{n}{2N}\sum_{k=1}^{N}[a_k\sin(\alpha_k - \alpha_j)] + \frac{\tilde{\mu}a}{2}a_j - \frac{\tilde{\Gamma}_\theta}{2n}\cos(\alpha_j - \tau) \\ & + \frac{(1+n^2)\tilde{\gamma}^2}{4n(1-n^2)}\cos(2\psi_j - \alpha_j) = 0.\end{aligned} \tag{3.13}$$

Notice that in this case the slow flow equations have an additional term compared to the general case. This extra term contains ψ_j, meaning the absorber response is dependent on the relative position of the absorber. This means the equations can change for systems if the number of absorbers changes. This will be discussed in more length later.

3.1.1.3 Case 3 : $n = 3$

This is the case for a six cylinder engine. When all the secular terms are collected and equated to zero, the following is found:

$$\begin{aligned}(2nC_j'i + 2n^2\sigma C_j + \frac{n^2}{N}\sum_{k=1}^{N} C_k - \kappa_0(6C_j^2\bar{C}_j + 12C_j\Lambda_j\bar{\Lambda}_j + \Lambda_j^3) \\ + n\tilde{\mu}_a C_j i - \frac{i\tilde{\Gamma}\theta}{2}e^{i\tau})e^{in\theta}0 = 0.\end{aligned} \tag{3.14}$$

Plugging in C_j, $\bar{C}_j$, Λ_j, $\bar{\Lambda}_j$ from equations (3.7) and Δ from equation (3.9) and separating into real and imaginary parts leads to the slow flow equations,

$$\begin{aligned}\textbf{RE}: \quad & -a_j\alpha_j' + na_j\sigma + \frac{n}{2N}\sum_{k=1}^{N}[a_k\cos(\alpha_k - \alpha_j)] - \frac{3}{4n}\kappa_0 a_j^3 \\ & - \frac{3}{2}\frac{\kappa_0 a_j\tilde{\gamma}^2}{n(1-n^2)^2} - \frac{\tilde{\Gamma}\theta}{2n}\sin(\alpha_j - \tau) - \frac{\kappa_0\tilde{\gamma}^3}{4n(1-n^2)^3}\sin(3\psi_j - \alpha_j) = 0 \\ \textbf{IM}: \quad & a_j' + \frac{n}{2N}\sum_{k=1}^{N}[a_k\sin(\alpha_k - \alpha_j)] + \frac{\tilde{\mu}_a}{2}a_j - \frac{\tilde{\Gamma}\theta}{2n}\cos(\alpha_j - \tau) \\ & + \frac{\kappa_0\tilde{\gamma}^3}{4n(1-n^2)^3}\cos(3\psi_j - \alpha_j) = 0\end{aligned} \tag{3.15}$$

Notice that in this case the slow flow equations are also dependent on ψ_j, similar to Case 2. This case will be examine in more detail later to show that it falls in to Case 1.

3.2 Time Trace of Response

Before the steady-state analysis is done for the different cases in the next few sections, it is beneficial to look at the responses seen in numerical simulations of the full equations of motion. This will show that, unlike in previous work, additional work will needed in order

to fully understand the results and compare them to analysis. Consider a system that has $\epsilon = .022276$, $\mu_a = .014921$, $n = 2$, $\sigma = 0$ and $N = 2$. The absorber response will be found for the case without gravity ($\gamma = 0$) and with gravity ($\gamma = .05$). The time trace without

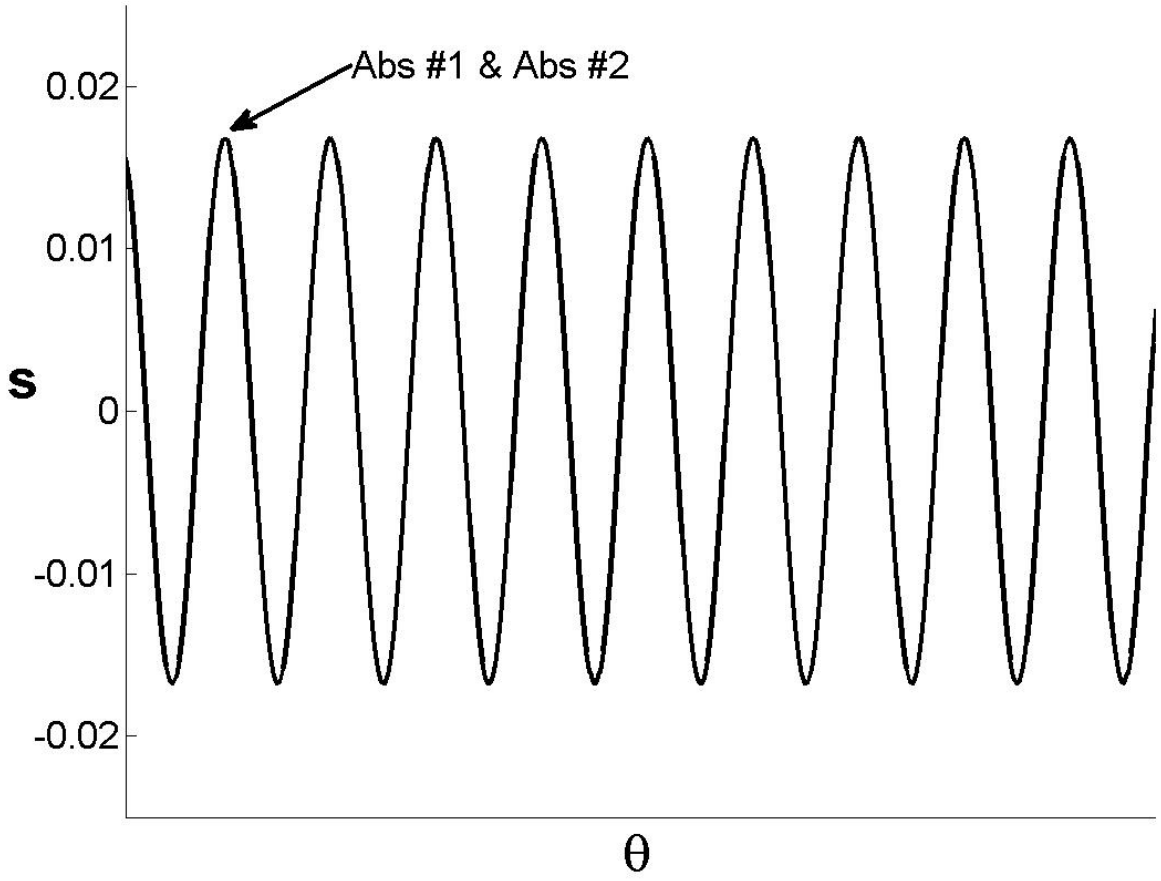

Figure 3.1: Time traces for two absorbers at order two without gravity.

gravity, (Figure 3.1), shows that absorbers have the same amplitude and are synchronous. The time trace that includes gravity, (Figure 3.2), shows that the two absorbers have the same response form but are phased differently. Using a fast Fourier transform (FFT) in MATLAB the amplitude and phases of the responses can be found. When this is done the

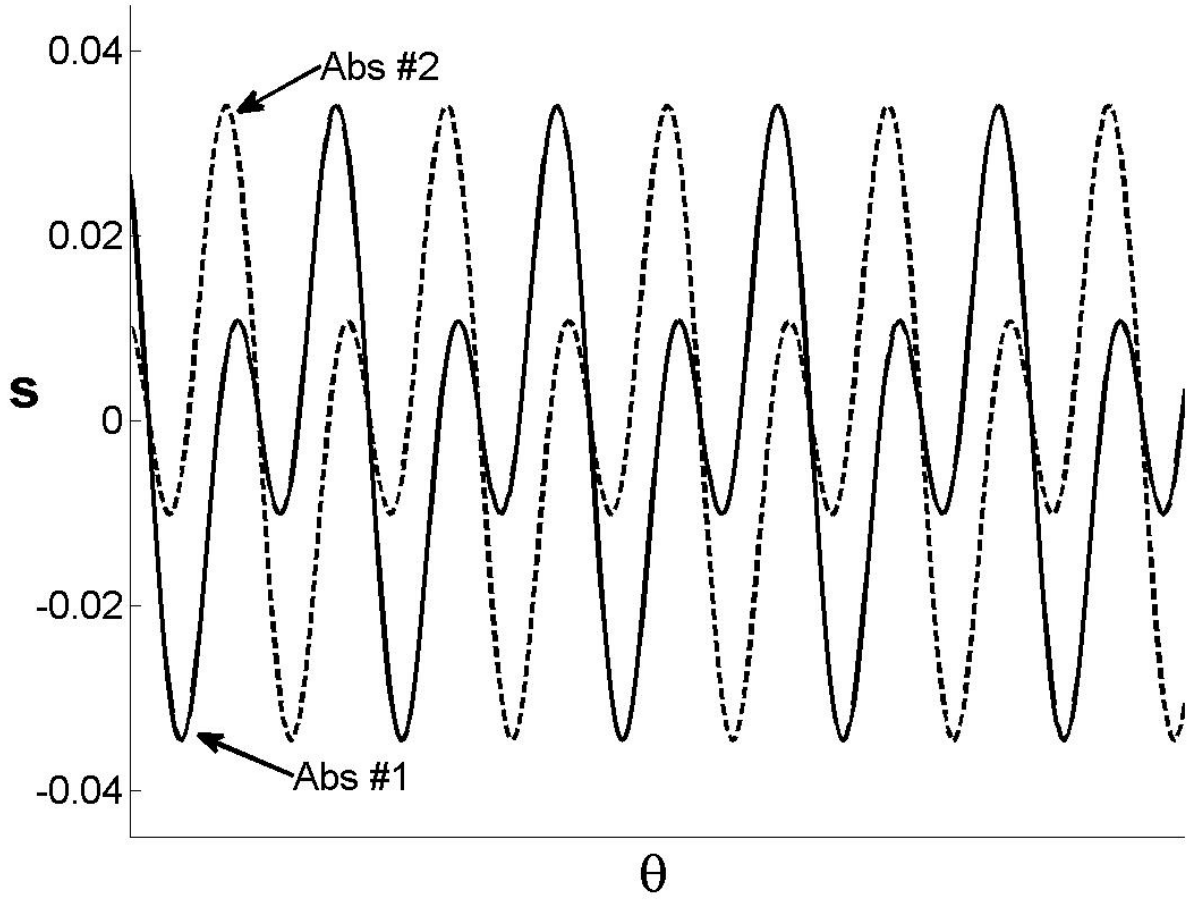

Figure 3.2: Time traces for two absorber at order 2 with gravity.

amplitudes of the responses at order one and order two are the same. The phase difference of the order two part of the response is zero. The phase difference of the order one part is π. When equation (2.57) is examined it can be seen that the order one part of the forcing $(\tilde{\gamma}\sin(\theta_j))$ is dependent on the position of the absorber. This introduces a phase difference between the order one responses of the two absorbers.

The number of absorbers and the order forcing has an impact on the different kinds of response that can be seen. Similar to the case of two absorbers, when the forcing order does

not equal two the response will have an order one and order n term. The order one response will have a phase difference that will be the same as the difference in the positions of the absorbers around the rotor, ψ_j. However, the case when the forcing order is two does not follow this. Figure 3.3 shows this case with four absorbers. A FFT is used to break down each response into its components. In this case the order one is the same as the other cases. However, in this case the phase differences between the order n responses is not equal to zero. This is due to the superharmonic response of the absorbers to gravitational forcing. This will be addressed more in future sections.

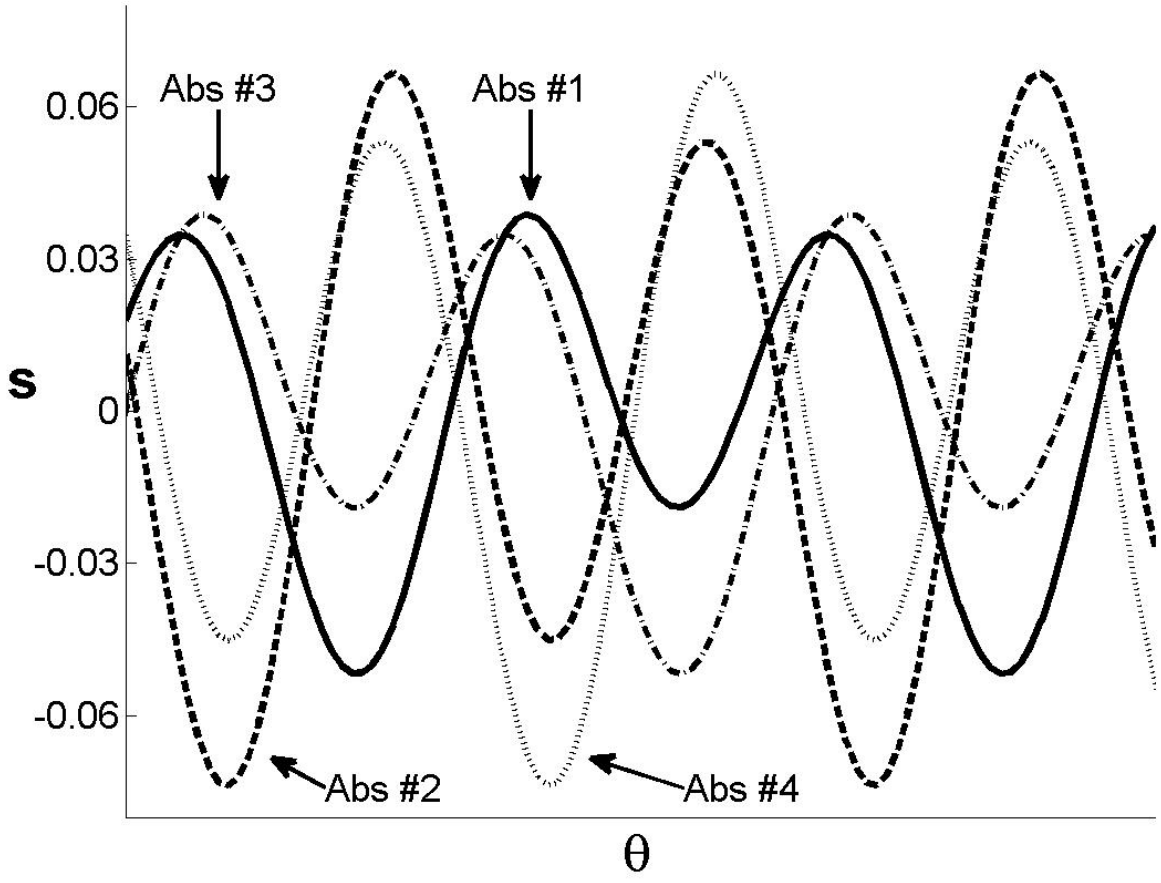

Figure 3.3: Time traces for four absorber at order two with gravity.

3.3 Steady-State Analysis

It is ideal to look at the steady-state of the system. In the absence of gravity unison motions have typically been sought by setting the absorber amplitudes and phases equal for all absorbers. This assumes that each absorber will have the same amplitude and phase, which has already been shown to not always be the case when gravity is present. This has an effect on the analysis but can easily be accounted for in the analysis of the slow flow equations. The chart in Figure 3.4 shows all of the special cases that were found, where S means that each absorber response is the same, V means that a quantity in the response varies, and D means that they are different with the number meaning the number of different amplitudes or phases. Each of the special cases of slow flow equations, that contain information about order n response, will now be analyzed.

Order 1 Response						
n / N	≠1,2,3		2		3	
	Amp	Phase	Amp	Phase	Amp	Phase
2	S	2 D	S	2 D	S	2 D
3	S	3 D	S	3 D	S	3 D
4	S	4 D	S	4 D	S	4 D

Order n Response						
n / N	≠1,2,3		2		3	
	Amp	Phase	Amp	Phase	Amp	Phase
2	S	S	S	S	S	S
3	S	S	3 D	V	S	S
4	S	S	2 D	V	S	S

Figure 3.4: Description of different cases and the responses that occur.

3.3.1 Case 1: $n \neq 1, 2, 3$

The steady-state condition corresponds to $a_j' = 0$ and $\alpha_j' = 0$. Applying this to equation (3.11) and setting $a_j = a$ and $\alpha_j = \alpha$ for a unison response at order n and gives the following:

$$\begin{aligned} \textbf{RE}: \quad & na[\sigma + \frac{1}{2} - \frac{3\kappa_0\tilde{\gamma}^2}{2n(1-n^2)^2}] - \frac{3}{4n}\kappa_0 a^3 \\ & - \frac{\tilde{\Gamma}\theta}{2n}\sin(\alpha - \tau) = 0 \\ \textbf{IM}: \quad & \frac{\tilde{\mu}a}{2}a - \frac{\tilde{\Gamma}\theta}{2n}\cos(\alpha - \tau) = 0 \end{aligned} \tag{3.16}$$

These equations can be combined into one equation:

$$(\frac{\tilde{\mu}a}{2}a)^2 + (n(\sigma + \frac{1}{2} - \frac{3}{2}\frac{\kappa_0\tilde{\gamma}^2}{n^2(1-n^2)^2})a - \frac{3}{4n}\kappa_0 a^3)^2 = (\frac{\tilde{\Gamma}\theta}{2n})^2 \tag{3.17}$$

It has been shown by Newland [15] that a certain amount of overtuning of the absorber is ideal in order to avoid the dangerous jump that can occur. This jump is harmful because the absorbers become amplifiers, and instead of reducing the vibration they will increase it. The desirable operating range of the absorber system precedes this jump. Equation (3.17) has a term that will be looked at more in depth and can be considered as an equivalent detuning:

$$\sigma_e = \sigma + \frac{1}{2} - \frac{3}{2}\frac{\kappa_0\tilde{\gamma}^2}{n^2(1-n^2)^2} \tag{3.18}$$

The gravity term is part of this equivalent detuning. It is desirable to have an equivalent over tuning that is positive and greater than $\frac{1}{2}$. It is known that σ will be positive for an over-tuned absorber. Thus the gravity factor is actually bringing the absorbers toward exact tuning and undertuning. As an engine slows down the effects of gravity will increase because

γ will increase. This can be seen in Figure 3.5.

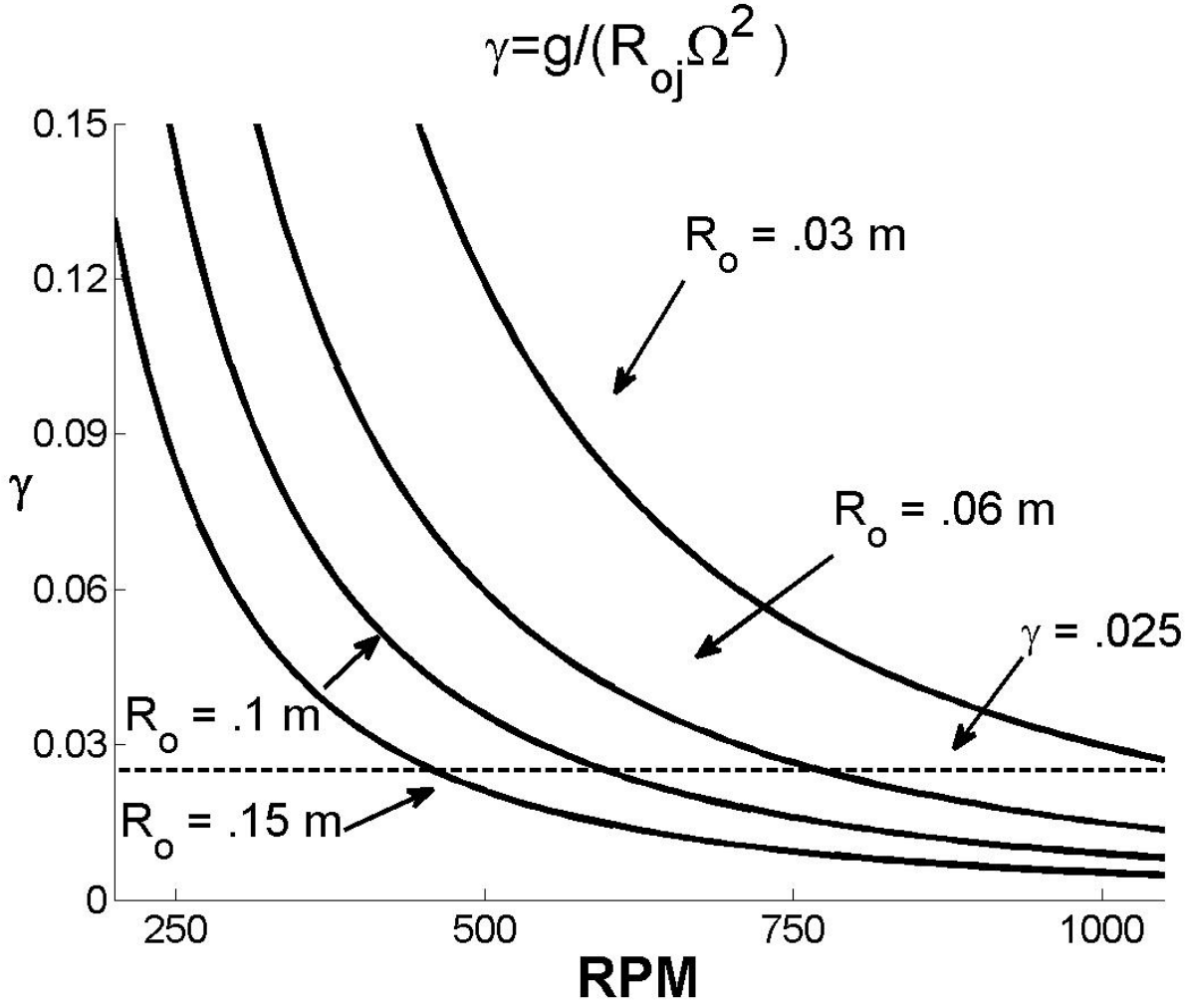

Figure 3.5: Change in γ with respect to RPM for various distance from the center of the rotor (R_{oj}) to the absorber point mass.

Since γ increases as the engine slows down the equivalent detuning will decrease. This can be beneficial but also dangerous. Absorbers will preform best when tuned exactly to the forcing order, i.e. $\sigma = 0$. However, when absorbers are perfectly tuned they are more susceptible to the nonlinear jump. As the engine speed decreases, Γ_θ will increase according to equation (2.41). There will be more alternating torque that needs to be corrected as

the engine slows down, but the absorbers' equivalent detuning tends towards the equivalent detuning of a perfectly tuned absorber allowing the system to absorb more of this alternating torque. Since the absorbers are tending towards the equivalent detuning of a perfectly tuned absorber, the predicted nonlinear jump will occur earlier than if gravity is left out of the analysis.

Equation (3.17) can be solved for $\tilde{\Gamma}_\theta(\tilde{\gamma}, \tilde{\mu a}, \sigma, \kappa_0, n)$ to give

$$\tilde{\Gamma}_\theta = 2n\sqrt{(\frac{\tilde{\mu}a}{2}a)^2 + (n^2(\sigma + \frac{1}{2} - \frac{3}{2}\frac{\kappa_0\tilde{\gamma}^2}{n(1-n^2)^2})a - \frac{3}{4n}\kappa_0 a^3)^2} \tag{3.19}$$

Now $\tilde{\Gamma}_\theta$ versus $|s|$ can be plotted. In the plots that follow the magnitude of the response is broken into harmonic components instead pf the total response which is a combination of the harmonics that includes their phasing. a is only the amplitude of the order n response. Equations (3.6) and (3.7) show that there is an order 1 as well as an order n response. The order one component is dependent only on the order of the absorbers and gravity. Thus it is a constant over all Γ_θ. This is shown in Figure 3.6. Now the effect of varying γ will be examined. Since the order one part is linearly based on γ it is uninteresting. However, γ has an effect on the order n part. For this only the order n curve will be examined, as shown in Figure 3.7. It can be seen that as γ increases the amplitude starts to increase more dramatically and the jump occurs early. It has been shown that a similar effect can be achieved by decreasing the tuning of the absorbers [1, 13]. This makes sense considering the equivalent detuning of equation (3.18) that was talked about earlier. It should be noted that the effect of gravity is very small for γ less than about 0.025, this will be shown to be true later in Section 3.4. This shows that the assumption used in previous models, that the

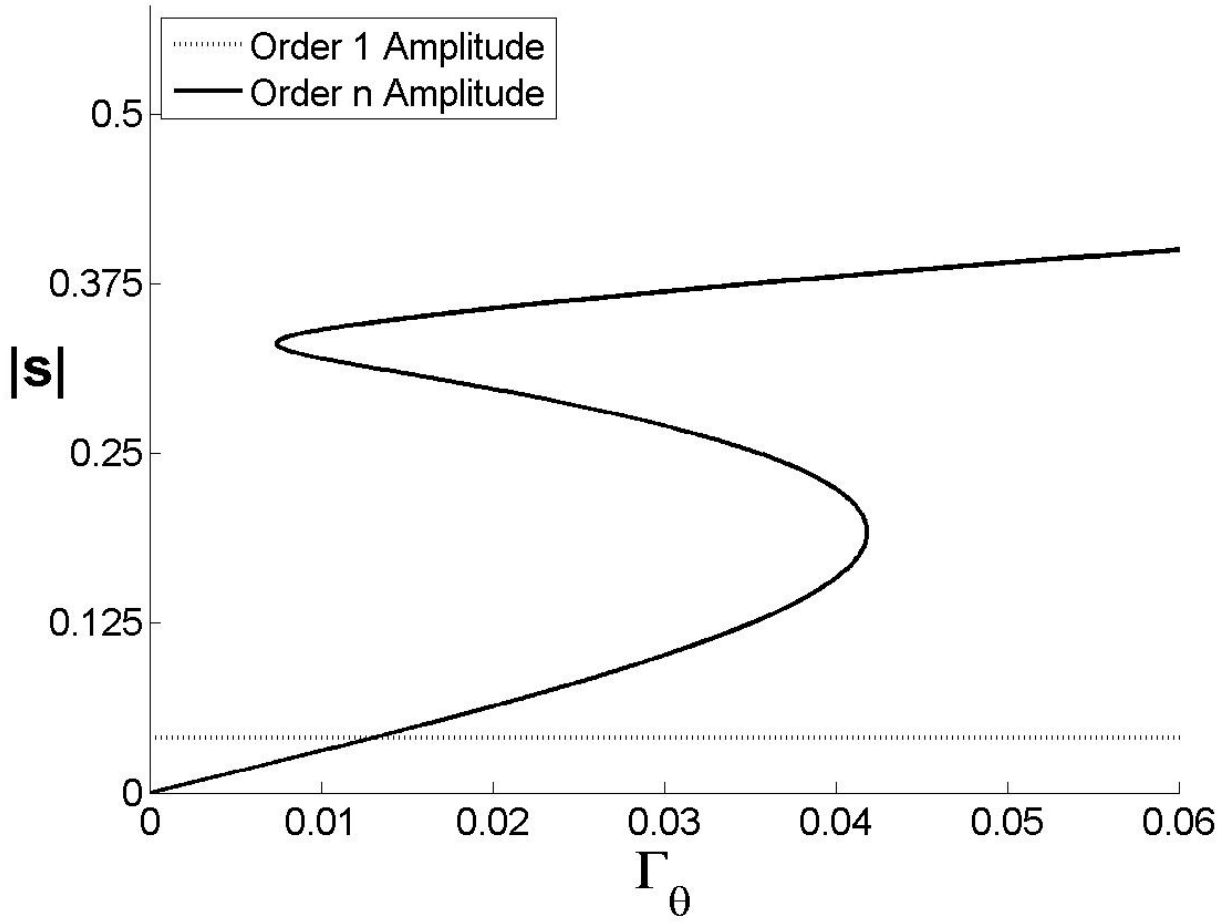

Figure 3.6: Analytical amplitudes of the harmonics of the non-dimensional absorber amplitude versus non-dimensional fluctuating torque, $\sigma = 0$.

effect of gravity was negligible, is true at least under certain parameter conditions. It can be seen in Figures A.1, A.2, A.3 and A.4, located in Appendix 4.2, that even as the value of ϵ (based on mass ratio) changes this assumption still holds true.

An important part of absorber design and analysis is the possibility that the absorber will hit the cusp. This has been addressed by Denman [5] but needs to be considered in the case of gravity. The cusp will tell us what the maximum value of the absorber path can be. When gravity is included, the absorber response can be thought of as having two parts: an

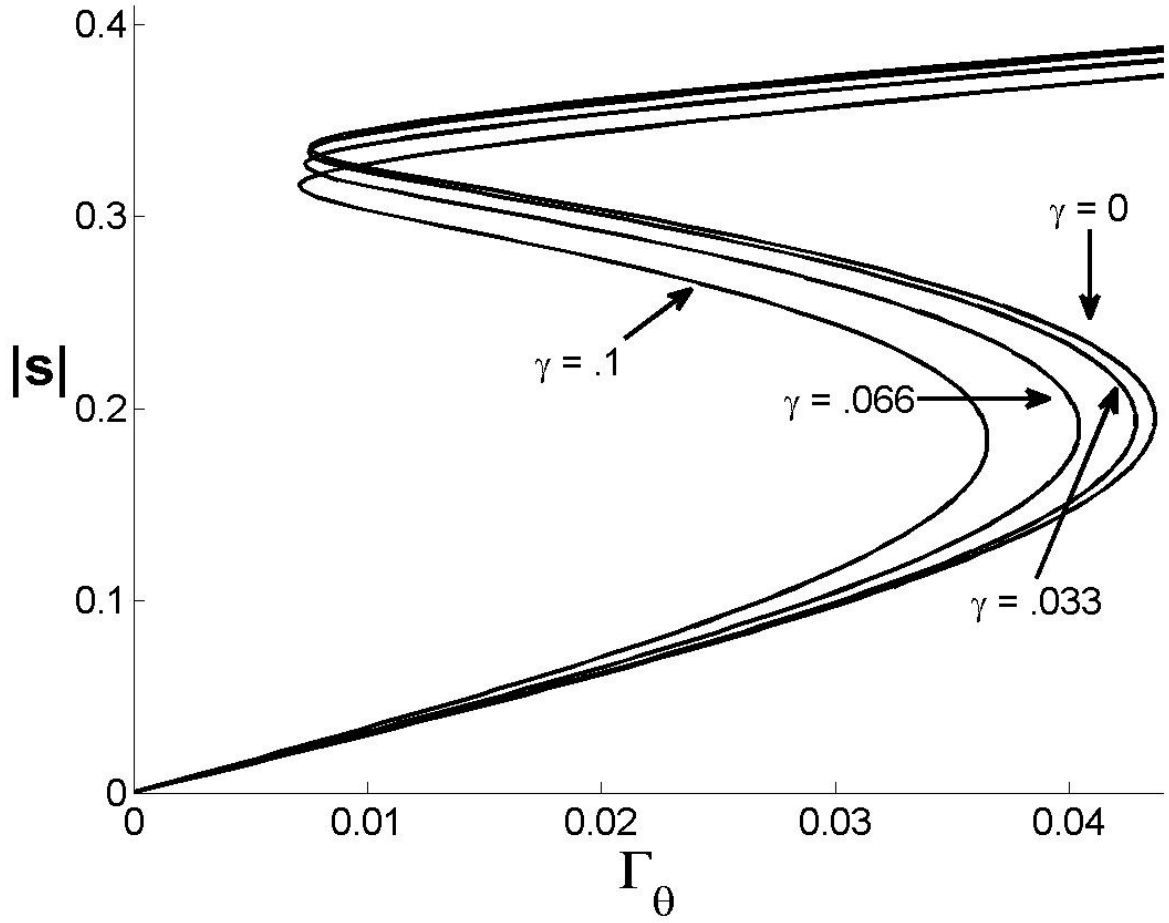

Figure 3.7: Analytical amplitudes of the harmonics of the non-dimensional absorber amplitude versus non-dimensional fluctuating torque for varying γ, $\sigma = 0$.

order one part and an order-n part. The phasing between these two parts, as well as what order-n actually is, plays a role in what the maximum absorber response can be. However, an upper bound on the absolute maximum absorber displacement could be obtained by a simple addition of the order one and order n magnitudes.

Now that the analytical model has been shown, it is ideal to compare the analytical model to numerical simulations to verify the findings. This was done using the software Mathematica. For the numerical simulations the full non-dimensional equations of motion

before scaling were used, Equations (2.35) and (2.36). This means that the full path equations stated in Table 2.2, 2.3 and 2.4 were used, not their truncated Taylor series expansions. Once the simulations were completed the responses needed to be analyzed. As was discussed in section 3.2, the response of each absorber contained components at different orders. These were primarily be at order one, due to gravity, and order n, due to the engine forcing. The amplitudes of these components were found using an FFT.

Figure 3.8 shows amplitudes of the harmonics of absorber responses of the analytical model versus numerical simulations for the case of a three cylinder engine. Thus $n = 1.5$. The other parameters used were $\mu_a = 0.014921$, $\epsilon = 0.022276$ and $\gamma = 0.05$. Since this analysis is for circular path absorbers $\lambda = 0$. Using equation (2.47) and (2.48) it can be found that $\kappa_0 = .2956$. κ_0 is dependent on the tuning of the absorbers ($\tilde{n}$), the type of path (λ) and the inertia ratio (ϵ). κ_0 will not be solved for each case that is examined but the information has been provided so that it can be determined in for each case tested. The responses of both absorbers are the same in amplitude. As was talked about earlier, the relative phases between the two can be different depending on the order. Looking at the order one component of the response, there are two lines based on the numerical simulations. One of these lines aligns with order one analytical model, while the other does not. The results that do not align well (the upper set of stars in the figure) correspond to when the absorbers have jumped. For the order n component of the response, the simulation matches the analytical model for the lower branch (LB). The results for the upper branch (UB) are not as accurate but this was expected. As was found by Nester [13] the jump occurred earlier in numerical simulations than predicted by the analytical model.

The overall goal of CPVAs is to reduce the rotor oscillation that is seen in the crankshaft

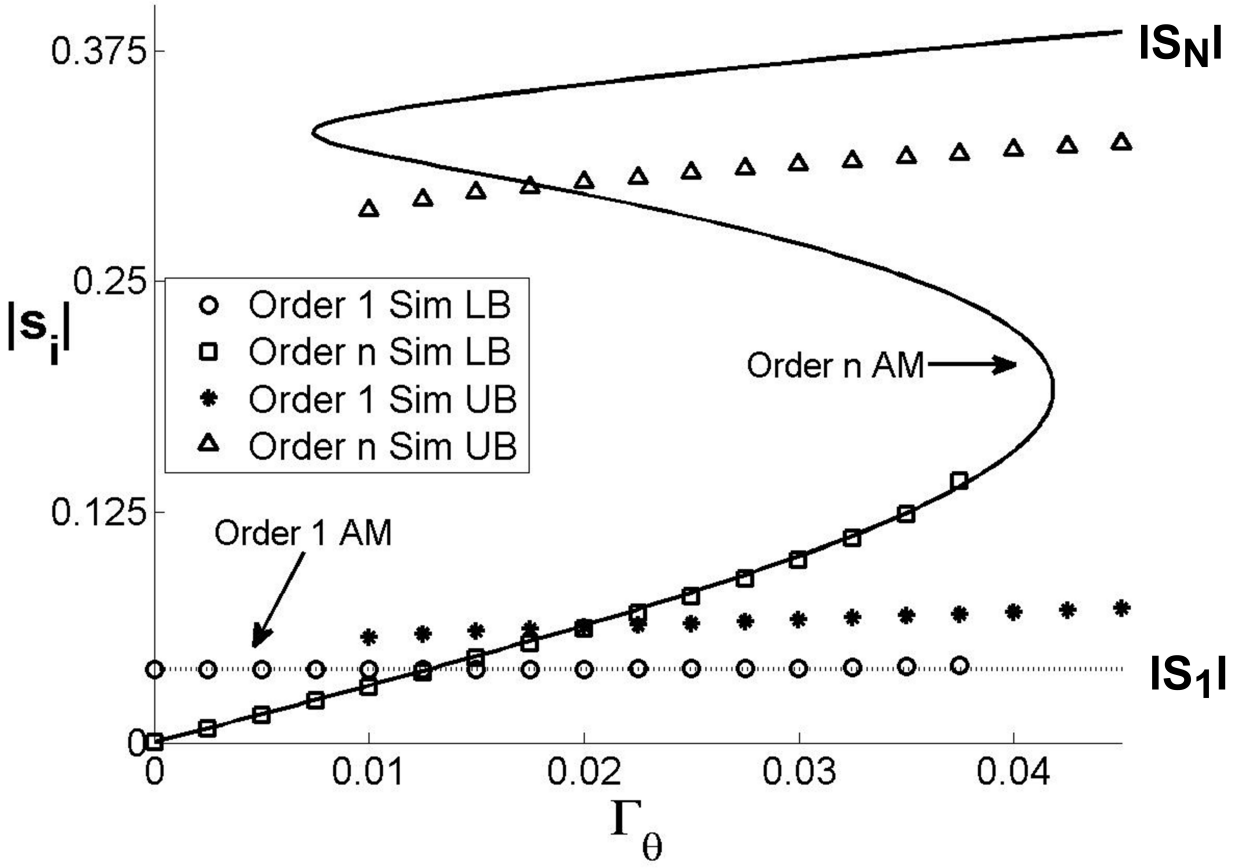

Figure 3.8: Analytical amplitudes of the harmonics of the non-dimensional absorber amplitude versus non-dimensional fluctuating torque comparison of numerical simulations to analytical model (AM), $\sigma = 0$.

and in other components. The non-dimensional rotor acceleration, $\nu\nu'$, will give insight into how CPVAs perform compared to an engine without absorbers. The non-dimensional rotor acceleration can also be looked at by rewriting equation (2.54) as

$$\nu\nu' = \epsilon(\tilde{\Gamma}_\theta \sin(n\theta + \tau) + \frac{1}{N}\sum_{j=1}^{N}(-\tilde{\gamma}\sin(\theta_j) + n^2 p_j)) \tag{3.20}$$

where the assumed solution for p_j is

$$p_j = a_j \cos(n\theta + \alpha_j) + \frac{\tilde{\gamma}}{(-1+n^2)} \sin(\theta + \psi_j) \tag{3.21}$$

As long as the assumption that more than one absorber is used, then the gravity term will cancel at the leading order out according to Appendix 4.2 and hence the rotor response has no order-1 contribution. Additionally, trigonometric identities are used to simplify the equation leading to

$$\begin{aligned} \nu\nu' = \epsilon[(\tilde{\Gamma}_\theta \cos(\tau) - \frac{1}{N}\sum_{j=1}^{N}(n^2 a_j \sin(\alpha_j)))\sin(n\theta) + (\tilde{\Gamma}_\theta \sin(\tau) \\ + \frac{1}{N}\sum_{j=1}^{N}(n^2 a_j \cos(\alpha_j)))\cos(n\theta)] \end{aligned} \tag{3.22}$$

Now it is important to note that Γ_θ is shown as a function of p_j and other parameters in equation (3.19). For this analysis $\tau = 0$ will be used. However some analysis has been done on what affect τ has in Section 3.5. It is convenient to plot $|\nu\nu'|$ vs $\tilde{\Gamma}_\theta$, as in Figures 3.9 and 3.10.

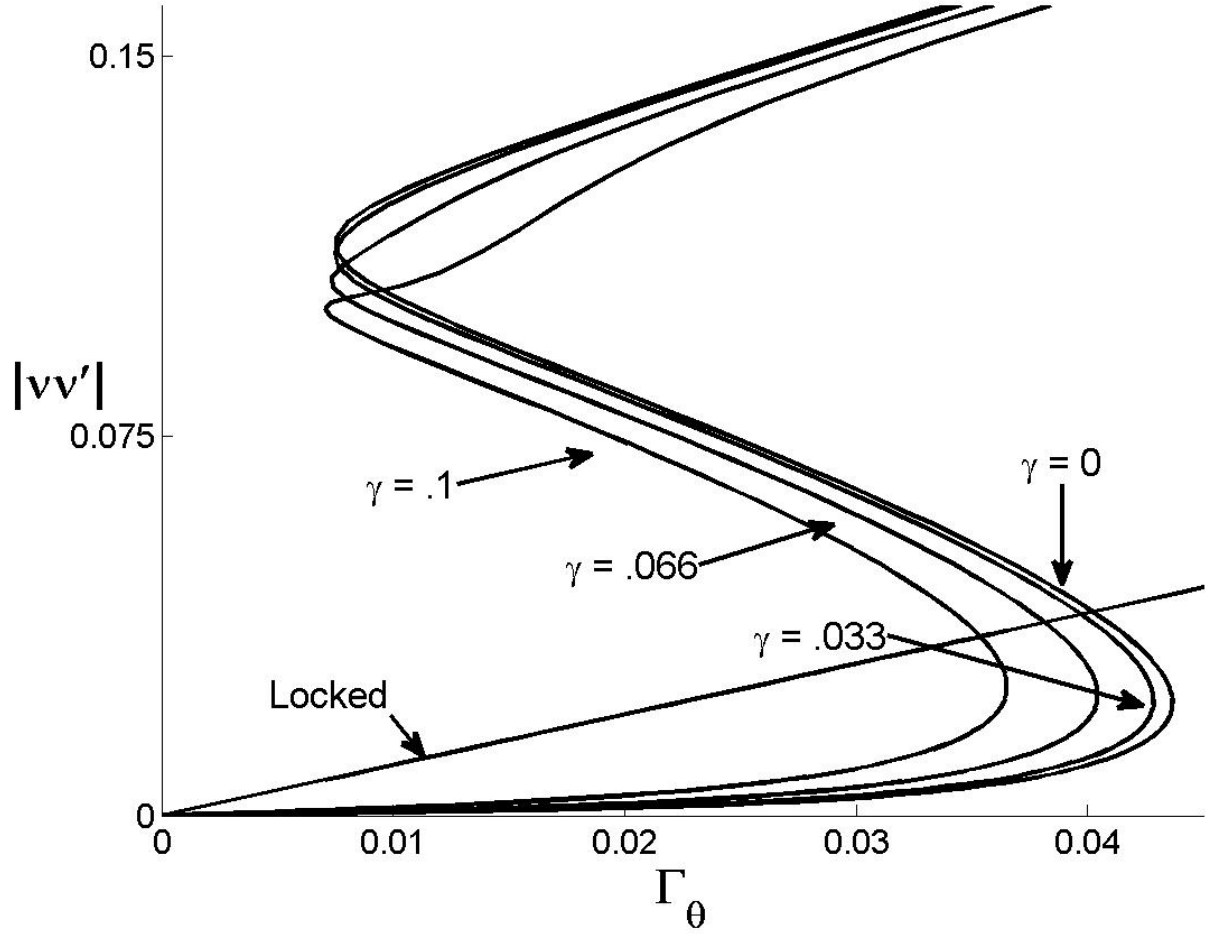

Figure 3.9: Non-dimensional rotor acceleration versus non-dimensional fluctuating torque for various values of γ, with 0% detuning

It can be seen in Figure 3.9 and Figure 3.10 that when gravity is included in the model with perfectly tuned absorbers the non-dimensional rotor acceleration increases as γ increases.

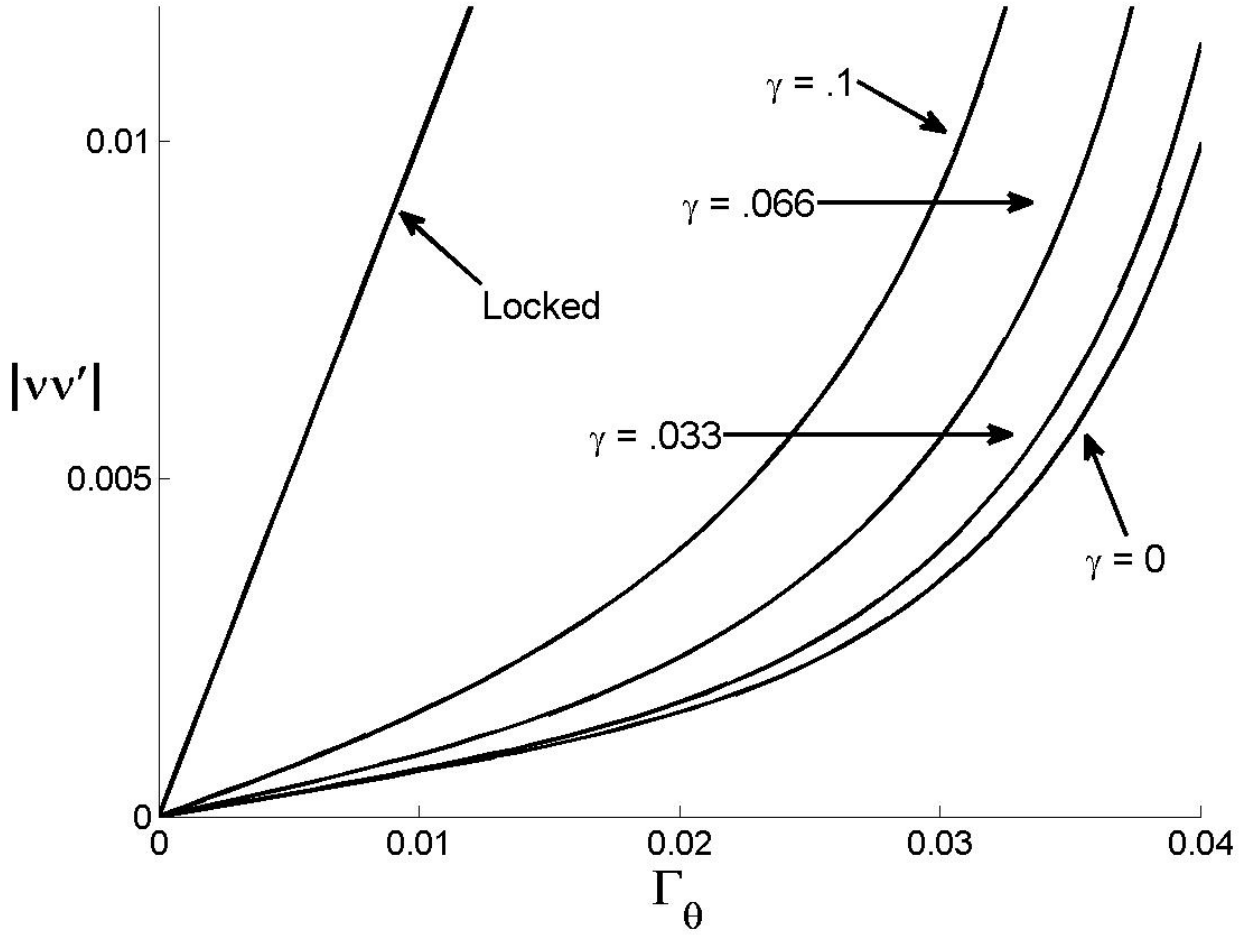

Figure 3.10: Non-dimensional rotor acceleration versus non-dimensional fluctuating torque for various values of γ, with 0% detuning, in the desirable operating region.

An interesting thing happens when the absorbers are over-tuned and $\tilde{\gamma}$ is varied. As γ is increased there is an improvement of the non-dimensional rotor acceleration in the desirable operating range. However, the jump occurs at a lower Γ_θ and this needs to be accounted for in design. This effect can be seen in Figure 3.11 and more easily in the magnified figure of the desirable operating range, Figure 3.12.

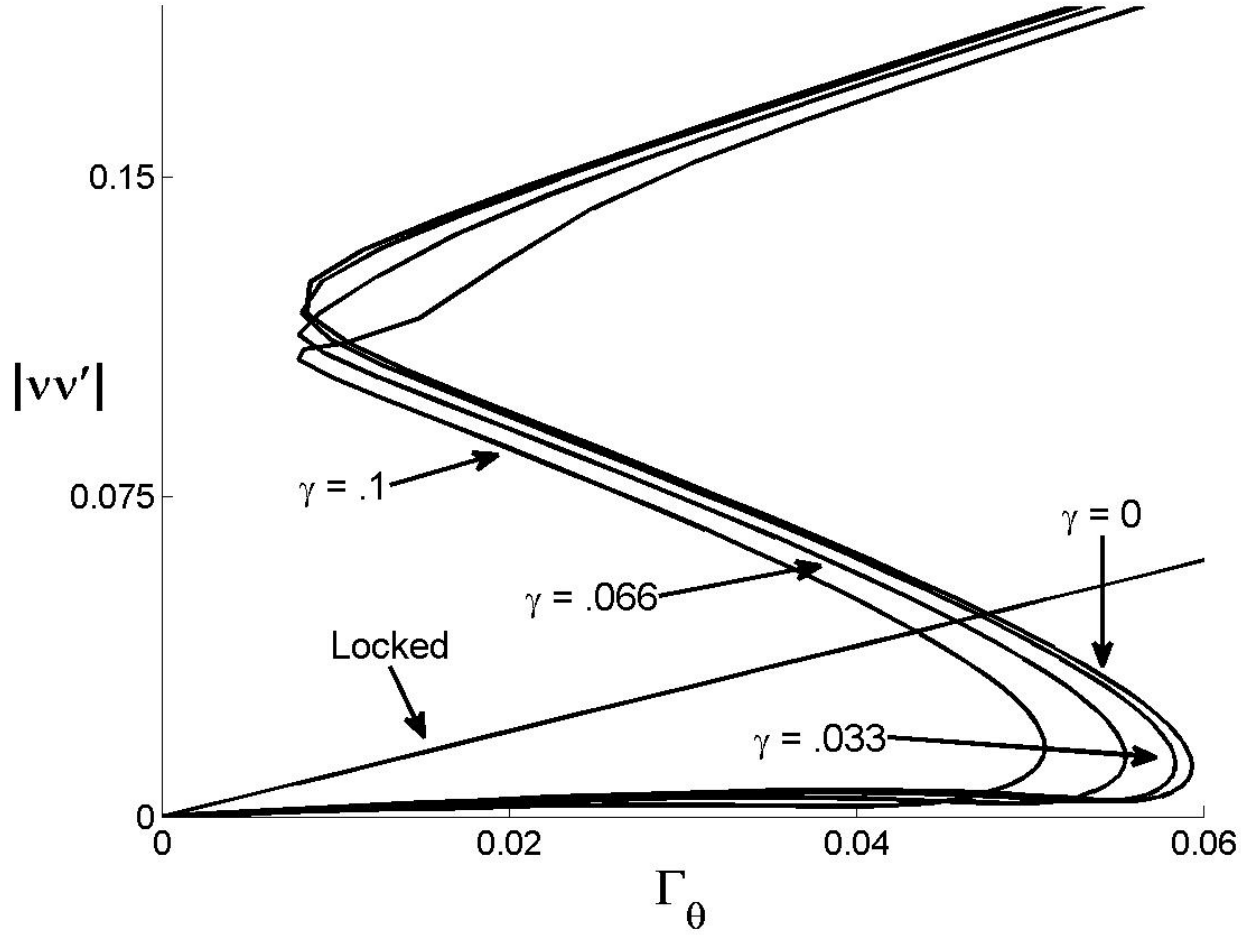

Figure 3.11: Non-dimensional rotor acceleration versus non-dimensional fluctuating torque for various values of γ, with 2% detuning.

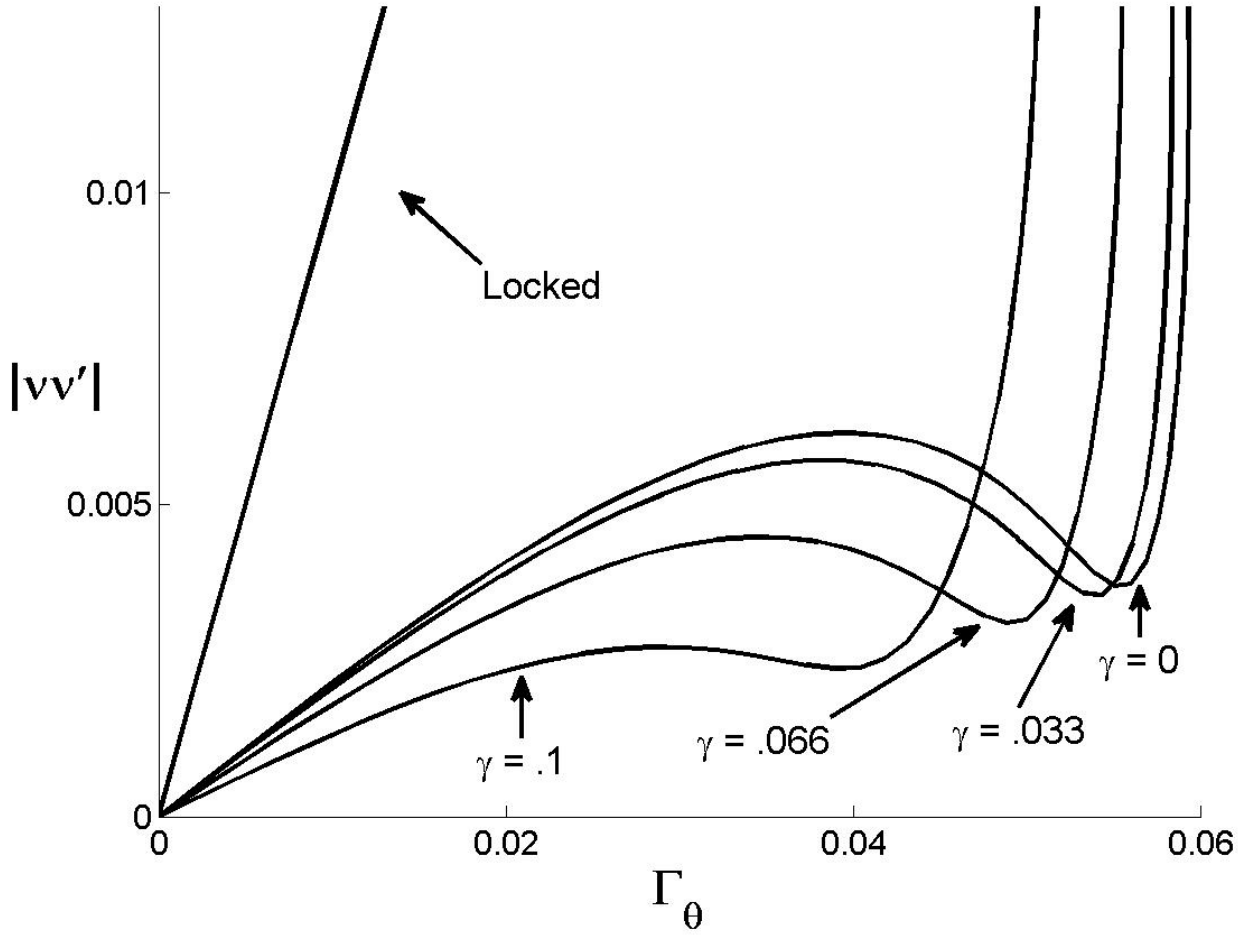

Figure 3.12: Non-dimensional rotor acceleration versus non-dimensional fluctuating torque for various values of γ, with 2% detuning, in the desirable operating region.

As was mentioned before the best performance is at $\sigma = 0$, or $\sigma_\epsilon = \frac{1}{2}$. Therefore from equation (3.18) there is a critical value of γ when the γ term balances with the intentional detuning of the absorbers. From equation (3.18) and (2.48) it is found that

$$\gamma_{\text{crit}} = \epsilon^{\frac{1}{2}} \sqrt{\frac{2\sigma n^2 (1-n^2)^2}{3\kappa_0}}. \tag{3.23}$$

In Figure 3.13 it can be seen that γ_{crit} is usually quite large even for small detuning. However, referring back to Figure 3.5 it is seen that γ can grow rapidly over a small decrease in RPM. Thus a small change in engine speed can change a well designed absorber from equivalently over-tuned to equivalent under-tuned as equation (3.18) states. The cases where γ_{crit} is small would involve low forcing orders. An example of a practical application that would fall into to this area would be a slightly detuned absorber for a three cylinder engine. However, γ_{crit} is also dependent on ϵ, as ϵ increases so will γ_{crit}, the inverse also being true.

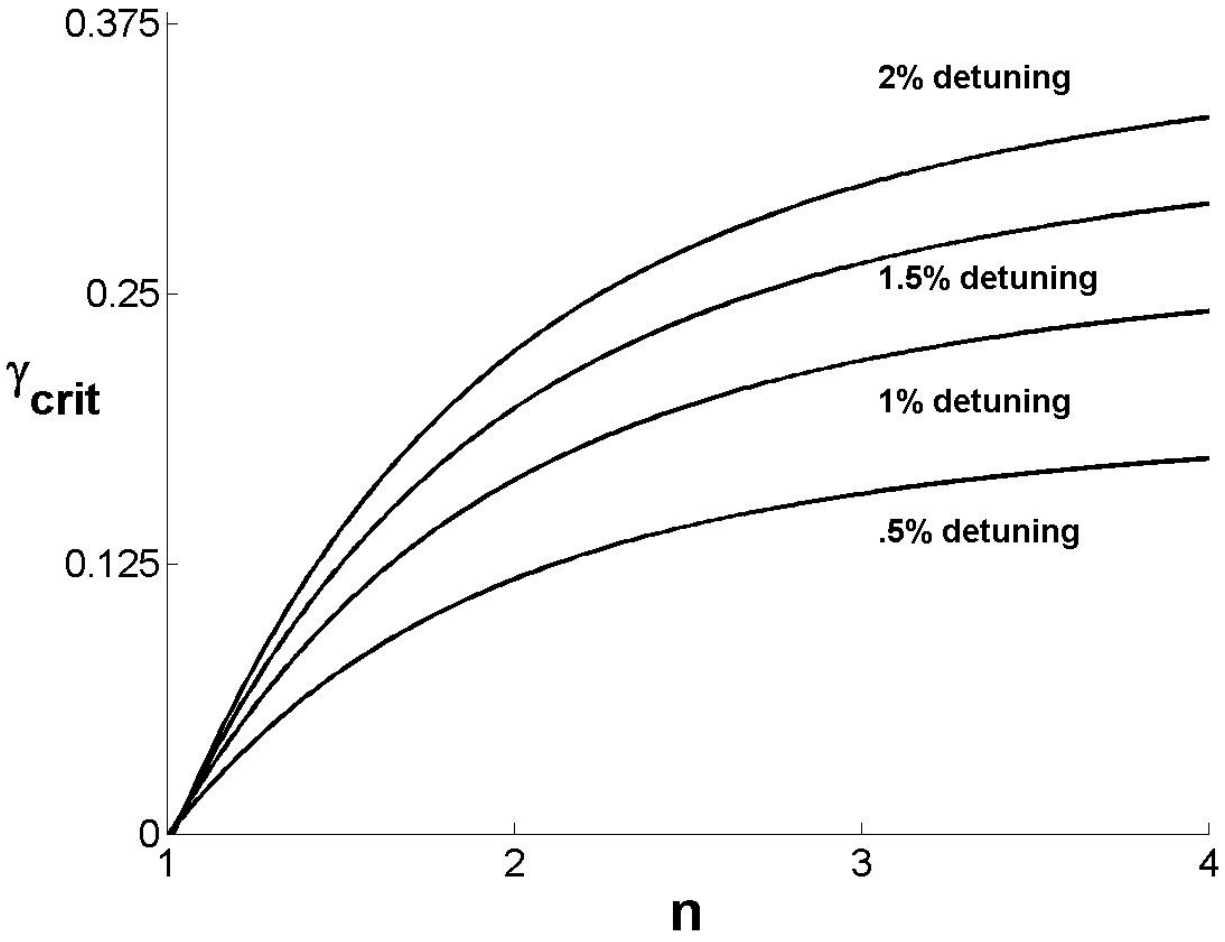

Figure 3.13: γ_{crit} versus forcing order, $\epsilon = .022276$.

The analytical model can be validated using numerical simulations. Figure 3.9 and 3.11 show that a jump occurs. The portion were the jump has occurred has been omitted during the numerical comparison. Additionally, referring back to equation (3.22), the gravity portion that would be at order one has canceled out. The parameters are the same as was used in Figure 3.8 but in this case we have tested with 0% and 2% detuning.

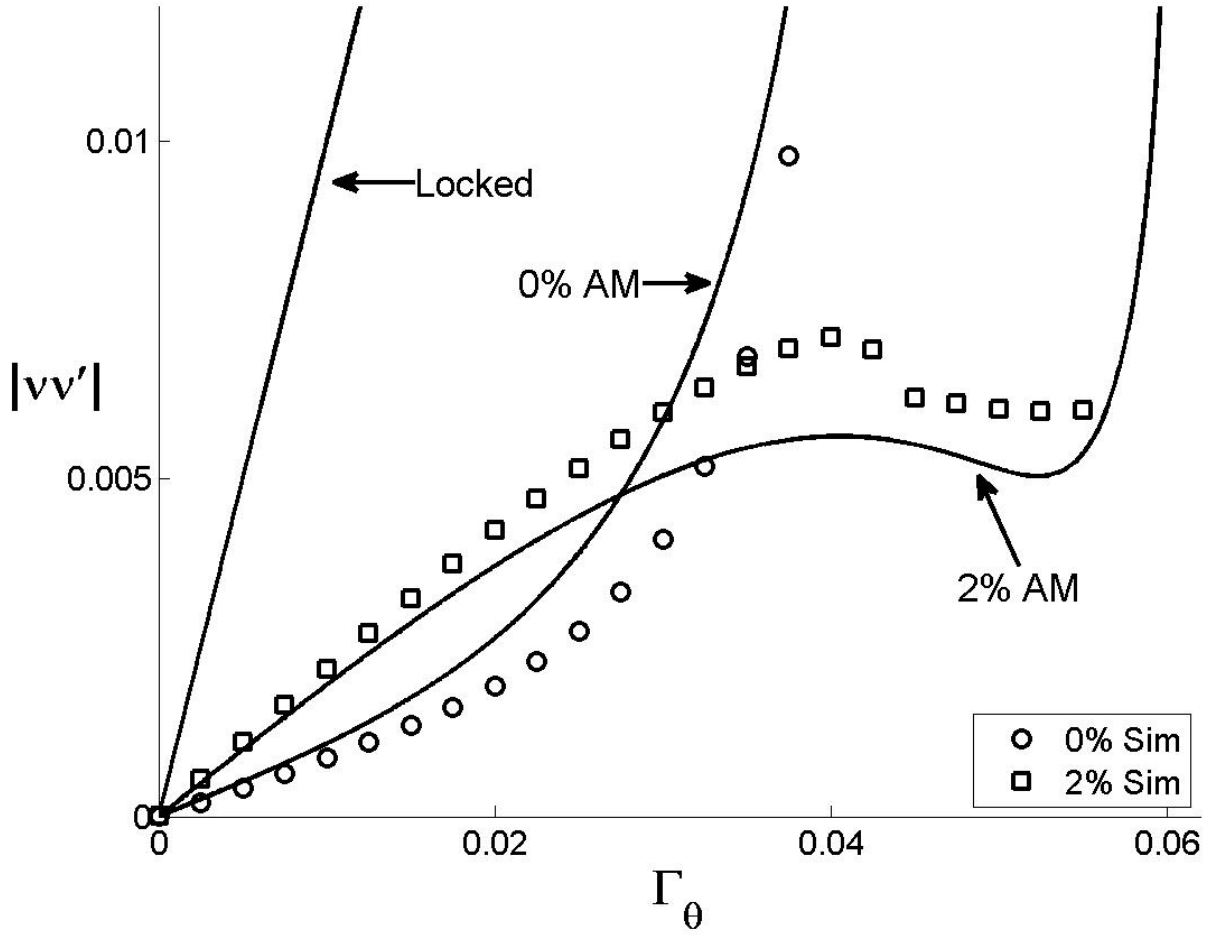

Figure 3.14: Non-dimensional rotor acceleration versus non-dimensional fluctuating torque at order 1.5 , analytical model vs numerical simulations, $\gamma = .066$.

Figure 3.14 shows that the simulations follow the analytical model. There is an improve-

ment in the rotor acceleration cause by the restoring force of the absorbers that is verified by the simulations. As was expected by the analytical model, over tuning the absorber increases the fluctuating torque that the system can handle before the jump occurs. This, however, does not come without drawbacks. The low end performance is sacrificed as was confirmed by the simulations. The effect gravity has on absorbers in the general case is the same as detuning. Thus when designing absorbers, the equivalent detuning, Equation (3.23), needs to be considered and can be broken into the following cases.

- If $\sigma_e = \frac{1}{2} \rightarrow$ Perfectly Tuned
  - Optimal correction in rotor acceleration
- If $\sigma_e > \frac{1}{2} \rightarrow$ over-tuned
  - Less correction in rotor acceleration in some regions.
  - Increased operating fluctuating torque range.
- If $\sigma_e < \frac{1}{2} \rightarrow$ under-tuned
  - Less correction in rotor acceleration.
  - Reduced operating fluctuating torque range.

3.3.2 Case 2: $n = 2$

For this case equation (3.13) will be used to evaluate the steady-state conditions. In this case it is very difficult to combine the amplitude and phase equations and solve for $\tilde{\Gamma}_\theta$. Instead mathematical software will be needed to solve the equations numerically and obtain the desired information. For the results shown, Mathematica was used. The equations were

simplified for their assumed steady-state and then a root solver was used to find amplitudes, phases and forcing. This case needs to be broken down even further because equation (3.13) is dependent on ψ_j which depends on the number absorbers that are being used. The cases of 2, 3 and 4 absorbers will be examined here.

3.3.2.1 2 Absorbers

When there are two absorber there are two sets of equations that define the steady state response:

$$\begin{aligned}
\textbf{RE}: \quad & na_1\sigma + \frac{n}{4}a_1 + \frac{n}{4}a_2\cos(\alpha_2-\alpha_1) - \frac{3}{4n}\kappa_0 a_1^3 \\
& - \frac{3}{2}\frac{\kappa_0 a_1\tilde{\gamma}^2}{n(1-n^2)^2} - \frac{\tilde{\Gamma}_\theta}{2n}\sin(\alpha_1-\tau) - \frac{(1+n^2)\tilde{\gamma}^2}{4n(1-n^2)}\sin(-\alpha_1) = 0 \\
\textbf{IM}: \quad & \frac{n}{4}a_2\sin(\alpha_2-\alpha_1) + \frac{\tilde{\mu}a}{2}a_1 - \frac{\tilde{\Gamma}_\theta}{2n}\cos(\alpha_1-\tau) \\
& + \frac{(1+n^2)\tilde{\gamma}^2}{4n(1-n^2)}\cos(-\alpha_1) = 0
\end{aligned} \tag{3.24}$$

and

$$\begin{aligned}
\textbf{RE}: \quad & na_2\sigma + \frac{n}{4}a_2 + \frac{n}{4}a_1\cos(\alpha_1-\alpha_2) - \frac{3}{4n}\kappa_0 a_2^3 \\
& - \frac{3}{2}\frac{\kappa_0 a_2\tilde{\gamma}^2}{n(1-n^2)^2} - \frac{\tilde{\Gamma}_\theta}{2n}\sin(\alpha_2-\tau) - \frac{(1+n^2)\tilde{\gamma}^2}{4n(1-n^2)}\sin(2\pi-\alpha_2) = 0 \\
\textbf{IM}: \quad & \frac{n}{4}a_1\sin(\alpha_1-\alpha_2) + \frac{\tilde{\mu}a}{2}a_2 - \frac{\tilde{\Gamma}_\theta}{2n}\cos(\alpha_2-\tau) \\
& + \frac{(1+n^2)\tilde{\gamma}^2}{4n(1-n^2)}\cos(2\pi-\alpha_2) = 0
\end{aligned} \tag{3.25}$$

Now assuming that $a_1 = a_2$ and $\alpha_1 = \alpha_2$ the two sets of equations can be reduced to one:

$$\begin{aligned}
\textbf{RE}: \quad & na\sigma + \frac{n}{2}a - \frac{3}{4n}\kappa_0 a^3 - \frac{3}{2}\frac{\kappa_0 a\tilde{\gamma}^2}{n(1-n^2)^2} \\
& - \frac{\tilde{\Gamma}_\theta}{2n}\sin(\alpha_1 - \tau) - \frac{(1+n^2)\tilde{\gamma}^2}{4n(1-n^2)}\sin(-\alpha) = 0 \\
\textbf{IM}: \quad & \frac{\tilde{\mu}a}{2}a - \frac{\tilde{\Gamma}_\theta}{2n}\cos(\alpha_1 - \tau) + \frac{(1+n^2)\tilde{\gamma}^2}{4n(1-n^2)}\cos(-\alpha) = 0
\end{aligned} \tag{3.26}$$

As before the order 1 will be a straight line that increases linearly as γ increases. Since the order 1 response is linear it has been left out of the figures below. The response in Figure 3.15 is similar to that of the general case seen in Figure 3.7. The difference between the two can be seen clearly in Figure 3.16. There is a superharmonic resonance of the absorbers with respect to gravity. This is evident because when $\Gamma_\theta = 0$ a response of the absorber at order two occurs. The magnitude of this response is less than that of the magnitude of the order *one* response.

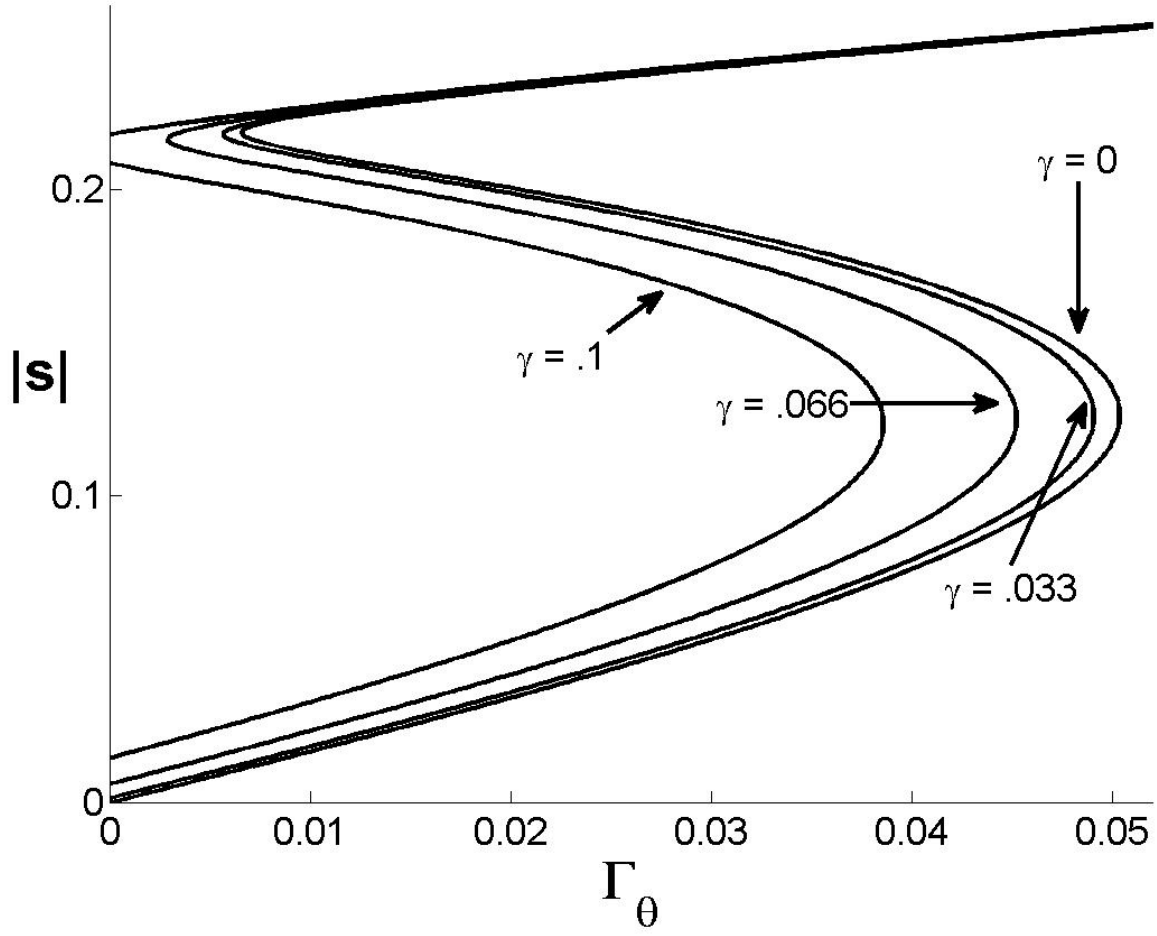

Figure 3.15: Order n harmonic of the non-dimensional absorber amplitude versus non-dimensional fluctuating torque at order $n = 2$, for two absorbers, with $\sigma = 0$, for various values of γ.

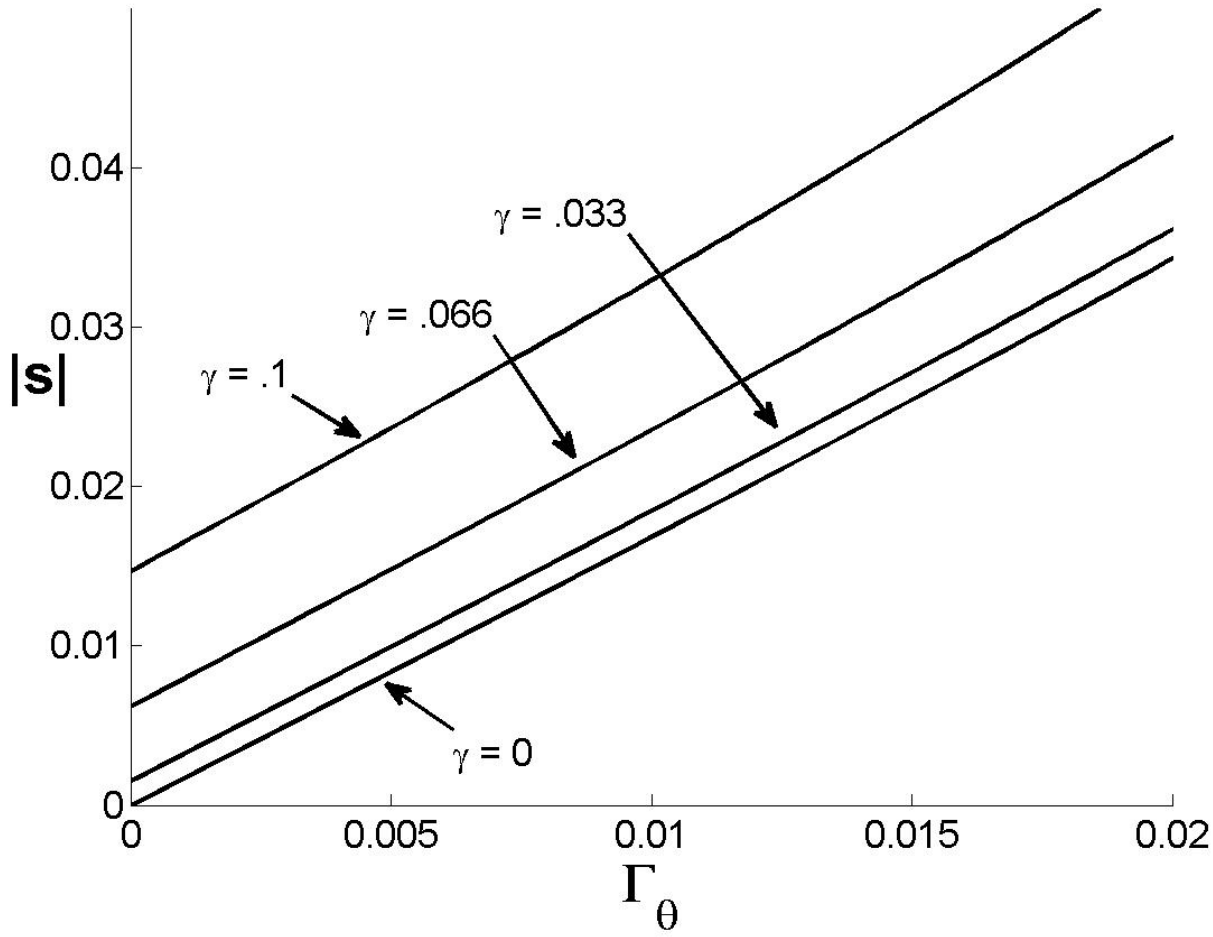

Figure 3.16: Order n harmonic of the non-dimensional absorber amplitude versus non-dimensional fluctuating torque near zero, at order $n = 2$, for two absorbers, with $\sigma = 0$, for various values of γ.

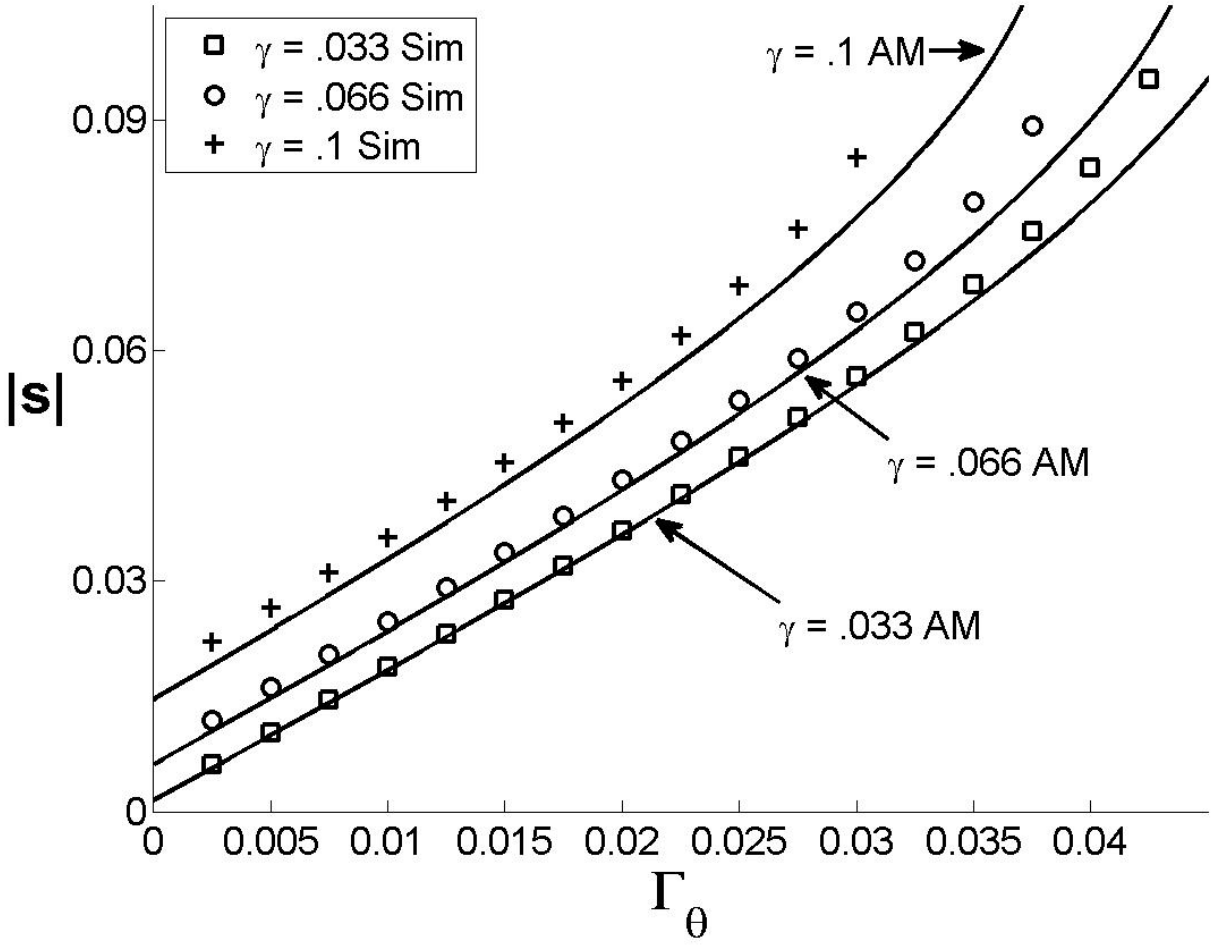

Figure 3.17: Order n harmonic of the non-dimensional absorber amplitude versus non-dimensional fluctuating torque near zero, at order $n = 2$, for two absorbers, comparison of simulations to analytical model.

Figure 3.17 shows numerical simulations of the full equations compared to the analytical model. In this figure the upper branch is not shown, although the steady-state solutions that correspond to the upper branch do exist. They are omitted for clarity. As was predicted by the analytical model, when the non-dimensional fluctuating torque is zero the absorbers show a response. In general the simulation matches the analytical model. The simulations

differ from the analytical results more as the non-dimensional gravity term increases. This is because the analysis employs the assumption the γ parameter is small. Thus as γ gets larger the analysis would be expected to break down.

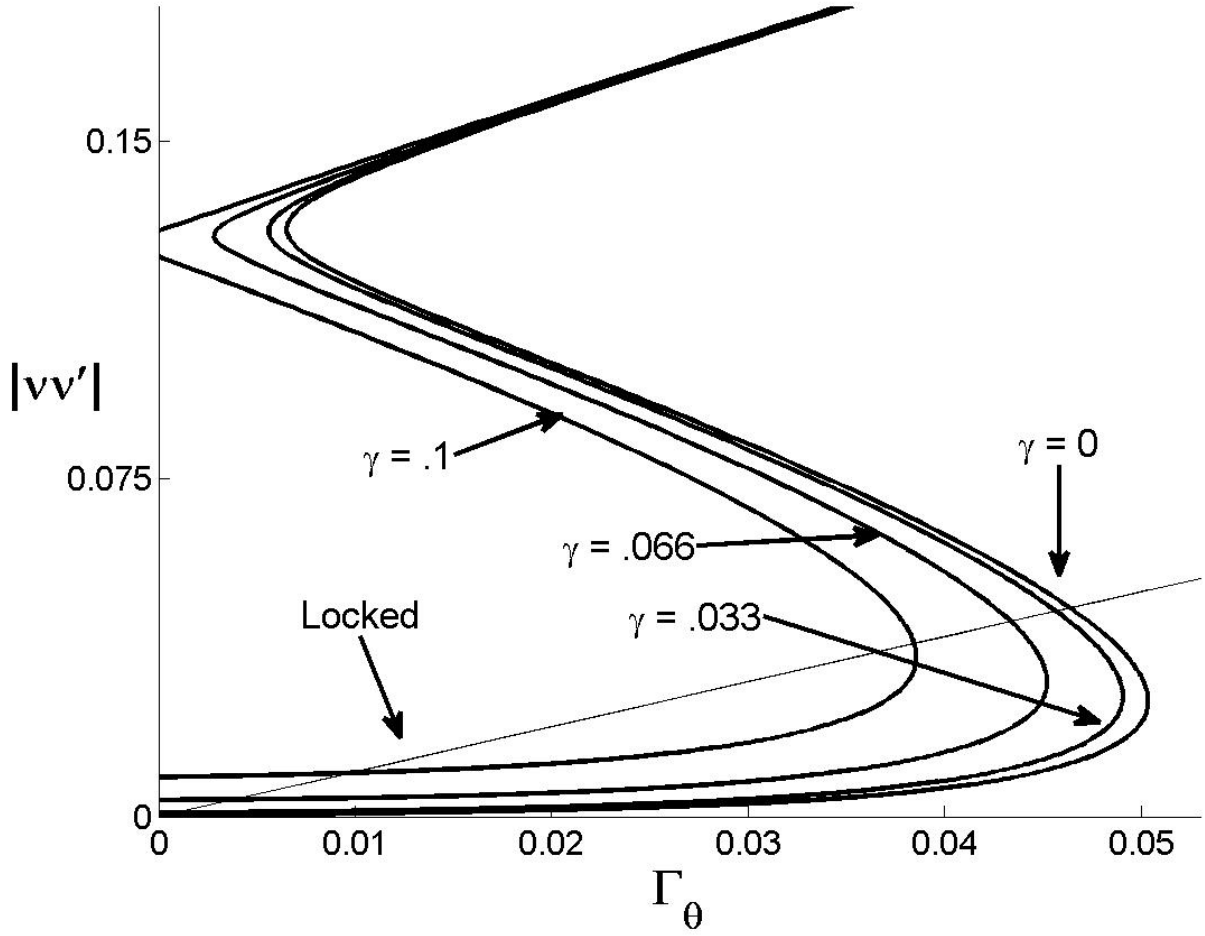

Figure 3.18: Order n harmonic non-dimensional rotor acceleration versus non-dimensional fluctuating torque at order $n = 2$, for two absorbers, with $\sigma = 0$, for various values of γ.

Similar to previous analysis the non-dimensional rotor acceleration versus the non-dimensional fluctuating torque can be solved for. The same equations, (3.21) and (3.22), will be used. When $\gamma \neq 0$, then $a \neq 0$ even when $\Gamma_\theta = 0$. This means that the non-dimensional rotor

acceleration will not be equal to zero, even when $\Gamma_\theta = 0$. This is a CPVA system that performs worse than a system without absorbers for values less than a certain Γ_θ. A potential case when this could happen though is with start-stop technology. In such a case the engine would be shut off thus eliminating the alternating torque due to the cylinders firing, causing Γ_θ to tend towards zero. The engine would slow down leading to a increase in γ. This could potentially cause the system to go through the range, were the system with CPVAs performs worse than one without, before the engine comes to a stop.

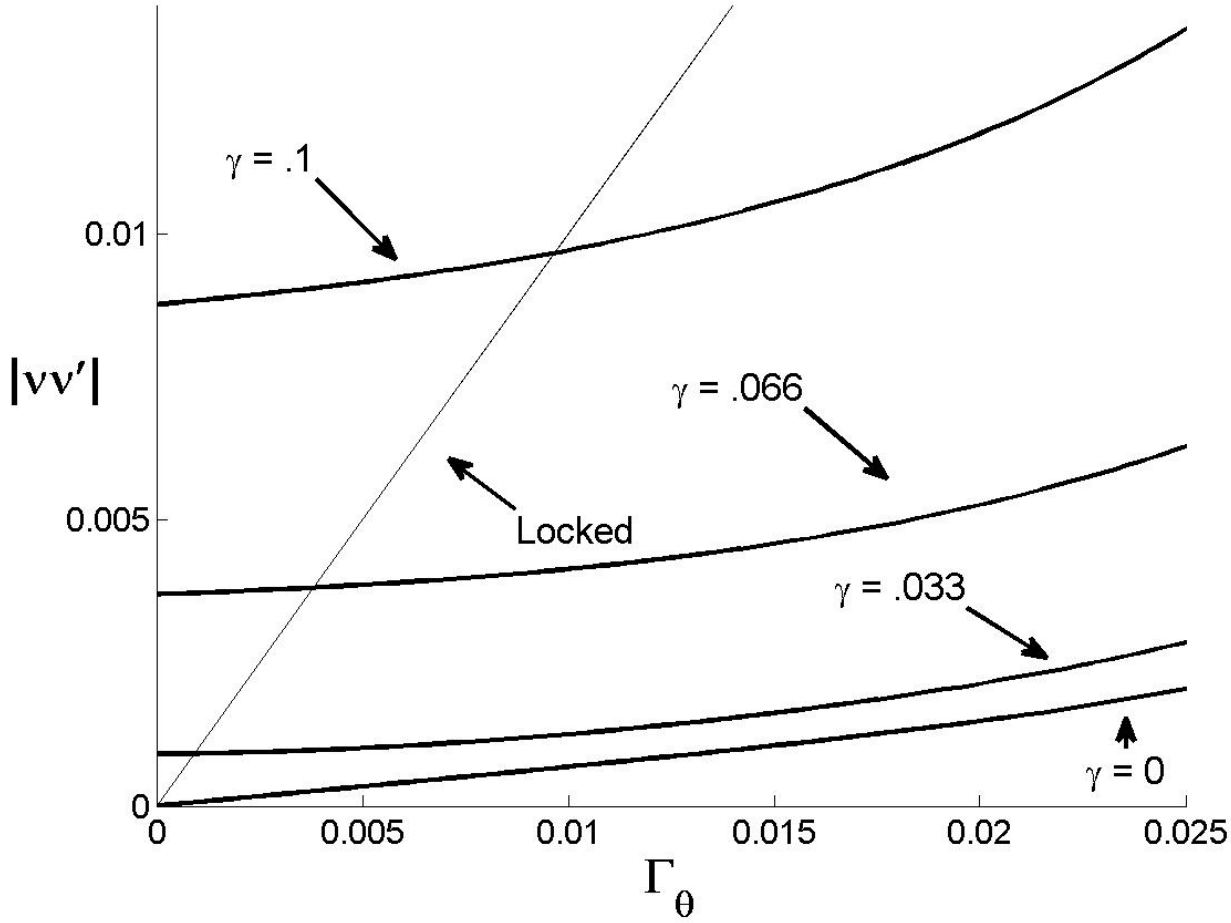

Figure 3.19: Order n harmonic of the non-dimensional rotor acceleration versus non-dimensional fluctuating torque near zero, at order $n = 2$, with $\sigma = 0$, for two absorbers for various values of γ.

Another interesting occurrence takes place if the absorbers are over-tuned instead of perfectly tuned. As was in the general case an improvement is seen in the non-dimensional rotor acceleration when the absorbers are initially over-tuned and γ is increased. It should be noted that the γ_{crit} value when $n = 2$ is different than in the general case. This would be solved from Equations (3.26) This is due to the superharmonic resonance that the $n = 2$

absorbers will experience. This makes γ_{crit} very difficult to find mathematically, but it can be found by varying γ in the equations and plotting.

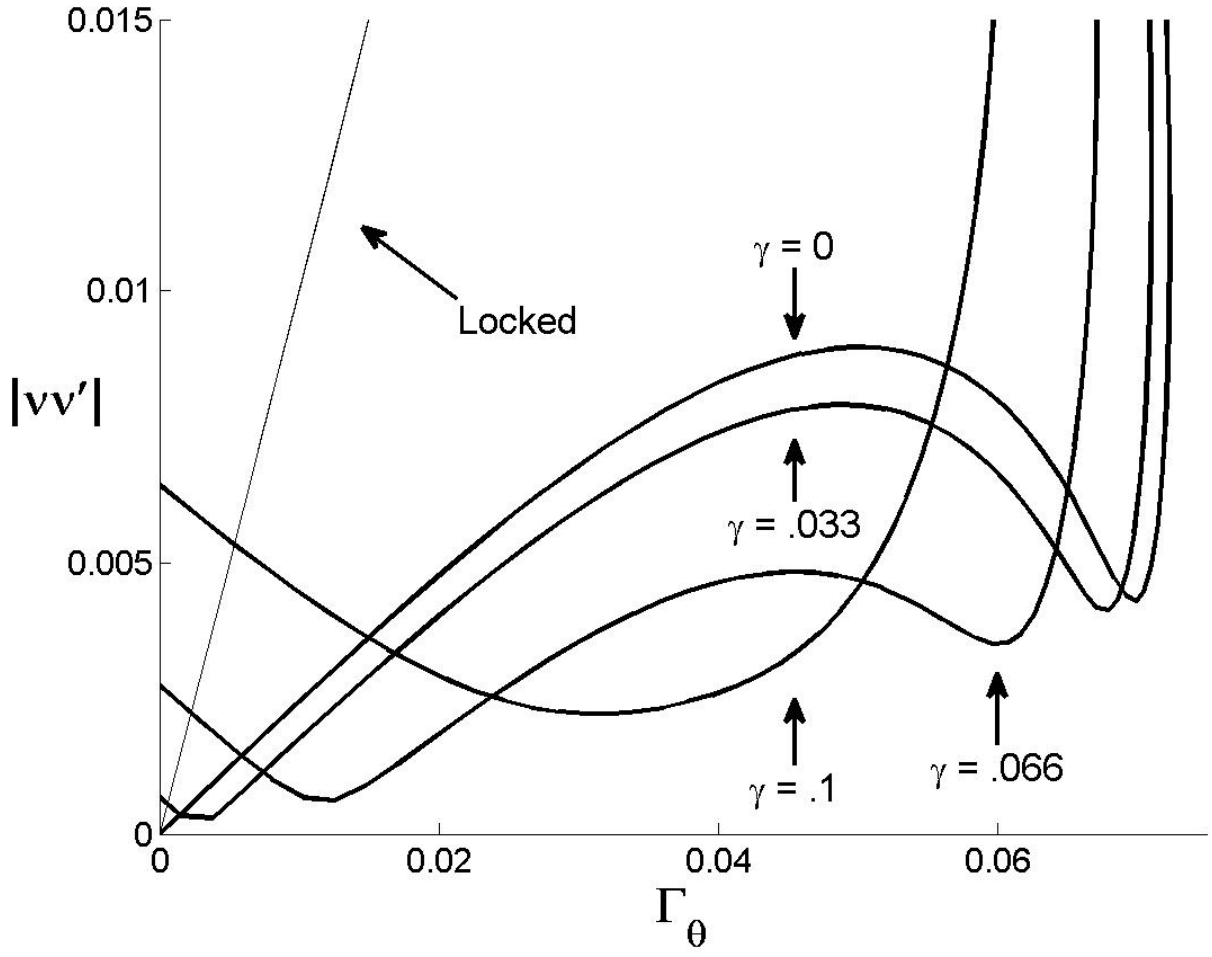

Figure 3.20: Order n harmonic of the non-dimensional rotor acceleration versus non-dimensional fluctuating torque near zero, at order $n = 2$, for two absorbers for various values of γ and 2% detuning.

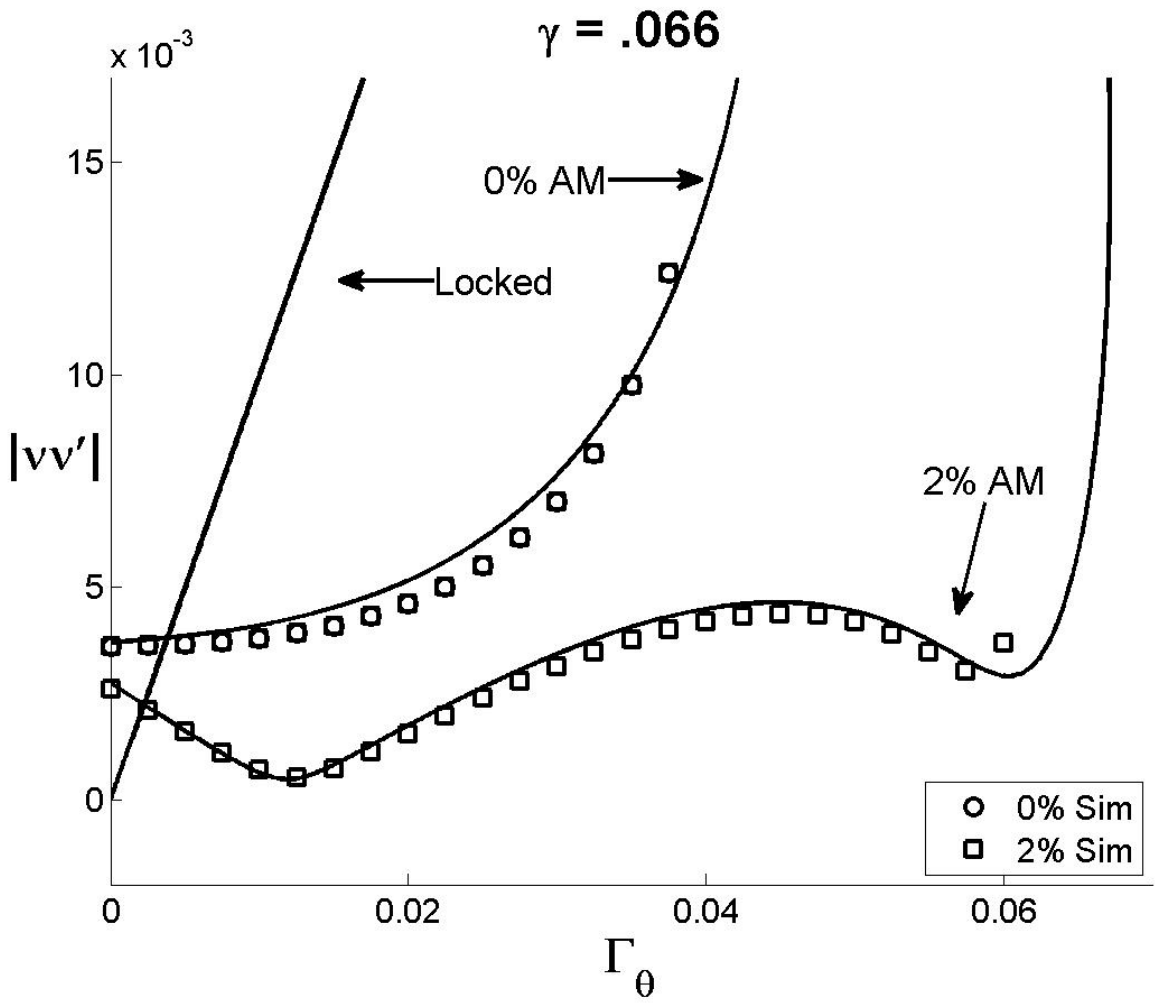

Figure 3.21: Order n harmonic of the non-dimensional rotor acceleration versus non-dimensional fluctuating torque near zero, at order $n = 2$, for two absorbers, comparison of simulations to analytical model.

Figure 3.21 demonstrates that the simulations follow the analytical model. The analytical model predicted that there is a region of low fluctuating torque where the rotor acceleration is greater with absorbers in action than if they are locked down. Of more interest though is the effect of over tuning the absorbers. The results found in Figure 3.14, which is for the general case, show that over tuning the absorbers does not improve the non-

dimensional rotor acceleration for all values of non-dimensional fluctuating torque before the jump occurs. However, in Figure 3.21, when the absorbers are for a second order engine, over tuning provides an improvement of the non-dimensional rotor acceleration across all the non-dimensional fluctuating torque before the jump. Additionally the simulation supports the analytical prediction that there is a range of Γ_θ in which the non-dimensional rotor acceleration approaches zero. If the idle condition of a four cylinder engine could be set with a two absorber system designed to correspond to this point, then the performance could be improved dramatically.

Since the equations were not solvable analytically it does make designing for this point more difficult, but it can still be done. An engine would need to be tested to determine Γ_θ vs. Ω. Once this is done a relationship between the two is known. Now an absorber design needs to be assumed. From this a graph similar to Figure 3.5 can be developed. A plot similar to Figure 3.21 can also be made. When this graph is made it should be done for a variety of different values of detuning at a constant value of γ that corresponds to the desired engine idle speed. Now the value of Γ_θ where $\nu\nu\prime$ is minimized can be determined from the graph. This can then be compared to the Γ_θ vs. Ω chart. For some engine speeds Γ_θ may be much larger than the Γ_θ corresponding to the minimum rotor acceleration. In this case a higher Ω would be chosen or a larger inertia ratio and the process repeated until the optimal conditions were found.

3.3.2.2 4 Absorbers

In the case of four absorbers there are four sets of equations developed from equation (3.12). For equally spaced absorbers, $\psi_1 = 0$, $\psi_2 = \frac{\pi}{2}$, $\psi_3 = \pi$, $\psi_4 = \frac{3\pi}{2}$. Normally when looking at the steady-state it is assumed that $a_j = a$ and $\alpha_j = \alpha$. If this is tried it can be found that

the four sets of equations do not simplify to one set. Instead, two sets of equations can be simplified to one set of equation, while the other two sets are equal to another set of equations. This means that the steady-state of four absorbers will behave differently than other cases. In the case of four absorbers absorber one will align with absorber three, while absorber two will align with absorber four. When it is assumed that $a_3 = a_1$, $a_4 = a_2$, $\alpha_3 = \alpha_1$ and $\alpha_4 = \alpha_2$ at steady-state, the four sets of steady-state equations can be simplified to two sets of equations as,

$$\begin{aligned}
\textbf{RE}: \quad & na_1\sigma + \frac{n}{4}a_1 + \frac{n}{4}a_2\cos(\alpha_2 - \alpha_1) - \frac{3}{4n}\kappa_0 a_1^3 \\
& - \frac{3}{2}\frac{\kappa_0 a_1\tilde{\gamma}^2}{n(1-n^2)^2} - \frac{\tilde{\Gamma}_\theta}{2n}\sin(\alpha_1 - \tau) + \frac{(1+n^2)\tilde{\gamma}^2}{4n(1-n^2)}\sin(\alpha_1) = 0 \\
\textbf{IM}: \quad & \frac{n}{4}a_2\sin(\alpha_2 - \alpha_1) + \frac{\tilde{\mu}_a}{2}a_1 - \frac{\tilde{\Gamma}_\theta}{2n}\cos(\alpha_1 - \tau) \\
& + \frac{(1+n^2)\tilde{\gamma}^2}{4n(1-n^2)}\cos(\alpha_1) = 0
\end{aligned} \tag{3.27}$$

and

$$\begin{aligned}
\textbf{RE}: \quad & na_2\sigma + \frac{n}{4}a_2 + \frac{n}{4}a_1\cos(\alpha_1 - \alpha_2) - \frac{3}{4n}\kappa_0 a_2^3 \\
& - \frac{3}{2}\frac{\kappa_0 a_2\tilde{\gamma}^2}{n(1-n^2)^2} - \frac{\tilde{\Gamma}_\theta}{2n}\sin(\alpha_2 - \tau) - \frac{(1+n^2)\tilde{\gamma}^2}{4n(1-n^2)}\sin(\alpha_2) = 0 \\
\textbf{IM}: \quad & \frac{n}{4}a_1\sin(\alpha_1 - \alpha_2) + \frac{\tilde{\mu}_a}{2}a_2 - \frac{\tilde{\Gamma}_\theta}{2n}\cos(\alpha_2 - \tau) \\
& - \frac{(1+n^2)\tilde{\gamma}^2}{4n(1-n^2)}\cos(\alpha_2) = 0
\end{aligned} \tag{3.28}$$

These equations can be solved numerically as has been done previously to get the non-dimensional absorber amplitude versus non-dimensional fluctuating torque, and non-dimensional rotor acceleration versus non-dimensional fluctuating torque. However, as is the case with three absorbers, when these equations were solved, unreasonable results were sometimes found. It is believed that this is because of the numerical solver that was used. The unrea-

sonable results were never found in numerical simulation and have been omitted. As was the case with two absorbers, when there is no non-dimensional fluctuating torque there is a response at order two by the absorbers. It can be seen in Figure 3.22 that the two sets of absorbers can have different amplitudes. This is confirmed by numerical simulations.

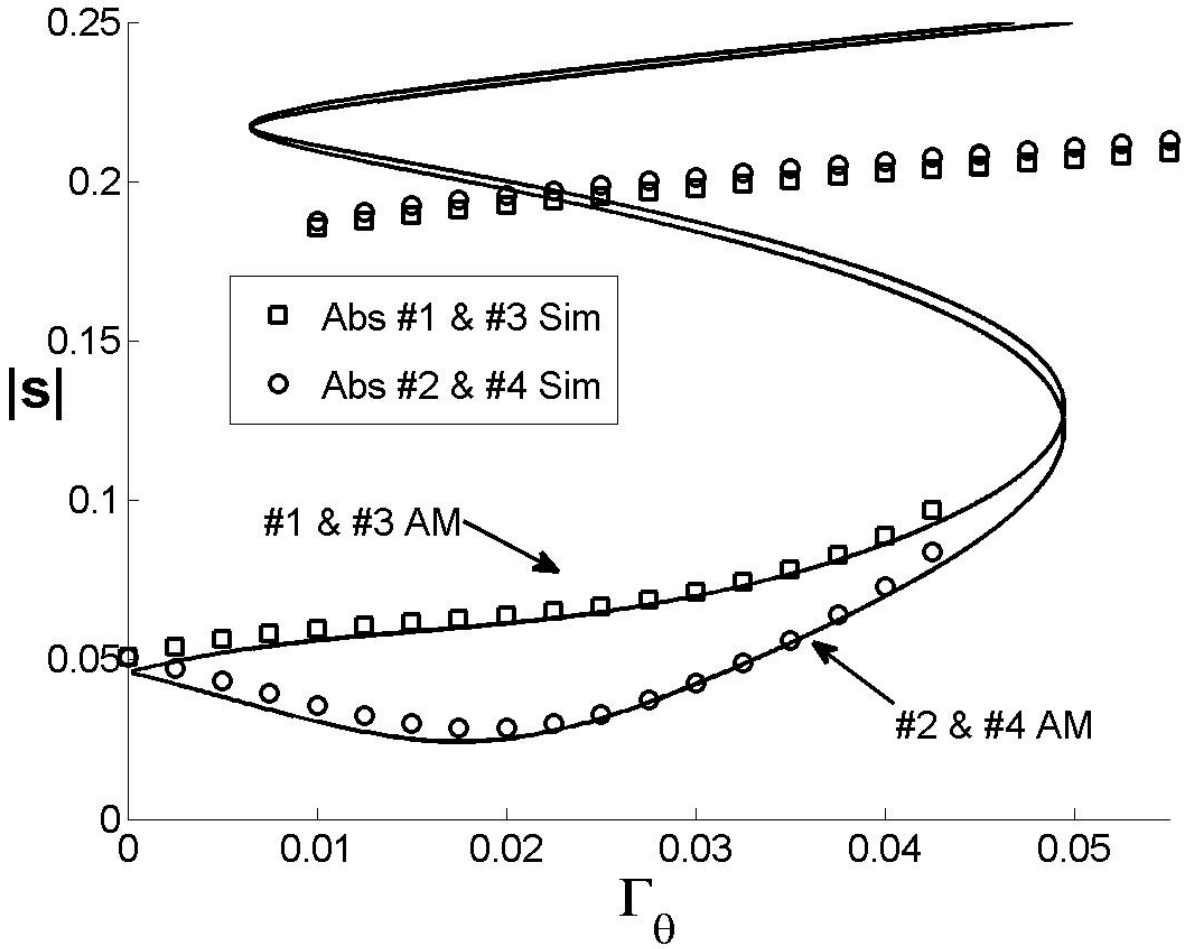

Figure 3.22: Order n harmonic of the non-dimensional absorber absorber amplitude versus non-dimensional fluctuating torque near zero, at order $n = 2$, with $\sigma = 0$ for four absorbers, with $\gamma = .05$.

As was the case with two absorbers, the same equations (3.28) can be plugged into (3.22)

and allow for the non-dimensional rotor acceleration to be examined.

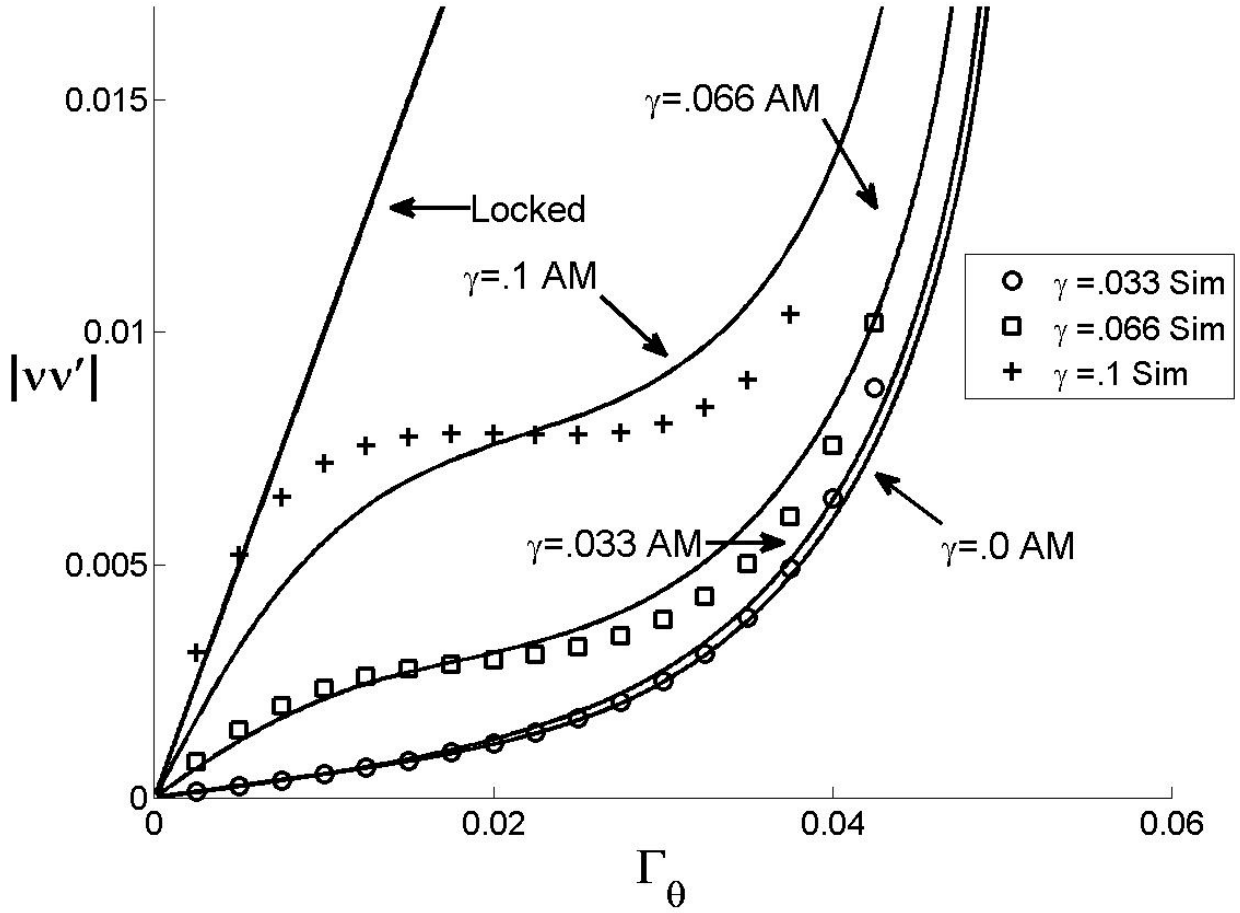

Figure 3.23: Order n harmonic of the non-dimensional rotor acceleration versus non-dimensional fluctuating torque near zero, at order $n = 2$, with $\sigma = 0$ for four absorbers, for various values of γ.

From Figure 3.22 and Figure 3.23 it can be seen that the numerical simulations align with the analytical model. The multiple amplitude responses are confirmed by the simulations. It can be seen in Figure 3.23 that as γ gets large the simulations start to vary from the analytical model, but this is likely because the analysis was an assumption that γ is small.

3.3.2.3 3 Absorbers

As was done previously, the three absorber set up is used to develop the sets of equations from equation (3.13). In this case, as was the case with four absorbers, it cannot be assumed that all the amplitudes and phases are the same for the steady-state response. This leads to three sets of steady-state equations that are coupled but can be solved numerically:

$$\begin{aligned}
\textbf{RE}: \quad & na_1\sigma + \frac{n}{6}a_1 + \frac{n}{6}a_2\cos(\alpha_2-\alpha_1) + \frac{n}{6}a_3\cos(\alpha_3-\alpha_1) - \frac{3}{4n}\kappa_0 a_1^3 \\
& - \frac{3}{2}\frac{\kappa_0 a_1\tilde{\gamma}^2}{n(1-n^2)^2} - \frac{\tilde{\Gamma}_\theta}{2n}\sin(\alpha_1-\tau) + \frac{(1+n^2)\tilde{\gamma}^2}{4n(1-n^2)}\sin(\alpha_1) = 0 \\
\textbf{IM}: \quad & \frac{n}{6}a_2\sin(\alpha_2-\alpha_1) + \frac{n}{6}a_3\sin(\alpha_3-\alpha_1) + \frac{\tilde{\mu}_a}{2}a_1 - \frac{\tilde{\Gamma}_\theta}{2n}\cos(\alpha_1-\tau) \\
& + \frac{(1+n^2)\tilde{\gamma}^2}{4n(1-n^2)}\cos(\alpha_1) = 0
\end{aligned} \tag{3.29}$$

and

$$\begin{aligned}
\textbf{RE}: \quad & na_2\sigma + \frac{n}{6}a_2 + \frac{n}{6}a_1\cos(\alpha_1-\alpha_2) + \frac{n}{6}a_3\cos(\alpha_3-\alpha_2) - \frac{3}{4n}\kappa_0 a_2^3 \\
& - \frac{3}{2}\frac{\kappa_0 a_2\tilde{\gamma}^2}{n(1-n^2)^2} - \frac{\tilde{\Gamma}_\theta}{2n}\sin(\alpha_2-\tau) + \frac{(1+n^2)\tilde{\gamma}^2}{4n(1-n^2)}\sin(\alpha_2-\frac{4\pi}{3}) = 0 \\
\textbf{IM}: \quad & \frac{n}{6}a_1\sin(\alpha_1-\alpha_2) + \frac{n}{6}a_3\sin(\alpha_3-\alpha_2) + \frac{\tilde{\mu}_a}{2}a_2 - \frac{\tilde{\Gamma}_\theta}{2n}\cos(\alpha_2-\tau) \\
& + \frac{(1+n^2)\tilde{\gamma}^2}{4n(1-n^2)}\cos(\alpha_2-\frac{4\pi}{3}) = 0
\end{aligned} \tag{3.30}$$

and

$$
\begin{aligned}
\textbf{RE}: \quad & na_3\sigma + \frac{n}{6}a_3 + \frac{n}{6}a_1\cos(\alpha_1-\alpha_3) + \frac{n}{6}a_2\cos(\alpha_2-\alpha_3) - \frac{3}{4n}\kappa_0 a_3^3 \\
& - \frac{3}{2}\frac{\kappa_0 a_3\tilde{\gamma}^2}{n(1-n^2)^2} - \frac{\tilde{\Gamma}_\theta}{2n}\sin(\alpha_2-\tau) - \frac{(1+n^2)\tilde{\gamma}^2}{4n(1-n^2)}\sin(\alpha_3-\frac{8\pi}{3}) = 0 \\
\textbf{IM}: \quad & \frac{n}{6}a_1\sin(\alpha_1-\alpha_3) + \frac{n}{6}a_2\sin(\alpha_2-\alpha_3) + \frac{\tilde{\mu}_a}{2}a_3 - \frac{\tilde{\Gamma}_\theta}{2n}\cos(\alpha_3-\tau) \\
& + \frac{(1+n^2)\tilde{\gamma}^2}{4n(1-n^2)}\cos(\alpha_3-\frac{8\pi}{3}) = 0
\end{aligned}
\tag{3.31}
$$

Now the equations can be solved numerically and allow for plots of the non-dimensional absorber amplitude versus the non-dimensional alternation torque. It can be seen that even when there is only forcing due to gravity that there is a response at order two by the absorbers. Also at this point all of the absorbers have the same amplitude. As the non-dimensional alternating torque increases, three different response amplitudes can be seen by the absorbers.

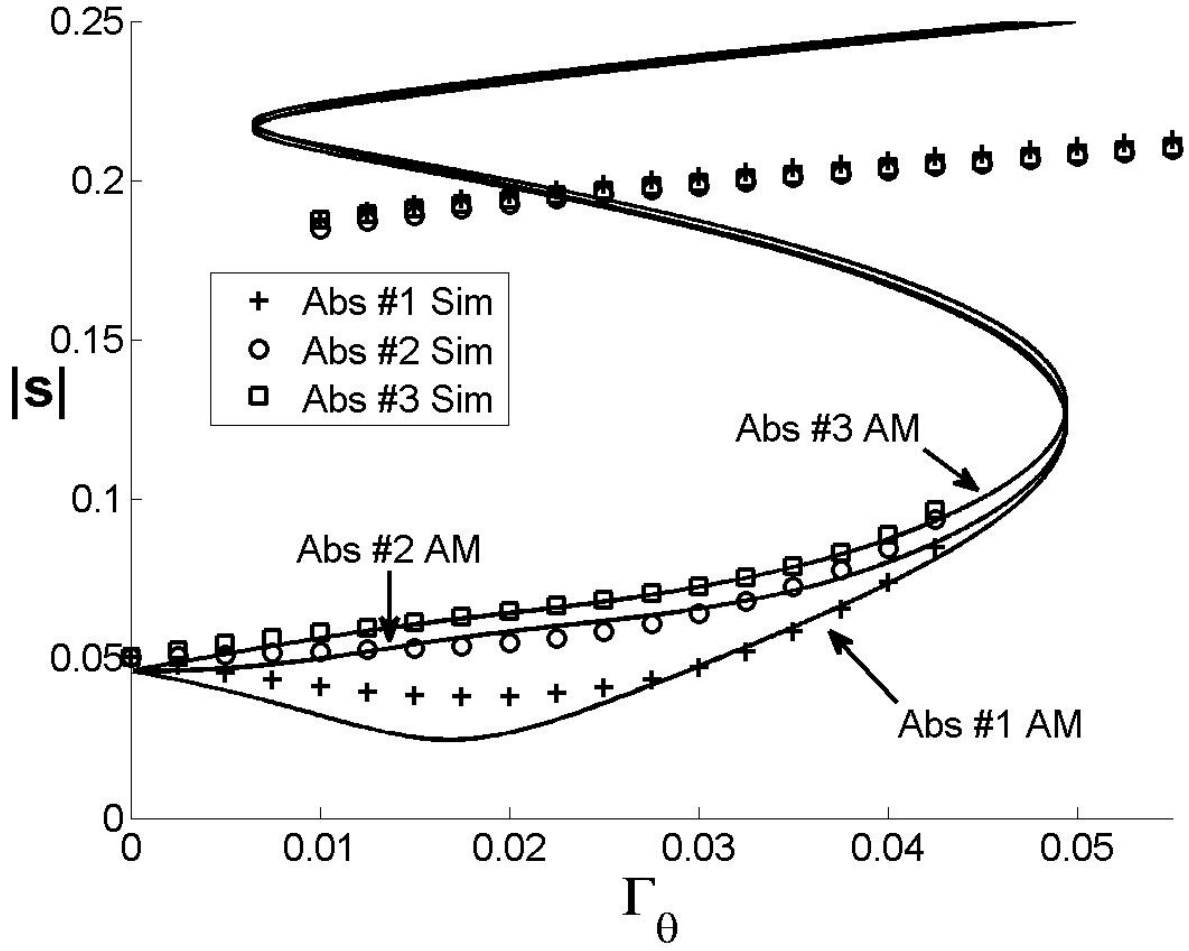

Figure 3.24: Order n harmonic of the non-dimensional rotor acceleration versus non-dimensional fluctuating torque near zero, at order $n = 2$, with $\sigma = 0$, for three absorbers, with $\gamma = .066$.

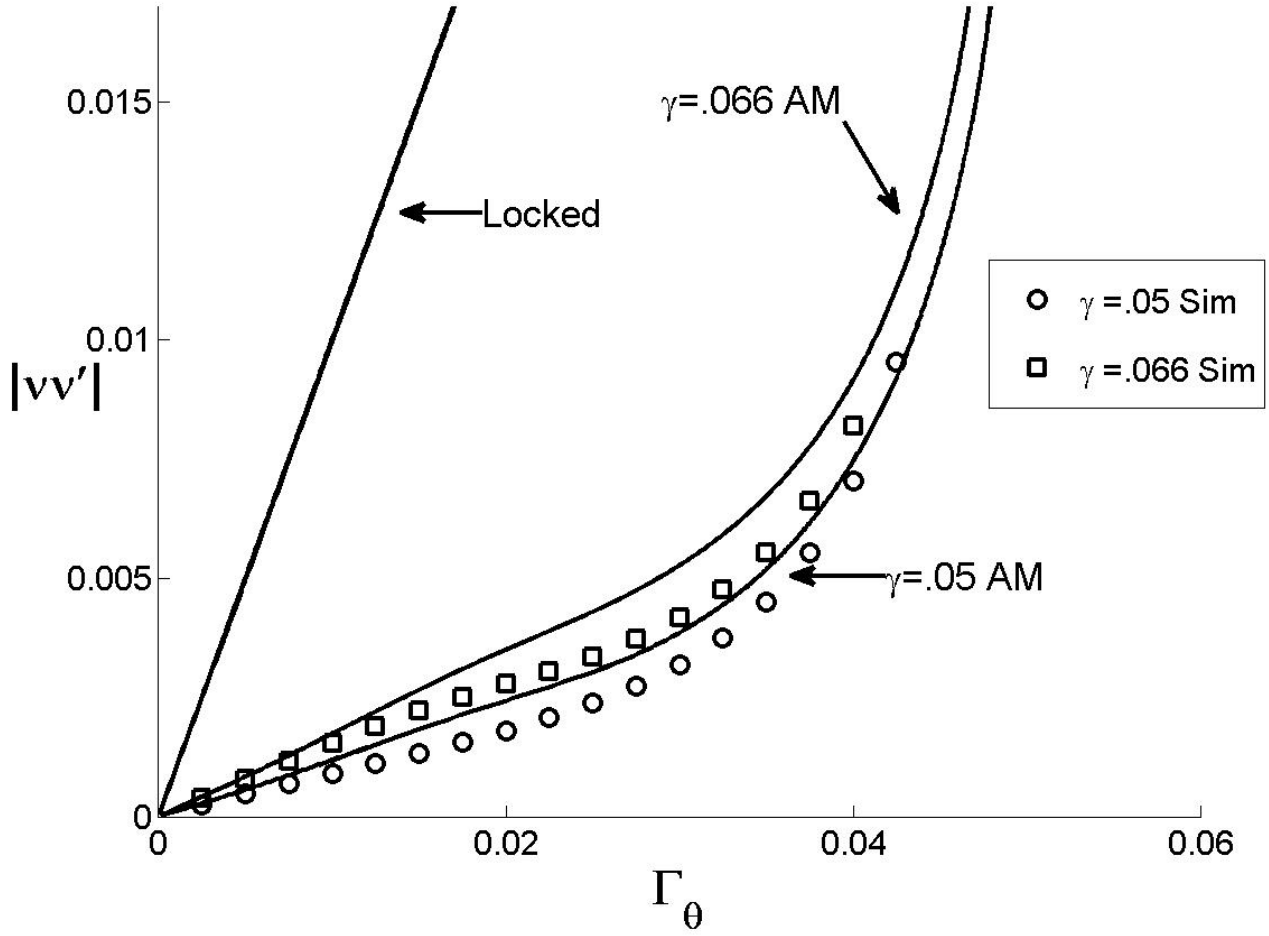

Figure 3.25: Order n harmonic of the non-dimensional rotor acceleration versus non-dimensional fluctuating torque near zero, at order $n = 2$, with $\sigma = 0$, for three absorbers, for various values of γ.

From Figure 3.24 and Figure 3.25 it can be seen that the numerical simulations align with the analytical model but not as well as in the other special cases.

3.3.2.4 Higher Numbers of Absorbers

Some general statements about cases that contain high numbers of absorbers can be made. If the number of absorbers is even then there exist a steady-state for which the number of distinct amplitudes at order two is half the number of absorbers. This is because of the arrangement of absorbers. When there is an even number of absorbers each absorber will be π radians from another absorber. The term in equation (3.13) that imposes multiple amplitudes at order two can be reconciled if $\psi = \pi$. However, if there are an odd number of absorbers this π phasing between two absorbers does not happen and thus the equation can not be reduced. This leads to each absorber having its own independent amplitude at order two.

3.3.3 Case 3: $n = 3$

An interesting occurrence is when the absorbers are tuned to order three. Similar to when the absorbers are tuned to order two, an extra term with a magnitude of $\frac{\kappa_0 \tilde{\gamma}^3}{4n(1-n^2)^3} = \chi$ appears in the slow flow equations. However, this extra term that is in equation (3.15) is typically very small. Breaking down the term it is seen that κ_0 is dependent on ϵ, $\tilde{n}$, and λ. Assuming that $\tilde{n} \approx 3$, and that if to maximize κ_0 then $\lambda = 0$, the extra variable can be solved to be a function of only two variables, γ and ϵ. Now the magnitude of this term will be examined by varying γ and ϵ in Figure 3.26.

This term only becomes relatively large when γ is large and ϵ is small. However, even in such instances the value of the magnitude is of the order 10^{-3}. This is orders of magnitude smaller than the other terms and thus the term can be dropped, which means that the cases when $n = 3$ falls into the general case. This can be shown graphically as well. Since it is

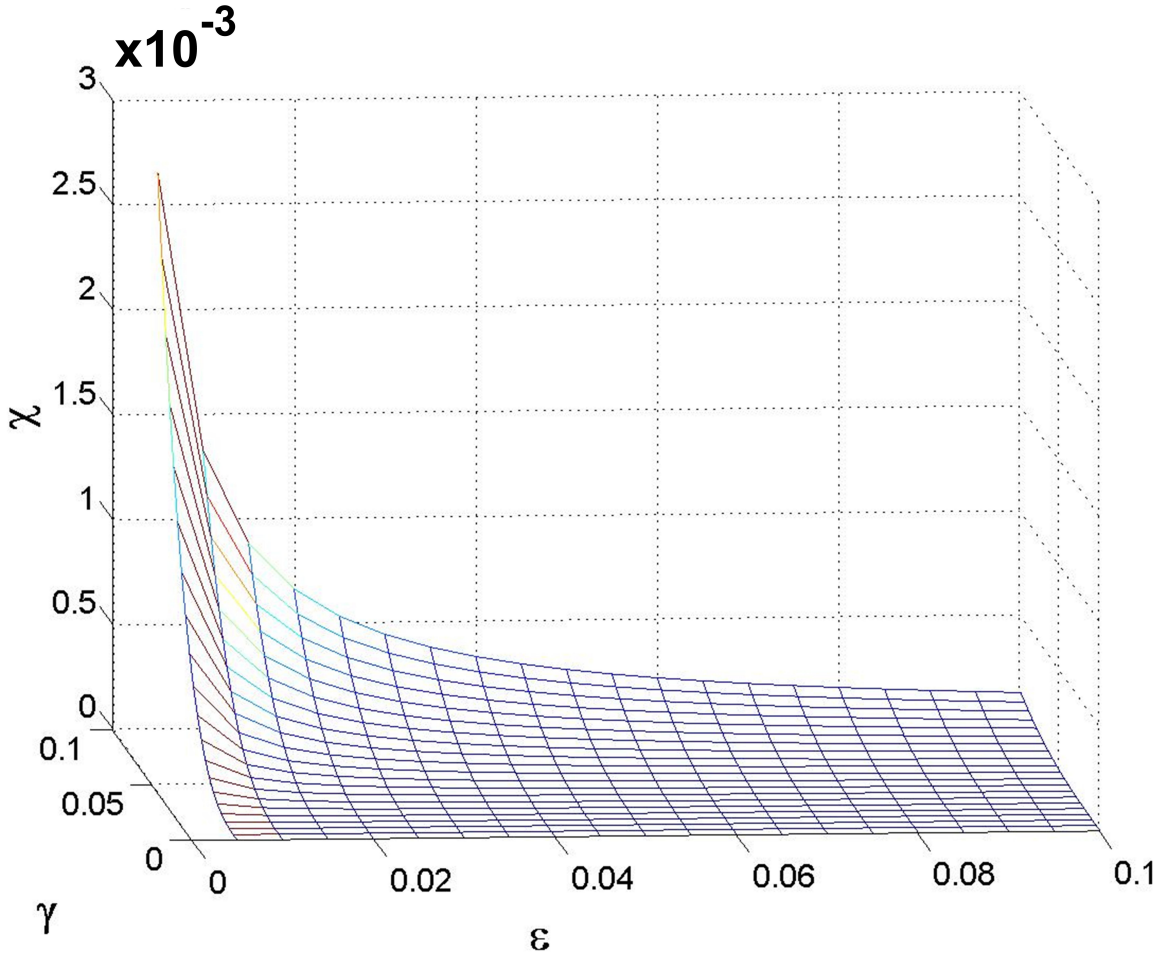

Figure 3.26: Evaluation of the magnitude of the special term χ in the $n = 3$ slow flow equations.

known where the extra term is largest that is where the equations will be tested. In Figure 3.27 only select points of the $n = 3$ analytical model are being compared with the line. This allows for the any differences in the lines to be seen.

It can be seen in Figure 3.27 that the numerical solution of the $n = 3$ analytical model coincides with that of the general case. It should be noted that as was the case when $n = 2$, there is a potential for different amplitudes based on the number of absorbers in the system. However, since it has been shown that this term is small the potential for different amplitudes

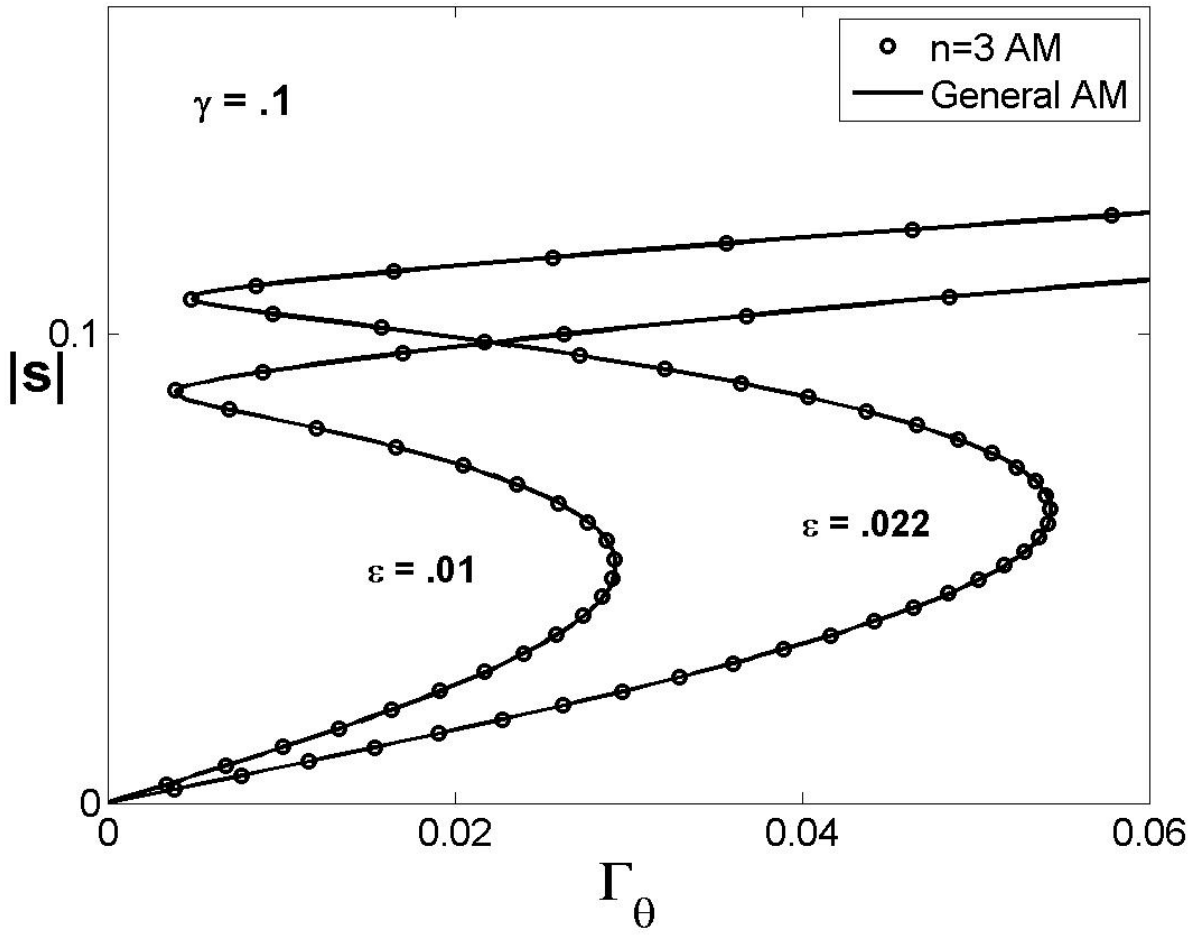

Figure 3.27: Comparison of order n harmonic of the non-dimensional absorber amplitude versus non-dimensional fluctuating torque between $n = 3$ analytical model and the general case.

is very small and is negligible. Additionally when this term is dropped the non-dimensional rotor acceleration also becomes the same as in the general case.

3.4 Ignoring Gravity

In order to determine at what values of γ the effects of gravity can be ignored, the saddle point at which the nonlinear jump occurs is examined. The difference between the value

of the non-dimensional fluctuating torque at which the saddle point occurs without gravity and with gravity was found. This was examined for both the non-dimensional absorber amplitude and the non-dimensional fluctuating torque amplitude. Additionally this will be examined for the case of $n = 1.5$ and $n = 2$, with $\mu_a = .014921$.

Table 3.1: Difference values given as % between the level of alternating torque at which the saddle-node bifurcation occurs, with respect to non-dimensional absorber amplitude, for various values of γ, for n=1.5, with $\sigma = 0\%$.

n	1.5			
Inertia Ratio(b)	5%	10%	15%	20%
γ=.01	0.49%	0.29%	0.16%	0.15%
γ=.02	1.98%	1.04%	0.66%	0.5%
γ=.03	4.42%	2.26%	1.5%	1.12%
γ=.04	7.82%	4.01%	2.69%	2.01%
γ=.05	12.12%	6.27%	4.17%	3.14%

Table 3.2: Difference values given as % between the level of alternating torque at which the saddle-node bifurcation occurs, with respect to non-dimensional fluctuating torque amplitude, for various values of γ, for n=1.5, with $\sigma = 0\%$.

n	1.5			
Inertia Ratio(b)	5%	10%	15%	20%
γ=.01	0.48%	0.25%	0.18%	0.12%
γ=.02	1.90%	1.0%	0.68%	0.5%
γ=.03	4.28%	2.24%	1.52%	1.12%
γ=.04	7.53%	3.98%	2.68%	2.01%
γ=.05	11.68%	6.18%	4.18%	3.14%

For the case of a three cylinder engine Tables 3.1 and 3.3 show that the impact of gravity decreases as the inertia ratio increases. It is desired that the difference be less than 2.5%.

Thus for all the inertia values examined γ must be less than .02. In typical applications R_O is between .05 m and .1 m. Thus when an engine is running above 950 RPM and 660 RPM respectively, gravity can be ignored.

Table 3.3: Difference values given as % between the level of alternating torque at which the saddle-node bifurcation occurs, with respect to non-dimensional absorber amplitude, for various values of γ, for n=2, with $\sigma = 0\%$.

n	2			
Inertia Ratio(b)	5%	10%	15%	20%
γ=.01	1.04%	0.4%	0.24%	0.15%
γ=.015	2.33%	0.94%	0.53%	0.35%
γ=.02	4.15%	1.59%	0.93%	0.63%
γ=.03	9.33%	3.61%	2.11%	1.42%
γ=.04	16.56%	6.42%	3.73%	2.54%
γ=.05	25.86%	10.07%	5.83%	3.96%

Table 3.4: Difference values given as % between the level of alternating torque at which the saddle-node bifurcation occurs, with respect to non-dimensional fluctuating torque amplitude, for various values of γ, for n=2, with $\sigma = 0\%$.

n	2			
Inertia Ratio(b)	5%	10%	15%	20%
γ=.01	1.04%	0.43%	0.24%	0.15%
γ=.015	2.33%	0.94%	0.53%	0.35%
γ=.02	4.15%	1.62%	0.93%	0.63%
γ=.03	9.33%	3.64%	2.11%	1.42%
γ=.04	16.56%	6.46%	3.73%	2.54%
γ=.05	25.87%	10.1%	5.83%	3.96%

The change in the saddle point was examined for the case of a four cylinder engine in Tables 3.2 and 3.4. It is desired that the difference be less than 2.5%. Thus for all the inertia

values examined γ must be less than .015. In typical applications R_O is between .05 m and .1 m. Thus when an engine is running above 1100 RPM and 775 RPM respectively, gravity can be ignored.

3.5 The Effects of τ

The effect of phasing the forcing due to the engine relative to the origin (τ), which is fixed by gravity, was briefly examined using perturbation results. Different values of τ were explored. Figure 3.28 shows that for any number of absorbers $n \neq 1, 2$, τ does not have an impact on the steady state response of the non-dimensional rotor acceleration. Figure 3.29 shows that when $n = 2$, τ will have a significant impact on the steady state response of the non-dimensional rotor acceleration. Therefore, when considering the effects of gravity, it is crucial to know the relative phases of gravity and the order n applied torque. These results will be seen for any number of absorbers but it is shown only for the simplest case of 2 absorbers.

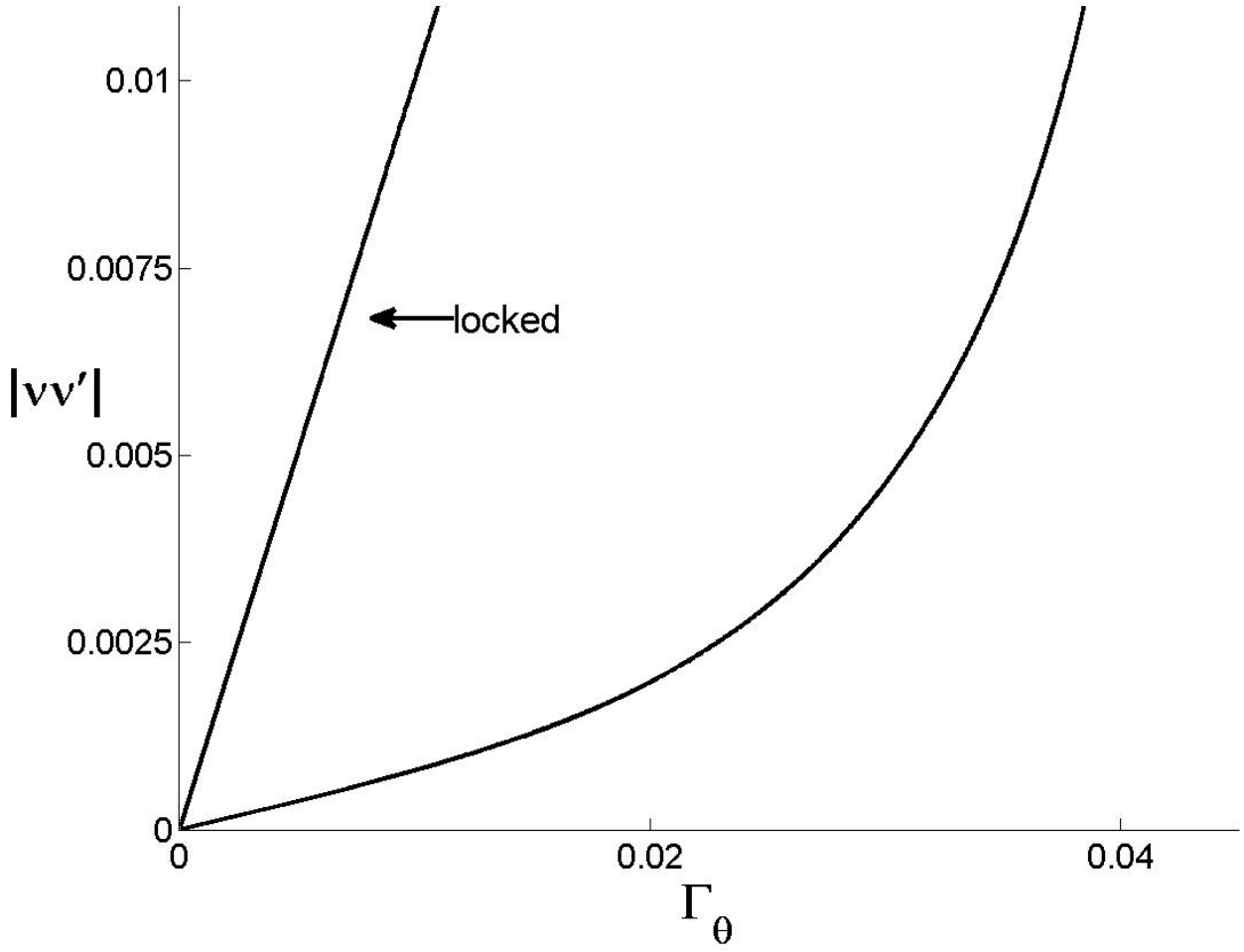

Figure 3.28: Diagram of $n \neq 1, 2$ pendulum type circular path absorbers order n rotor acceleration as a function of Γ_θ for various τ, τ has no effect, the locked response is for reference only.

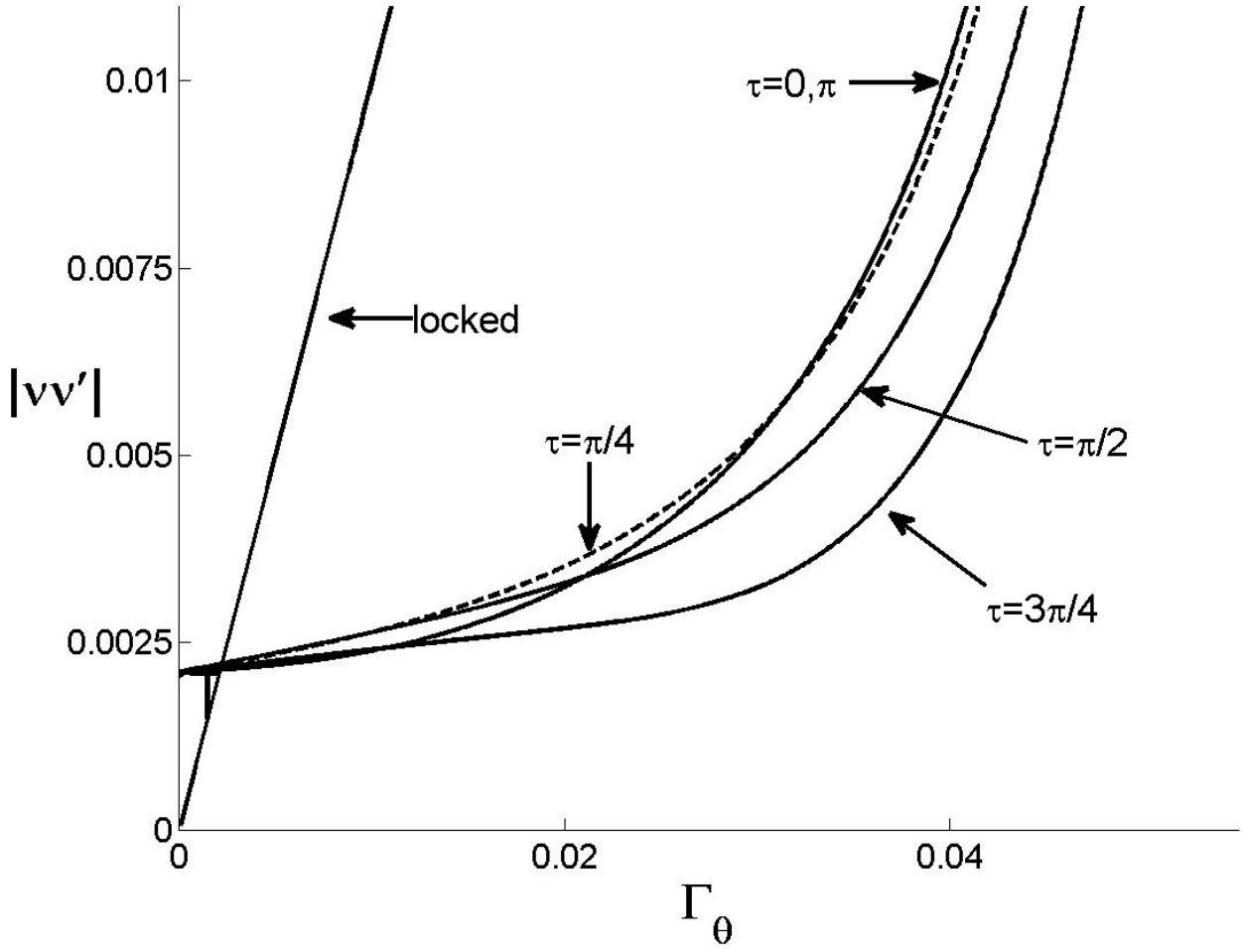

Figure 3.29: Diagram of two $n = 2$ pendulum type circular path absorbers order n rotor acceleration as a function of Γ_θ for various τ, response are distinct for each τ, the locked response is for reference only.

Chapter 4

Conclusions and Recommendation for Future Work

4.1 Summary of Results and Conclusions

The purpose of this investigation was to systematically investigate the effects gravity has on the dynamics and effectiveness of CPVAs. This was done using a mathematical model, which was studied by perturbation analysis and numerical simulations. Gravity provides both direct and parametric forcing of CPVAs at engine order 1 (one cycle per revolution), which can interact with engine order n vibrations under certain circumstances, leading to rich dynamic behavior.

The thesis provides a brief background of CPVAs, including previous relevant work and various applications. The analysis of gravity begins by developing model equations of motion for a rotor spinning about a horizontal axis, subjected to torsional excitation of order n, fitted with N identical general path CPVAs, and the entire system is acted on by gravity.

The model equations were rescaled and transformed into a form suitable for perturbation analysis. This procedure included small parameter assumptions that are consistent with values encountered in applications. The absorber equations of motion were uncoupled from the rotor equation to leading order in the small parameter, which allows one to find approximate response solutions for the absorbers, from which the rotor dynamics can then be recovered. The method of multiple scales was used to obtain the slow flow equations governing the amplitudes and phases of the absorbers. A numerical root solver was used to solve the for zeros of the slow flow equations, yielding steady-state conditions that were used for parameter studies. Direct numerical simulations of the full EOM were used to verify the theoretical results. Stability of these responses was not considered, except by observations from these simulations. When the fluctuating torque is zero the absorbers experience equal magnitudes of an order two super harmonic response from gravity, however the absorbers phases are not equal. For the cases when $N > 2$ and $n = 2$ the root solver frequently had difficulties with convergence; the initial conditions used in the root solver were extremely important to successfully finding a solution.

It was determined that it is important to include the effects of gravity when the ratio of gravity to centrifugal acceleration, $\gamma = g/(R_0\Omega^2)$, is sufficiently large (assuming reasonable absorber/rotor inertia ratios in the range 5%-20%). For example, it is found that gravity must be accounted for when $\gamma > 0.02$ for $n = 1.5$, and for $\gamma > 0.015$ for $n = 2$. The corresponding range of engine speeds depends, of course, on the distance from rotor center to absorber center of mass, R_0. For typical automotive engines, R_0 is in the range of 0.05-0.1 meters, which implies that one should consider gravitational effects for rotor speeds below about 70-99 radians/second, that is, about 660-950 rpm for $n = 1.5$ and below about 80-115

radians/second, that is, about 775-1100 rpm for $n = 2$. These are precisely in the range of engine idle speeds.

In addition to these general observations, it was found that nonlinear dynamic interactions can occur under certain conditions. These arise from interplay between gravity (of order 1) and fluctuating torques (of order n) when they are internally resonant. For most values of n, specifically, for $n \neq 1, 2, 3$, the system response is essentially linear, that is, the responses of order 1 and n can be determined separately and combined to obtain the overall response. In these cases it was shown that the effects of gravity can be accounted for by using an equivalent detuning parameter that is smaller than the detuning between order n and the absorber order $\tilde{n}$. This means that gravity has the effect of lowering the torque threshold at which the dangerous jump instability occurs for circular path absorbers. For $n = 3$ it was shown that, even though there are subharmonic interactions, these effects are very small and can generally be ignored. The special cases of $n = 1, 2$ proved to be the most interesting. In this work we focused on the $n = 2$ case, since it has particular relevance to four cylinder engines. The equally rich $n = 1$ case is left for future study.

For $n = 2$ it was determined that the number of absorbers N has an effect on the types of responses that can occur. The simplest response occurs when there are two absorbers, $N = 2$, in which case the steady-state responses of both absorbers have the same amplitude and phase at order n. The order one response of the absorbers, from gravity, has the same amplitude, but with a phase difference of π, due to the angular spacing of the absorbers. It is also shown that the $n = 2$ absorbers have a superharmonic response to the order one gravitational forcing. The superharmonic response leads to an interesting finding regarding the rotor acceleration, which is a measure of rotor torsional vibration. It was found that if

the absorbers are over-tuned (as is the case in practice) and the gravity parameter exceeds a certain level, for zero relative phase between the applied torque and gravity there is parameter region in which the nondimensional rotor acceleration shows a minimum value as the fluctuating torque is varied, and this minimum is lower than the value experienced without gravity. Thus, it may be possible to design absorbers so that gravity actually reduces second order torsional vibration levels under engine idle conditions. Cases for $N = 3, 4$ absorbers were explored throughly, while general comments were made for $N > 4$. It was also found that when $N > 2$, depending on the value of the fluctuating torque, different absorber amplitudes and phases are possible. When $N > 2$, the amplitude of the order one response was the same for all absorbers, but the phases are not equal. More interesting is the observation that in this case synchronous order two responses were not found to occur. In general, even numbers of absorbers will display $\frac{N}{2}$ unique responses among sets of absorbers, that is, there are $\frac{N}{2}$ groups of mutually synchronous absorbers. For N odd it was observed that the absorbers display N unique responses.

4.2 Recommendations for Future Work

While a number of interesting results were obtained in this study, several important topics remain to be explored. A list of possible topics for future work along these lines includes the following:

- Compare the analytical model and numerical simulations against physical experiments; these tests are being planned for the MSU test facility, with a horizontal axis of rotation.

- Symmetry techniques may be very useful to sort out the cases where the absorber re-

sponses are synchronous and non-synchronous, and the details of the non-synchronous responses.

- Investigate the effects of gravity on absorbers with different absorber paths, including cycloids and tautochronic epicycloids; the basic resonance cases will be the same, but the quantitative effects may differ.

- The present study focused on the case where the applied order n torque had a zero phase relative to gravity, that is $\tau = 0$; the effects of this phase need to be studied in more detail.

- Complete a stability analysis of the slow flow equations that include gravity, in order to carry out a parameter study to determine specific parameter conditions for the jump, non synchronous, and subharmonic instabilities.

- Explore the effects of absorber damping on the results; this would be motivated by specific case studies of practical interest.

- Further explore the torque condition that minimizes the rotor acceleration, and see if it has a practical application to engine idle.

- Numerical solution of the steady-state responses for order 2 absorbers was extremely sensitive when there were more than two absorbers; the source of this sensitivity, and its resolution, would be beneficial to future investigations.

- This work assumes that the absorbers are identical and equally spaced around the rotor, but in some cases absorbers of different orders may be employed, and the effects of gravity on these systems may prove interesting as well.

Appendices

Appendix A

Additional Figures

The following figures examine the effect that arise from varying the value of ϵ from .015 to .06 has on the absorber response. Figures A.1 through Figure A.4 are from perfectly tuned absorbers $\sigma = 0$.

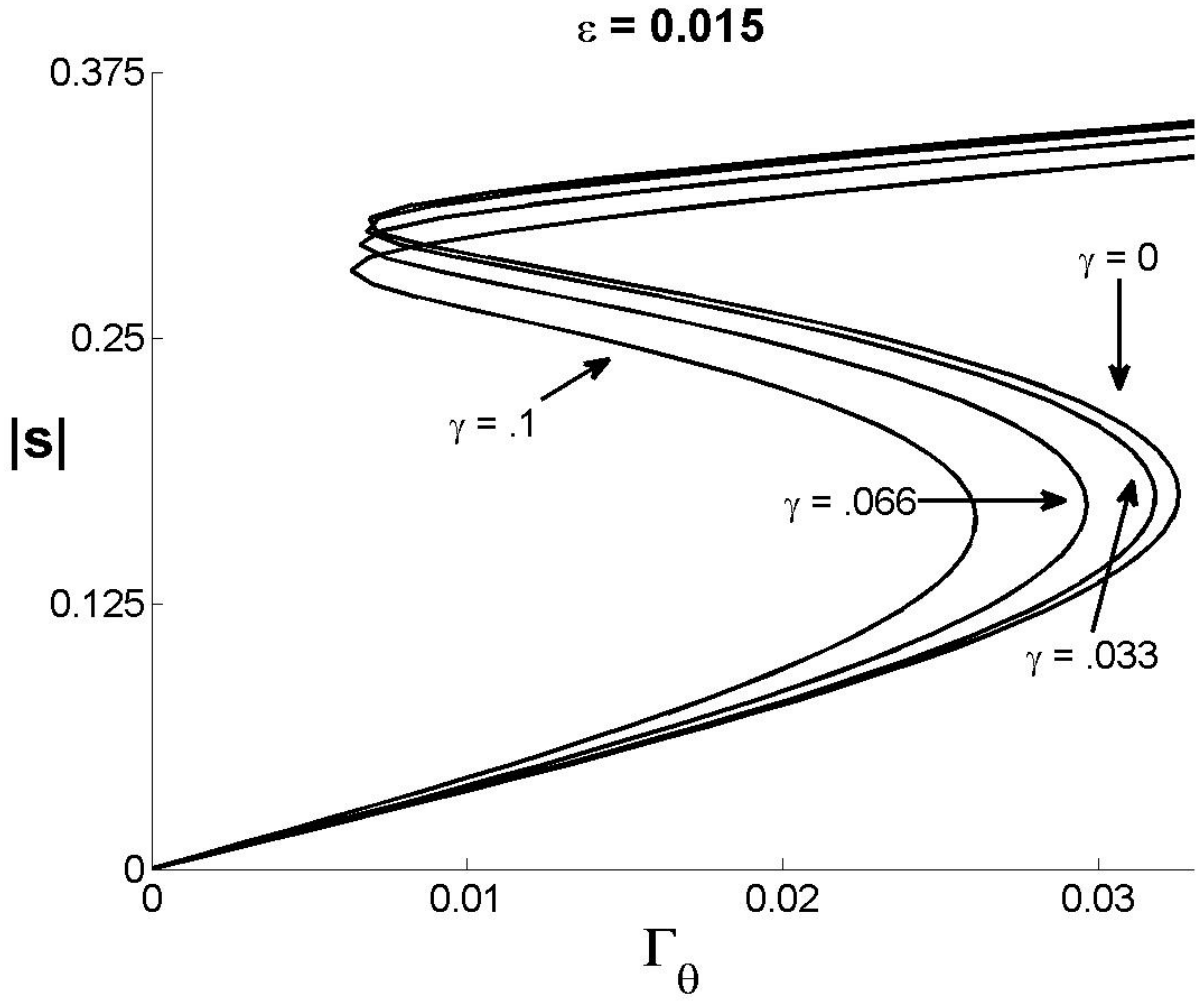

Figure A.1: Non-dimensional absorber amplitude versus non-dimensional fluctuating torque at order n for $\epsilon = .015$.

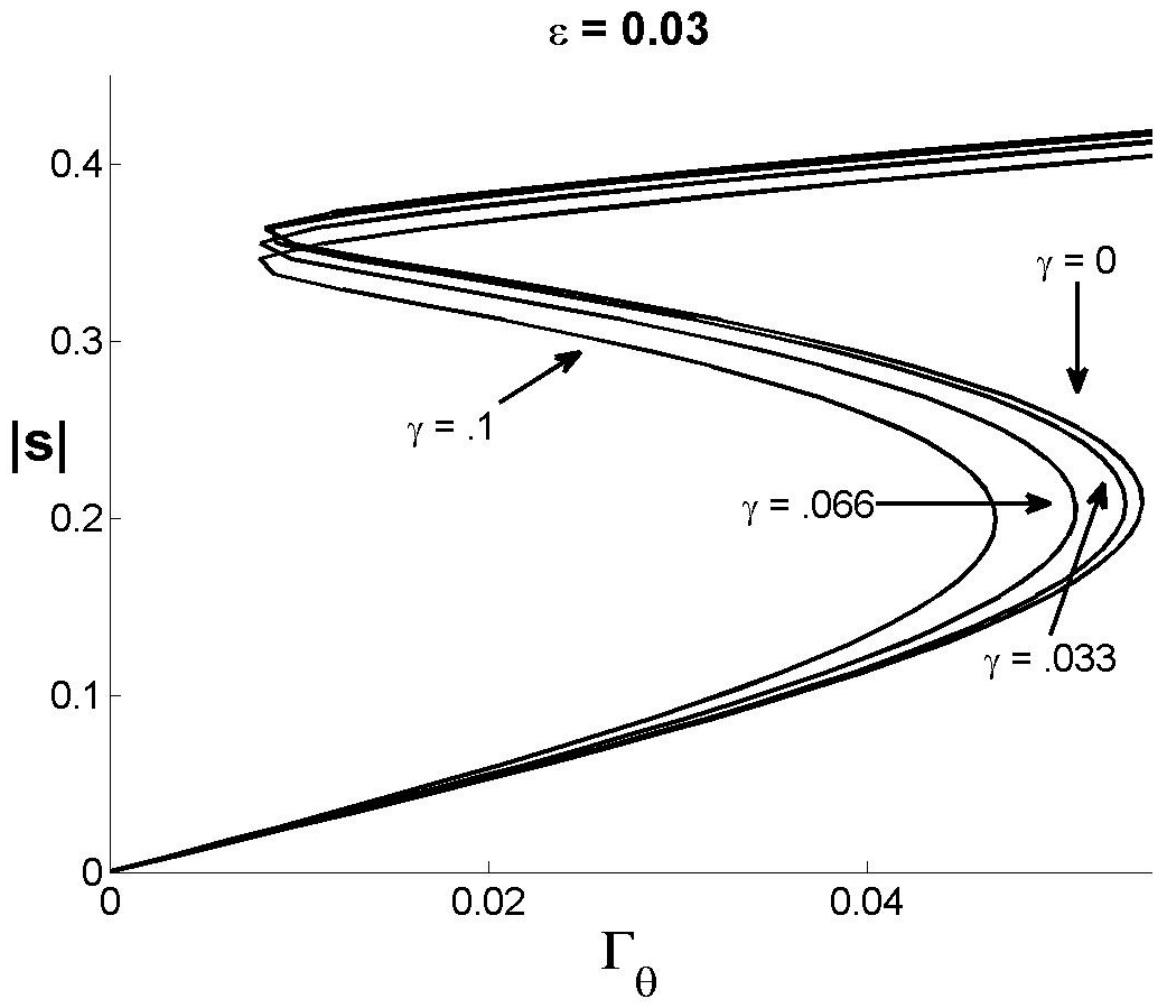

Figure A.2: Non-dimensional absorber amplitude versus non-dimensional fluctuating torque at order n for $\epsilon = .03$.

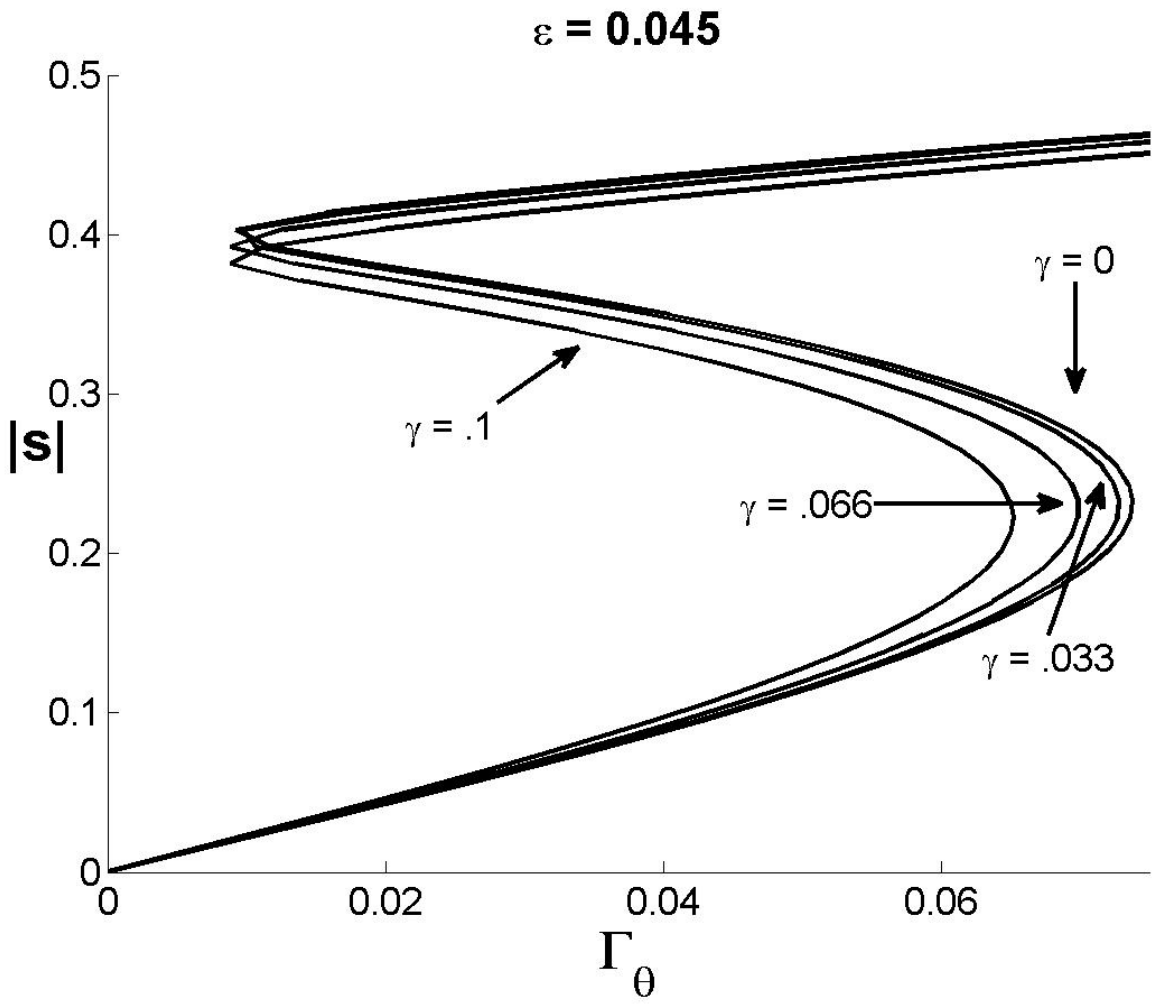

Figure A.3: Non-dimensional absorber amplitude versus non-dimensional fluctuating torque at order n for $\epsilon = .045$.

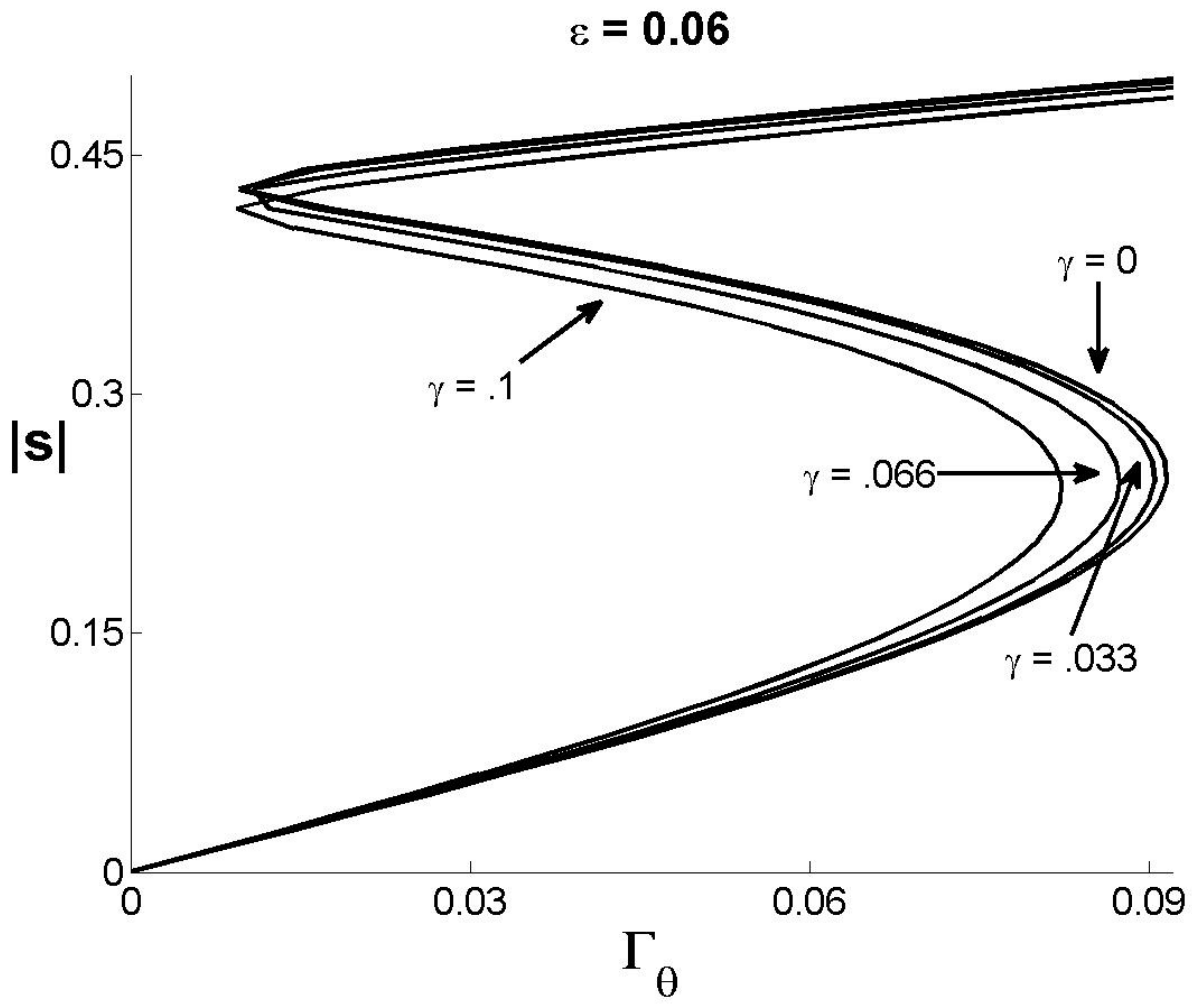

Figure A.4: Non-dimensional absorber amplitude versus non-dimensional fluctuating torque at order n for $\epsilon = .06$.

Appendix B

Elimination of Gravity Term

For the analysis there are always two or more identical absorbers equally spaced around the rotor, a typical arrangement for balancing. In this case the gravitation effects that appear in the scaled rotor equation can be simplified, essentially by symmetry properties of the system. Consider the term that shows up twice in equation (2.55),

$$\sum_{j=1}^{N}[\sin(\theta_j)] = \sum_{j=1}^{N}\sin(\theta + (j)\frac{2\pi}{N}) = \frac{1}{2i}e^{i\theta}\sum_{j=1}^{N}e^{i\frac{j2\pi}{N}} - \frac{1}{2i}e^{-i\theta}\sum_{j=1}^{N}e^{-i\frac{j2\pi}{N}}, \tag{B.1}$$

where $\psi_j$in θ_j has been shifted without affecting the results. By changing the exponential form back to its trigonometric form the following is found,

$$\sum_{j=1}^{N}e^{i\frac{j2\pi}{N}} = \sum_{j=1}^{N}\cos(\frac{j2\pi}{N}) + \sum_{j=1}^{N}i\sin(\frac{j2\pi}{N}). \tag{B.2}$$

It can be shown that

$$\sum_{j=0}^{N}\cos(jX) = \frac{\cos(\frac{NX}{2})\sin(\frac{(N+1)X}{2})}{\sin(\frac{X}{2})} \tag{B.3}$$

and

$$\sum_{j=0}^{N}\sin(jX) = \frac{\sin(\frac{NX}{2})\sin(\frac{(N+1)X}{2})}{\sin(\frac{X}{2})}. \tag{B.4}$$

$X = \frac{2\pi}{N}$ can be inserted into equations (B.3) [20] and (B.4) [21] which will simplify equation (B.2) and consequently equation (B.1). Note that the summations in equations (B.3) and (B.4) contains the $j = 0$ term. When this is accounted for it is found that

$$\sum_{j=1}^{N}[(\sin(\theta_j))] = 0, \tag{B.5}$$

which simplifies the equations of motion.

Appendix C

Higher Order Harmonics Induced by Absorber Motions

When the absorbers move along their paths in an order n response, they produce a torque on the rotor that contains harmonics of order n, as well as higher harmonics. These can be modeled as terms of the form,

$$\sum_{j=1}^{N} z_m \sin(m(\theta + j\frac{2\pi}{N})) \tag{C.6}$$

where m is a multiple of n. Here we show that for some harmonics these terms add, rather than cancel, as was the case for gravity, for which $n = 1$. In this case the number of absorbers also becomes an important part of the analysis. In application if there is no forcing from the engine ($\Gamma_\theta = 0$) harmonics will appear from the coupling between the absorbers, which are driven by gravity, and the rotor. Typically order 2 is of comparable size to order 1, while other higher orders are significantly smaller. It is important to realize is that since the harmonics stem from gravity they remain to have a phase dependence in them.

Case 1: N≠m

It is known that

$$\sum_{j=0}^{N} \sin(jX) = \frac{\sin(\frac{NX}{2})\sin(\frac{(N+1)X}{2})}{\sin(\frac{X}{2})} \tag{C.7}$$

where in this case $X = \frac{m2\pi}{N}$ and, as before, accounting for the $j = 0$ term, it is found that,

$$\sum_{j=1}^{N} z_m \sin(m(\theta + j\frac{2\pi}{N})) = 0 \tag{C.8}$$

Case 2: N=m

Here the summantion is given by,

$$\sum_{j=1}^{N} z_m \sin(m\theta + (\frac{mj2\pi}{N}) = \sum_{j=1}^{N} z_m \sin(N\theta + j2\pi) = N z_m \sin(N\theta) \tag{C.9}$$

Notice that in this case the term does not cancel out, they actually add up. In most cases z_m is a very small value and even if multiplied by the number of absorbers the value is still small.

Implications

It has been seen that in applications of absorbers with gravity, the absorbers produce a significant amount of 2^{nd} order torque that appears in the rotor acceleration. Thus in the case of 2 absorbers there is a noticeable amount of 2^{nd} order torque of non-dimensional rotor acceleration, even when there is no alternating torque from the engine. For the case of 3 and 4 absorbers z_m is typically very small and thus even when summed can be ignored.

Appendix D

Pendulum Type Absorber

The future work that can be done on this topic contains experimental testing, in which case a pendulum style absorber would likely be used. A pendulum style absorber would have a radius of gyration that would alter the analysis and are circular path. As was done by Nester [13] and Vidmar [18] the equations of motion can be normalized so that they can be compared to the results derived in this work.

Equations of Motion

Largrange's equations will be used to find the EOM as was done in this work. The kinetic and potential Energy can be found from the model. Figure 4.2 shows the model that is used to develop the equations of motion.

$$T = \frac{1}{2}J_R\dot{\theta}^2 + \frac{1}{2}J_{pj}(\dot{\theta}+\dot{\phi})^2 + \frac{1}{2}\sum_{j=1}^{N} m_{pj}R^2\dot{\theta}^2 + \ell^2(\dot{\theta}+\dot{\phi})^2 + 2R\dot{\theta}\ell(\dot{\theta}+\dot{\phi})\cos\phi \quad \text{(D.10)}$$

Where J_{pj} is the mass moment of inertia of the pendulum absorber and can be stated as $J_{pj} = m_j\rho^2$. Where ρ is the radius of gyration. The potential energy can be found to be.

$$g\sum_{j=1}^{N}[m_{p_j}(R\cos\theta_j + \ell(\cos\phi\cos\theta_j + \sin\phi\sin\theta_j))]. \quad \text{(D.11)}$$

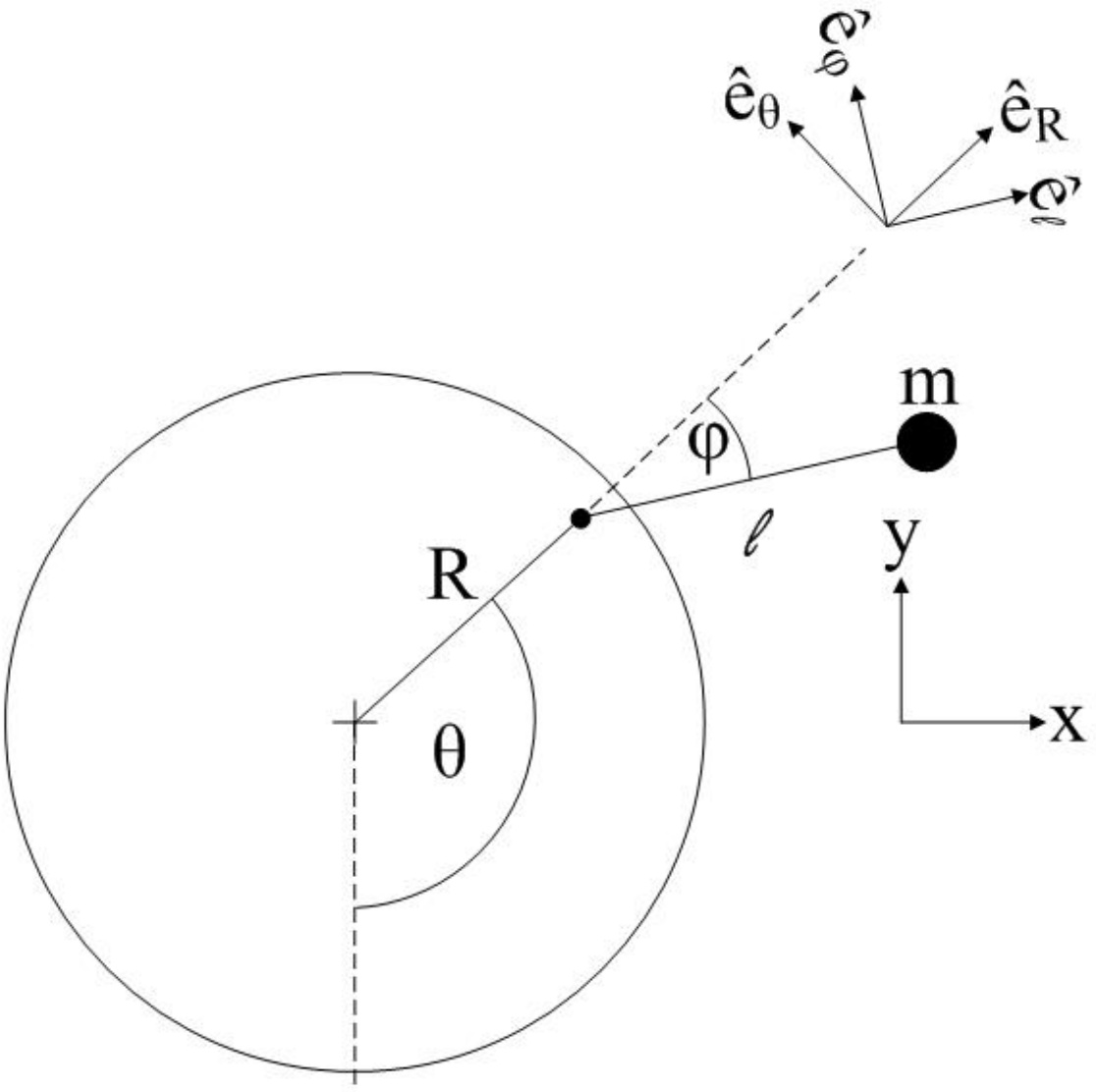

Figure D.5: Diagram of pendulum type circular path absorbers.

Using Lagrange's Equations the EOM can be found. The rotor equation is given by

$$\begin{aligned}
&[J_R + \sum_{j=0}^{N}[m_j(R^2+\ell^2+\rho^2+2R\ell\cos\phi)]]\ddot{\theta} + [\sum_{j=0}^{N}[m_j(\rho^2+\ell^2+R\ell\cos\phi)]]\ddot{\phi} \\
&- \sum_{j=0}^{N}[m_j R\ell(2\dot{\theta}+\dot{\phi})\dot{\phi}\sin\phi] + g\sum_{j=0}^{N}[m_j[R\sin\theta_j + \ell(\cos\phi\sin\theta_j - \sin\phi\cos\theta_j)]] \\
&= -c_o\dot{\theta} + T_0 + T_f\sin n\theta
\end{aligned} \tag{D.12}$$

and the absorber equations are to be found,

$$\begin{aligned}
&[m_j(\ell^2+\rho^2+R\ell\cos\phi)]\ddot{\theta} + [m_j(\ell^2+\rho^2)]\ddot{\phi} + m_j R\ell\sin\phi\ \dot{\theta}^2 \\
&+ m_j g\ell(\sin\phi\cos\theta_j - \cos\phi\sin\theta_j) = -c_{aj}\dot{\phi}
\end{aligned} \tag{D.13}$$

When the absorber is analyzed it can be found that the natural frequency of the absorber, when the rotor spins at a constant rate, is porportional to the mean angular velocity. This allows for the natural frequency to be expressed in an order which is given by,

$$\tilde{n} = \sqrt{\frac{R\ell}{\ell^2+\rho^2}}. \tag{D.14}$$

Non-dimensionalizing and Comparison

The same process is used as was for the general path that was done previously.

$$\nu = \frac{\dot{\theta}}{\Omega} \tag{D.15}$$

Additionally the following is true.

$$\dot{\phi} = \nu\Omega(\phi)' \tag{D.16}$$

$$\ddot{\phi} = \nu^2\Omega^2(\phi)'' + \Omega^2\nu\nu'(\phi)' \tag{D.17}$$

$$\ddot{\theta} = \Omega^2\nu\nu' \tag{D.18}$$

It is desired to change the angle ϕ into a non-dimensional arc length s. It is necessary in order to compare the pendulum style circular path absorbers to the analysis that has already been done that a new parameter β be introduced and solved for later.

$$s = \frac{L\phi}{\beta} \tag{D.19}$$

When these equations are inserted into the equations of motion and expanding trig functions to the third power the following is found,

$$\begin{aligned}
&[1 + \sum_{j=1}^{N}[\frac{m_{pj}}{J_R}(R^2 + \ell^2 + \rho^2 + 2R\ell(1 - \frac{s_j^2\beta^2}{2\ell^2})]\nu\nu' \\
&+ \sum_{j=1}^{N}[(\frac{m_{pj}\beta}{\ell J_R}(R\ell + \ell^2 + \rho^2) - \frac{m_{pj}R\beta^3 s_j^2}{2\ell^2 J_R})(\nu\nu' s_j' + \nu^2 s_j'')] \\
&- \sum_{j=1}^{N}[(\frac{m_{pj}R\beta^3 s_j^2}{\ell^2 J_R})(\nu s_j')^2(s_j - \frac{s_j^3\beta^2}{6\ell^2})] - \sum_{j=1}^{N}[(\frac{m_{pj}R\beta^2}{\ell J_R})\nu^2 s_j'(2s_j - \frac{s_j^3\beta^2}{3\ell^3})] \\
&+ \sum_{j=1}^{N}[(\frac{gm_{pj}R}{J_R\Omega^2} + \frac{gm_{pj}\ell}{J_R\Omega^2} - \frac{gm_{pj}s_j^2\beta^2}{2\ell J_R\Omega^2})\sin(\theta_j)] - \sum_{j=1}^{N}[(\frac{gm_{pj}s_j\beta}{J_R\Omega^2} - \frac{gm_{pj}s_j^3\beta^3}{6\ell^2 J_R\Omega^2})\cos(\theta_j)] \\
&+ \frac{c_0}{J_R\Omega}\nu = \frac{T_0}{J_R\Omega^2} + \frac{T_f}{J_R\Omega^2}\sin(n\theta)
\end{aligned} \tag{D.20}$$

$$
\begin{aligned}
&s_j'\nu'\nu + \nu^2 s_j'' + \frac{R\ell}{\ell^2+\rho^2}(s_j - \frac{s_j^3\beta^2}{6\ell^2})\nu^2 + \frac{R\ell^2}{\beta(\ell^2+\rho^2)}(-\frac{\beta^2 s_j^2}{2\ell^2} + \frac{R\ell+\ell^2+\rho^2}{R\ell})\nu\nu' \\
&+ (\frac{g\ell s_j}{(\ell^2+\rho^2)\Omega^2} - \frac{g\beta^2 s_j^3}{6\ell(\ell^2+\rho^2)\Omega^2})\cos(\theta_j) - (\frac{g\ell^2}{\beta(\ell^2+\rho^2)\Omega^2} - \frac{g\beta s_j^2}{2(\ell^2+\rho^2)\Omega^2})\sin(\theta_j) \\
&+ \frac{c_a}{m_p\Omega(\ell^2+\rho^2)}\nu s_j' = 0
\end{aligned}
\tag{D.21}
$$

These equations can be compared to equations (2.39) and (2.40). When this is done it can be seen that β can be solved for by expanding the $\tilde{g}(s_j)$ and comparing the $\nu\nu'$ terms.

$$
\tilde{g_i}(s) = (1 - \frac{\epsilon^2(n^2+n^4)s_j^2}{2}) = \frac{R\ell^2}{\beta(\ell^2+\rho^2)}(-\frac{\beta^2 s_j^2}{2\ell^2} + \frac{R\ell+\ell^2+\rho^2}{R\ell})
\tag{D.22}
$$

It can easily be seen that

$$
\beta = \ell(1+\tilde{n}^2)
\tag{D.23}
$$

Similar comparisons can be made fore other terms as well. The following parameter definitions were derived by Vidmar [18],

$$
\begin{aligned}
b_o &= \frac{m_o\beta}{J_R\ell}(R\ell+\ell^2+\rho^2) \\
\mu a &= \frac{c_a}{m_p\Omega(\ell^2+\rho^2)} \\
\mu_o &= \frac{c_o}{J_R\Omega} \\
\Gamma_0 &= \frac{T_0}{J_R\Omega^2} \\
\Gamma_\theta &= \frac{T}{J_R\Omega^2}
\end{aligned}
\tag{D.24}
$$

Carrying out a similar analysis for the gravitational terms yields the following relationships,

$$\begin{aligned} -\gamma \frac{dx_{pi}(s)}{ds_j} \sin(\theta_j) &= -\left(\frac{g\ell^2}{\beta(\ell^2+\rho^2)\Omega^2} - \frac{g\beta s_j^2}{2(\ell^2+\rho^2)\Omega^2}\right) \sin(\theta_j) \\ -\gamma\left(1 - \frac{(1+\tilde{n}^2)^2 s^2}{2}\right) &= -\left(\frac{g\ell^2}{\beta(\ell^2+\rho^2)\Omega^2} - \frac{g\beta s_j^2}{2(\ell^2+\rho^2)\Omega^2}\right) \\ \gamma &= \frac{g\ell^2}{\beta(\ell^2+\rho^2)\Omega^2} \end{aligned} \tag{D.25}$$

These results provide the relationships required to compare results for compound pendulum absorbers with single point suspensions with those derived for point mass absorbers.

BIBLIOGRAPHY

BIBLIOGRAPHY

[1] A. S. Alsuwaiyan. *Performance, Stability, and Localization of Systems of Vibration Absorbers*. PhD thesis, Michigan State University, 1999.

[2] A. S. Alsuwaiyan and S. W. Shaw. Steady-state response in systems of nearly-identical torsional vibration absorbers. *Journal of Vibration and Acoustics*, 125:80–87, 2003.

[3] C. P. Chao and S. W. Shaw. The effects of imperfections on the performance of the subharmonic vibration absorber system. *Journal of Sound and Vibration*, 215(5):1065–1099, 1998.

[4] C.P. Chao, C.T. Lee, and S. W. Shaw. Stability of the unison response for a rotating system with multiple tautochronic pendulum vibration absorbers. *ASME Journal of Applied Mechanics*, 64:149–156, 1996.

[5] H. H. Denman. Tautochronic bifilar pendulum torsion absorbers for reciprocating engines. *Journal of Sound and Vibration*, 159(2):251–277, 1992.

[6] B. K. Geist. Hingemaster: Calculating bifilar cut-outs for a pendulum absorber. Technical report, PCTR7380 (Chrysler technical report), 2007.

[7] J. P. Den Hartog. *Mechanical Vibrations*. Dover Publications Inc. New York, 1985.

[8] J.P. Den Hartog. *Stephe Timoshenko 60th Anniversay Volume, Tuned pendulums as torsional vibration eliminators*. The Macmillan Company, New York, 1938.

[9] C.T. Lee and S.W. Shaw. A comparative study of the nonlinear centrifugal pendulum vibration absorber. *Nonlinear and Stochactic Dynamics ASME*, AMD-Vol.192/DE-Vol. 78:91–98, 1994.

[10] J. Madden. Constant frequency bifilar vibration absorber. Technical report, United State Patent No. 4218187, 1980.

[11] R. J. Monroe. *Transients*. PhD thesis, Michigan State University, 2011.

[12] A. H. Nayfeh and D. T. Mook. *Nonlinear Oscillations*. A Wiley-Interscience Publication, John Wiley & Sons, INC., 1995.

[13] T. M. Nester. Experimental investigation of circular path centrifugal pendulum vibration absorbers. Master's thesis, Michigan State University, 2002.

[14] T. M. Nester, A. G. Haddow, and S. W Shaw. Experimental observations of centrifugal pendulum vibration absorbers. In *10th International Symposium on Transport Phenomena and Dynamics of Rotating Machinery (ISROMAC-10), Honolulu, Hawaii*, 2004 2004.

[15] D.E. Newland. Nonlinear aspects of the performance of centrifugal pendulum vibration absorbers. *ASME Journal of Engineering for Industry*, 86:257–263, 1964.

[16] P. M. Schmitz. Experimental investigation into epicycloidal centrifugal pendulum vibration absorbers. Master's thesis, Michigan State University, 2003.

[17] S. W. Shaw and B. K. Geist. Tuning for performance and stability in systems of nearly tautochronic torsional vibration absorbers. *Journal of Vibration and Acoustics*, 132, 2010.

[18] B. J. Vidmar. The effects of coulomb friction on the performance of centrifugal pendulum vibration absorbers. Master's thesis, Michigan State University, 2009.

[19] A. Wedin. Rduction of vibrations in engines using centrifugal pendulum vibration absorbers. Master's thesis, Chalmers University of Technology, 2011.

[20] E. W. Weisstein. *"Cosine" From MathWorld–A Wolfram Web Resource.*

[21] E. W. Weisstein. *"Sine" From MathWorld–A Wolfram Web Resource.*

[22] W. Ker Wilson. *Paractical Solutions of Torsional Vibration Problems*, volume IV. Champman and Hall Ltd, London, 1968.